Functional and proteomics analysis of GNAQ mutant melanocytes

By:
Eva Jin B.Sc.
Dr. Julia V Burnier's Lab
Department of Pathology
McGill University
Montreal, Quebec, Canada

A thesis submitted to McGill University in partial fulfillment of the requirements of the degree of M.Sc.

Table of Contents

Acknowledgements

I would like to acknowledge a number of great people I have met throughout this journey of my graduate studies, without whom I could not have gotten to where I am today.

Firstly I would like to thank my supervisor Dr. Julia V Burnier whom I was fortunate enough to meet and work with. She gave me the opportunities, guidance, and encouragement throughout my studies which were indispensable to my growth as a student and scholar.

I would like to thank Dr. Zorychta and the McGill Department of Pathology for their continuous support during my master's degree, who always had the students' best interests in mind. I would also like to thank my committee advisors: Dr. Carlos Telleria and Dr. Jason Karamchandani, for their presence and support during my committee meetings and presentations, and for their valuable suggestions and comments.

Each and every one of my lab members needs to be acknowledged as well for their daily help and encouragement in the laboratory. Particular thanks to our research assistant Thupten Tsering, and our PHD candidate Prisca Bustamante who helped me troubleshoot and taught me various experimental techniques. Members of Dr. Miguel Burnier's laboratory also helped me greatly, especially Dr. Alicia Goyeneche who introduced me to cell culture and related cell assays, and Christina Mastromonaco for her help in setting up the solar simulator. I am grateful for our neighboring labs of Dr. Alex Gregorieff, Dr. Peter Metrakos, Dr. Labbé, and Dr. Livia Garzia for their generosity in sharing resources and advice.

My project was made possible with funding from Alcon, and studentships from Research Institute of McGill University Health Center (RI-MUHC) and McGill Faculty of Medicine. Technical services and help from Genome Quebec and proteomic platform at RI-MUHC were also indispensable to my research.

Finally, I would like to thank my family, for their unconditional support in whatever I choose to pursue.

Preface / contribution of authors

This is to certify that I have conducted all experiments described in this thesis, under the supervision of Dr. Julia V Burnier. The isolation of normal choroidal melanocytes and western blot results in Chapter 6 were completed as collective work with our research assistant Thupten Tsering M.Sc.

Abstract

Uveal melanoma (UM) is a rare but deadly disease that currently lacks effective preventative or systemic treatment. Key genetic events at different stages of disease progression have been identified in recent years. However, a clear understanding of the mechanistic role of each event in the development of the disease is still lacking.

We are interested in one of the early mutations identified, guanine nucleotide-binding protein G(q) subunit α (*GNAQ)*. Interestingly, *GNAQ* mutations have also been found in over 80% of nevi cases, which mostly remain benign. This indicates that *GNAQ* mutation alone is not sufficient for malignancy in UM. In order to study the biological effects of a *GNAQ* mutation in the disease-originating cells, we aimed to create an *in vitro* system using human normal choroidal melanocytes (NCM) and a lentiviral transduction system.

Furthermore, blue light (BL) has been implicated as a risk factor for UM. To test whether BL exposure compounds with the effect of *GNAQ* mutation to progress to malignancy in melanocytes, we exposed *GNAQ*-mutant NCM to BL in the wavelength range of 400-500nm, at 0.3sun intensity for 3hrs per day over 4 days, and observed functional and proteomic changes that took place.

We demonstrated that a lentiviral transduction system using NCMs provides a viable and useful system to study UM development *in vitro*. Our results characterized $GNAQ^{Q209L}$ mutation as a weak oncogenic event in NCMs. While our results did not capture a transforming effect of BL exposure in $GNAQ^{Q209L}$-transduced melanocytes as hypothesized, we showed that BL acts as an environmental stressor to non-malignant NCM but not UM cells. Our study could set the path for future investigations to clarify the role of BL in development of UM, as it may be valuable promoting the use of BL-filtering intraocular lens or other eye-protections if a preventative value is established.

Abstract (French)

Le mélanome uvéal (MU) est une maladie rare mais mortelle qui n'a actuellement aucun traitement préventif ou systémique efficace. Des événements génétiques clés à différents stades de la maladie ont été identifiés au cours des dernières années. Cependant, une compréhension du rôle mécaniste de chaque événement dans le développement de la maladie fait toujours défaut.

Nous nous intéressons à l'une des premières mutations qui se produit dans la progression de cette maladie, dans la sous-unité α de la protéine de liaison de nucléotides de guanine G(q) (*GNAQ)*. Fait intéressant, des mutations *GNAQ* ont également été trouvées dans plus de 80% des cas de naevus, qui restent pour la plupart bénins. Cela indique que la mutation *GNAQ* seule n'est pas suffisante pour la malignité dans le MU. Afin d'étudier les effets biologiques d'une mutation *GNAQ* dans les cellules à l'origine de la maladie, nous avons cherché à créer un système *in vitro* utilisant des mélanocytes choroïdiens normaux humains (NCM) et un système de transduction lentiviral.

De plus, la lumière bleue (LB) a été impliquée comme facteur de risque pour l'UM. Pour tester s'il y a un effet de la LB en conjonction avec l'effet de la mutation GNAQ qui mène à une évolution vers une tumeur maligne dans les mélanocytes, nous avons exposé les NCM mutant GNAQ à la LB dans la gamme de longueurs d'onde de 400 à 500 nm, à une intensité de 0,3 soleil pendant 3 heures par jour pour 4 jours, et observé les changements fonctionnels et protéomiques qui ont eu lieu.

Nous avons démontré qu'un système de transduction lentiviral utilisant des NCM fournit un système viable et utile pour étudier le développement du MU *in vitro*. Nos résultats ont caractérisé la mutation $GNAQ^{Q209L}$ comme un événement oncogène faible dans les NCM. Bien que nos résultats n'aient pas capturé un effet oncogène de l'exposition à la LB dans les mélanocytes transduits par le $GNAQ^{Q209L}$, comme nous l'avons fait l'hypothèse, nous avons montré que la LB agit comme un facteur de stress environnemental pour les cellules NCM non malignes mais pas les cellules UM. Notre étude pourrait ouvrir la voie à de futures investigations pour clarifier le rôle de la LB dans le développement du MU, car il pourrait être utile de promouvoir l'utilisation de lentilles intraoculaires filtrant le LB ou d'autres protections oculaires si une valeur préventive est établie.

List of figures

List of tables

List of abbreviations

BAP1	BRCA1 associated protein 1
BL	blue light
CM	cutaneous melanoma
GNAQ	guanine nucleotide-binding protein G(q) subunit α
GPCR	G protein coupled receptor
hTERT-NCM	human normal choroidal melanocytes immortalized with *hTERT*
hTERT-NCM^{mGNAQ}	immortalized human normal choroidal melanocytes transduced with mutant *GNAQ* plasmid
IOL	intraocular lens
MAPK	mitogen-activated protein kinase
Melan-A^{mGNAQ}	murine melanocytes transduced with mutant *GNAQ* plasmid
Melan-A^{wt}	murine melanocytes transduced with wildtype *GNAQ* plasmid
NCM^{mGNAQ}	human normal choroidal melanocytes transduced with mutant *GNAQ* plasmid
NCM^{wt}	human normal choroidal melanocytes non-transduced
ROS	reactive oxygen species
TPA	tetradecanoyl phorbol acetate
UM	uveal melanoma
UV	ultraviolet
YAP1	YES-associated protein 1

Introduction / background literature

1. Uveal melanoma

Uveal melanoma (UM) is the most common intraocular malignancy found in adults[1], accounting for 82.5% of all ocular melanomas[2]. Nevertheless, it is still a relatively rare disease representing only 5% of all melanomas. Its incidence rate is approximately 4.9 per million in the US[2], and the number has remained relatively constant from 1970s to current day[3].

UM arises from the melanocytes of the uveal tract in the eye, which is composed of the iris, ciliary body, and choroid, with 90% of tumors found in the choroid[4]. While iris UMs are comparatively less malignant[5], choroidal UMs are more fatal due to their propensity to develop metastasis. Due to yet unclear biological properties, UM metastasis has a high affinity and specificity for the liver. Despite advances over the years in local control of UM, there is yet any effective systemic therapies once the metastatic stage is reached, resulting in the fatality of the disease.

1.1. Risk factors

Risk factors for UM include fair skin and light eye colors[4]. Incidence rates have been reported to be higher for Caucasian populations[2]. Although UM can be diagnosed at any age[6], incidence rate increases with age[4]. The median age of onset lies between 55-60[6], with a peak in the age group of 70[4]. Some have reported gender to be important too. According to Singh *et al.*, between the years 1973 and 2008, there was a significant difference in incidence rates between the two sexes, with male having a higher incidence rate of 5.8 compared to 4.4 of females[7].

Other risk factors suggest a role in genetic factors, including the pre-existence of choroidal nevi, chromosomal abnormalities and mutations, and certain familial factors[6]. Ocular melanocytosis, dysplastic nevus syndrome, and germline BRCA1 Associated Protein 1 (*BAP1*) mutations are also suggested to confer risks[3].

1.2. Genetic signatures

Despite both arising from neural crest-derived melanocytes, cutaneous melanoma (CM) and UM are very different diseases, and UM has a unique genetic signature from its cutaneous counterpart. While in CM, *BRAF* and *NRAS* mutations are important driver mutations, mutations in the same genes have not been found in UM[5]. Additionally, while ultraviolet (UV) exposure contributes significantly to CM etiology, with 80% of CM patients presenting the C>T DNA base transitions characteristic of UV damage[8], the role of UV exposure in UM development remains debatable. No UV damage DNA signature has been reported[9].

Compared to other cancers, UM has a particularly low mutational burden, and relatively clear mutation profiles. Mutations in *GNAQ* and *GNA11* are thought to be the initiating events in UM. In one study with 900 UM patients, *GNAQ* mutation was found in 57% and *GNA11* in 41% of UM tumors[8]. Interestingly, tumors with mutations in neither initiating mutation contain mutations in either *PLCB4* or *CYSTLR2*, two other genes within the *GNAQ/11* pathway[8]. *GNAQ/11* are however considered to be weak oncogenes and are also found in nevi[10]. As such, these mutations appear to be required but not sufficient for malignancy.

While *GNAQ* and *GNA11* are important early mutations, *BAP1*, *SF3B1*, and *EIF1AX* are important secondary driver genes in UM and relate to metastatic risk[8]. *BAP1* is known as a deubiquitinating enzyme that can act as a tumor suppressor by interacting with *BRCA1* in homology-directed DNA repair, however its role in UM could be different and remains unclear[8]. Patients with mutations in *BAP1* often present the disease at younger ages of between 30-49[3]. *BAP1* mutations are found in 47% of primary UM patients and 84% of metastatic patients[3]; thus the presence of *BAP1* mutations is correlated with worse prognosis[3]. Splicing Factor 3b Subunit 1 (*SF3B1*), as its name suggests, is a splicing factor subunit, and mutated *SF3B1* leads to dysregulated splicing of RNA[8]. *EIF1AX* codes for a eukaryotic initiation factor that is responsible for stabilizing the ribosome during translation.

Patterns of genetic aberrations generally also associate with specific chromosomal alterations. For instance, *BAP1* mutations are associated with loss of chromosome 3 and gain of chromosome 8q. Importantly, *BAP1* itself is located

on chromosome 3 as well. *EIF1AX* and *SF3B1* mutations commonly associate with chromosome 6p gain[11].

Metastatic risk in UM is generally divided into three groups – that of high, intermediate, and low metastatic risk. Traditionally, various clinical and histological characteristics are used to estimate the metastatic risk of UM patients, such as tumor size, extraocular extension, and cell type (epithelioid or spindle)[8]. However genetic aberrations have recently shown potential for higher reliability in predicting disease progression[12]. Metastatic risk of patients harboring *BAP1*, *SF3B1*, and *EIF1AX* are considered high, intermediate, and low respectively[8]. In general, higher metastatic risk is associated with chromosome 8q gain and loss of chromosome 3, while lower metastatic risk associates with gain of chromosome 6p[8].

1.3. Pathogenesis

It is believed that the pathogenesis of UM involves uncontrolled activation of the mitogen-activated protein kinase (MAPK) pathway, which has been shown to drive oncogenesis of various other cancers[13]. However, investigations of mutational profiles of primary and metastatic UMs did not show mutation of signaling components of *RAS*, *B-RAF*, or *MEK1* as previously shown in mutation profiles in CM[14, 15]. This suggests that tumor development in UM follows a distinct molecular pathway from that of CM.

Choroidal nevi have a prevalence rate of 4.6% to 7.9% in the USA[16]. However the true incidence rate is most likely higher since unlike skin nevi, choroidal nevi are less noticeable, generally asymptomatic, and often found during ophthalmic exams for other reasons. In rare occasions, nevi growths have been observed to undergo malignant transformation into UM. In an analysis of 2514 choroidal nevi cases, malignancy developed after one, five, and ten years in 2%, 9%, and 13% of the cases respectively[17]. Several clinical factors have been determined that would predict higher likelihood of nevi to UM transformations. The seven factors are: tumor thickness greater than 2mm, subretinal fluid, symptoms, orange pigment, tumor margin 3mm of optic disc, ultrasonographic hollowness, and halo absence[17].

One proposed model of UM disease progression is as depicted in the schematics of Figure 1. A normal melanocyte first obtains an initiating mutation in *GNAQ/11*, that gives it a survival and proliferating advantage. Then through a yet unknown stimulation, gains a secondary oncogenic event that makes it progress into melanoma. After maligancy is established, it could either gain chromosome 6p to develop a less aggressive clinical form, or lose chromosome 3 to progress to a more aggressive tumor class[5].

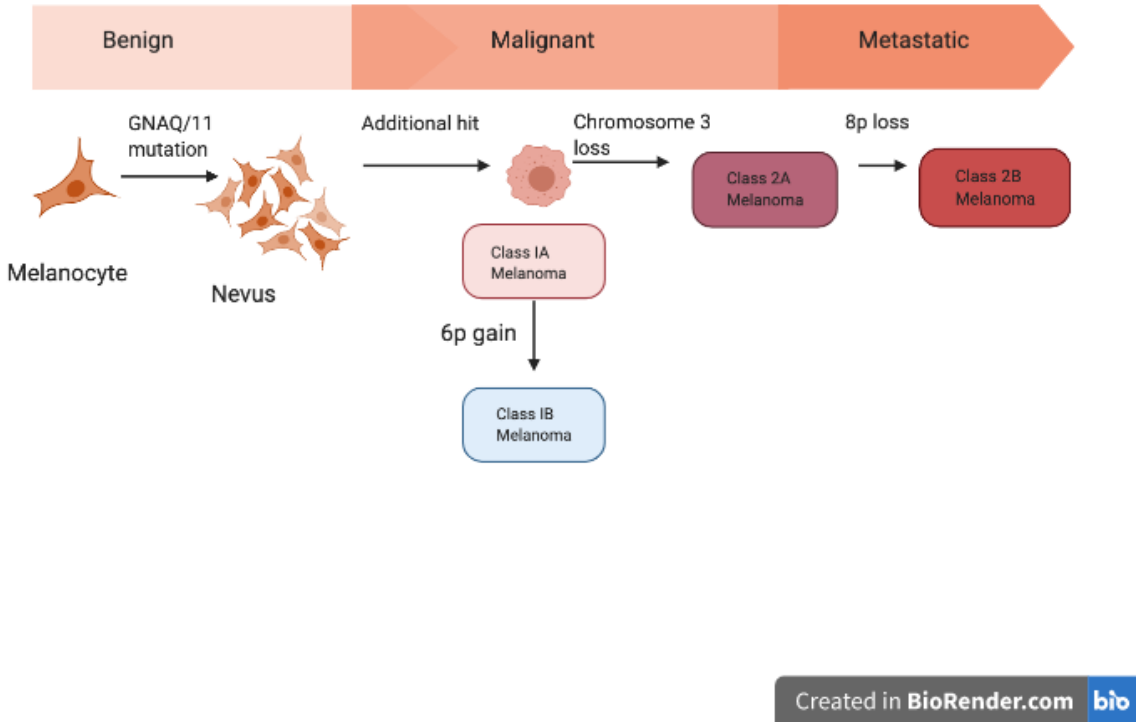

Figure 1: Proposed disease progression schematics of UM (Adapted from Sodhi, A. and S. Merbs, Molecular Genetics of Choroidal Melanoma. Vol. 3. 2012. 2247-2253.)

1.4. Treatments

Current treatment options include resection, radiation, and enucleation[4]. Treatment methods over the years have undergone a shift towards more eye-sparing techniques[7]. Following the 2006 Collaborative Ocular Melanoma Study (COMS) that showed enucleation did not exhibit a more favorable outcome compared with iodine-125 brachytherapy, it has become more common in the US to opt for plaque brachytherapy as primary treatment[3]. Options of eye-preserving surgical procedures include transretinal endoresection and transscleral resection.

However the visual acuity benefit of transscleral resection must be weighed against the higher rates of recurrence[3].

Despite improvements in treatments over the last decades, the 5-year survival rate for UM patients has not improved significantly and remains at around 81.6%[7]. Long-term survival rate for UM patients is severely compromised by the incidence of liver metastasis[4]. Although at time of primary tumor diagnosis, most patients do not present with detectable metastasis, it is believed that for patients that go on to developing metastases, micro-metastases had already developed at the time of primary treatment[18]. For patients with detectable metastasis, survival is estimated to be less than a year[19]. Much still remains to be known regarding the mechanisms of metastasis in UM and the conditions of tumor dormancy. Metastasis can occur after several years after primary disease diagnosis, but it could also occur only after several decades[8]. This latency of UM may be driven by tumor dormancy and this hypothesis is under investigation by many groups[20, 21].

As previously stated, there is currently no effective treatment for metastatic UM, and therapies that have demonstrated success in CM have not showed similar success in UM[8]. Chemotherapy in UM has shown disappointing response rates[22]. Immunotherapy that has shown promising results in CM has not showed promise in UM, and this may be partly attributed to the immune privilege of the eye[8]. Based on the importance of *GNAQ/11* pathway in UM, therapeutic efforts have been made to target its downstream signaling components. MEK inhibitor selumetinib showed promising preliminary results, however it lost efficacy when resistance eventually develops; thus resistance remains an unsolved obstacle in inhibitor-based therapeutics aiming to block the *GNAQ/11* pathway[8]. Other therapeutics under development include histone deacetylase inhibitors and spliceosome inhibitors[8].

2. *GNAQ/11* as initiating mutations in UM

GNAQ encodes for the α subunit of heterotrimeric G-proteins that work downstream of G protein-coupled receptors (GPCR)[3]. Both *GNAQ* and *GNA11*

belong to the same family of Gα proteins and are 90% homologous at their amino acid level[23].

Under normal circumstances, once a ligand binds to the GPCR, a binding pocket opens for the heterotrimetric G protein complex that consists of Gα subunit and a β-γ dimer[23]. Upon binding to the GPCR, the Gα protein exchanges its bound GDP to GTP, dissociates from the trimer complex and becomes activated to signal to its downstream targets. The Gα protein has intrinsic GTPase activity, which under normal circumstances would return the protein to its resting activity state bound to GDP.

GNAQ mutations in UM occur selectively on exon 5[24], with 95% of mutations occurring at position Q209 and the other 5% occurring at R183[25]. The mutations occur in the RAS-like domain of the protein that contains its GTPase activity. Mutation in Q209 results in a complete loss of GTPase activity while mutation at R183 results in a partial loss[26]. The loss-of-function mutations prevents the Gα subunit from returning to GDP-bound state, thus locking the protein in its activated form and making the mutant protein constitutively active. An over-stimulation of the downstream pathways results[24].

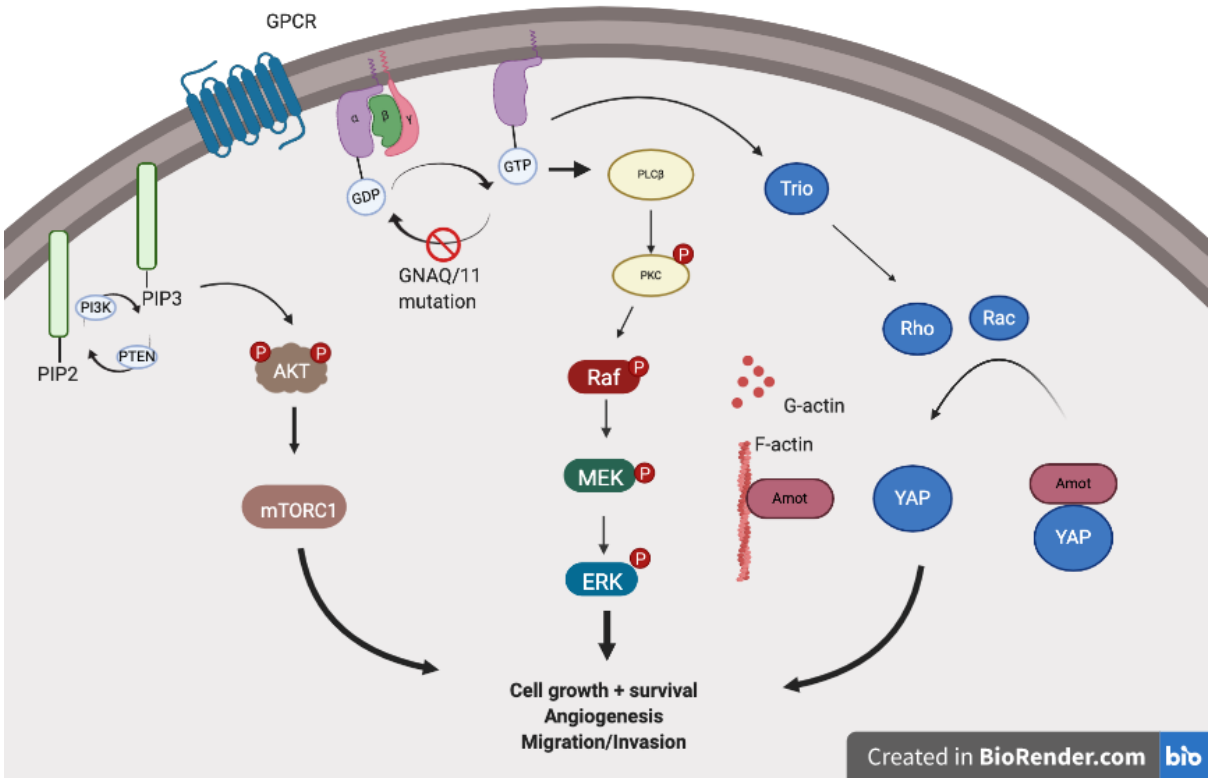

Figure 2:Signal pathway downstream of GNAQ/11 (adapted from Yang, J., et al., Treatment of uveal melanoma: where are we now? Therapeutic Advances in Medical Oncology, 2018. 10: p. 175883401875717.)

2.1. MAPK pathway

There are three identified pathways involved downstream of GNAQ, with all pathways leading to cell growth and proliferation. The most well-known pathway downstream of active GNAQ is the mitogen-activated protein kinases (MAPK) pathway (RAS/RAF/MEK/ERK)[25].

GNAQ relays signal to phospholipase C (PLCβ), which functions to hydrolyze membrane phospholipid into second messengers of inositol 1,4,5-trisphosphate (IP3) and diacylglycerol (DAG)[25]. DAG functions as binding site for PKC enzymes, while IP3 triggers calcium release which can also in turn activate PKC enzymes[25].

Although the detailed mechanistic link between GNAQ and MAPK activation had been unclear, it has been demonstrated that activation of PKC is an

important link[25]. Knockdown of GNAQ or PKC inhibited cell proliferation of GNAQ-mutant UM cells[26]. Activation of PKC in UM cell lines has been shown to be a direct result of mutated GNAQ/11, and UM cell lines without GNAQ/11 mutations did not exhibit high PKC activity[26].

The role of PKC in the GNAQ-mutant pathway has been closely studied. There are many isoforms of PKCs with significant homology with each other. However siRNA knockdown of PKC δ and ε alone led to partial inhibition of phosphorylated MEK (pMEK) and pERK, and knockdown of both isoforms resulted in pMEK and pERK inhibition level similar to knockdown of GNAQ[25]. These results suggest a vital role for the δ and ε isoforms of PKC in GNAQ-mutant UM cells.

Downstream of PKC, a RasGEF, RasGRP3, has been found to mediate MAPK activation specifically in GNAQ/11 mutated UM cells, and is activated by phosphorylation by PKC[25].

Interestingly, cell lines with BRAF and NRAS mutations resulted in increases of pERK but not p-MARCKS (a PKC substrate), demonstrating that despite sharing an upregulation of MAPKs, there is a specificity for PKC dependency downstream of GNAQ/11 mutations[26]. It has been shown *in vitro* that UM cell lines harboring GNAQ mutations are more sensitive to PKC inhibition[26, 27]. Collectively these results show that in GNAQ/11 mutated cell lines, MAPK activation depends heavily on PKC activity. PKC inhibition alone however is not sufficient to inhibit MAPK activity, thus it has been proposed that combination of PKC and MEK inhibitors would act synergistically to induced apoptosis in GNAQ/11 mutant cells[26].

2.2. YAP Pathway

In addition to the MAPK pathway, GNAQ also lies upstream of the phosphatidylinositol3-kinase (PI3K)/AKT and Yes-associated protein1 (YAP1) pathways[3]. The Hippo/YAP pathway has been implicated in a number of cancers[28]. Canonically, YAP1 is regulated by the Hippo tumor suppressor. The activated YAP is translocated to the nucleus and promotes proliferation by regulating transcription factors TEADs and SMADs. The Hippo pathway

suppresses YAP by phosphorylating it through large tumor suppressor 1/2 (LATS1/2), which retains YAP in cytoplasm.

There is evidence that YAP may be responsible for at least a portion of oncogenic effects of mutant GNAQ/11. It has been found that mutant GNAQ/11 cell led to YAP/TAZ dephosphorylation, and the knockdown of YAP significantly inhibited tumorigenic abilities in *GNAQ*-mutant cells[29].

Interestingly, YAP activation through GNAQ signaling is demonstrated to occur through a non-canonical Hippo-independent pathway. This pathway involves the guanine nucleotide exchange factor Trio, and its downstream GTPases Rho and Rac. A cytoskeleton-associated regulation for YAP has been proposed, where mutant GNAQ results in actin polymerization and increases polymerized F-actin. F-actin has been shown to bind angiomotin (AMOT), and AMOT in turn is associated with YAP[30]. Although the exact mechanism in which actin polymerization results in upregulation of YAP activity is not completely known, it is proposed that it occurs through F-actin which binds and sequesters AMOT, which in turn results in release of YAP that would otherwise be sequestered by AMOT[30].

2.3. PI3K-AKT Pathway

Through yet unclear mechanisms, phosphatidylinositol-3 kinase (PI3K) signaling has been shown to be upregulated in *GNAQ*-mutant UM cells[23]. PI3K signals through AKT and ultimately the mammalian target of rapamycin (mTOR) to promote proliferation. Inhibitors for mTOR, the downstream effector of AKT, have been explored as plausible treatment approaches for UM patients[31]. It was shown that *GNAQ/11*-mutant tumors had higher levels of pAKT compared to normal choroidal cells[32]. Studies investigating effects of inhibitors showed that inhibition of MEK or PI3K alone does not sufficiently induce apoptosis in UM cell lines, further supporting that MAPK is not the sole pathway downstream of GNAQ/11[33].

2.4. Importance of GNAQ pathway in UM

In tumors that do not harbor *GNAQ/11* mutations, it has been found that there are much rarer mutations in either phospholipase$C\beta 4$ (*PLCβ4*) or G-protein

coupled receptor cysteinyl leukotriene receptor 2 (*CYSLTR2*). Both are also involved in G-protein coupled receptor signaling pathway, with PLCβ4 acting downstream of GNAQ/11 and responsible for hydrolysis of PIP2 and generation of second messengers, and CYSLTR2 acting upstream of GNAQ/11. This furthers illustrates the important role this pathway plays in UM[3]. As such, it is thought that the pathogenesis of all cases of UM are defined by a mutually exclusive mutation in *GNAQ*, *GNA11*, *PLCB4* or *CYSLTR2*.

While GNA11 mutations has been found to be more frequently represented in metastatic UM cases[34], it was shown that GNAQ mutations did not correlate with disease-free survival (DFS), and cannot be used to predict progression of disease[24]. More than one study has also found that GNAQ mutations did not correlate with clinicopathological parameters such as age, gender, largest tumor diameter, scleral extension, and other prognostic paramters[35, 36]. The presence of GNAQ mutation in benign blue nevi also is evidence that despite its wide presence in UM, mutation in the GNAQ pathway alone is insufficient for malignancy.

3. Light exposure

3.1. UV exposure and UM

UV light is divided into three categories according to its wavelength, with the longest wavelengths consisting of UV-A (~315-400nm), intermediate wavelengths in UV-B (~280-315nm), and shortest wavelengths being UV-C (~100-280nm)[37].

The effect of UV exposure on cells have been extensively studied. It is generally believed that UV exposure drives oncogenic mutations via formations of cyclobutane pyrimidine dimers and (6-4) photoproducts. However not all UV wavelengths induce damage in the same way. While UV-B and UV-C are directly absorbed by DNA base pairs, UV-A induces damage indirectly via generating oxidative stress[37].

Several suggested risk factors of UM indicate a role of light exposure in UM incidence, including: increasing latitude in European populations, light iris color, and Caucasian ethnicity[6]. However overall, literature has been inconsistent regarding the role of sun and UV exposure in the development of UM, and

epidemiological studies have showed inconclusive results correlating UV exposure to UM incidence[4].

Furthermore, genetic evidence also suggests UV exposure to be unlikely to contribute dominantly to the development of UM. For instance, it is known that in cutaneous melanoma, the V600E BRAF mutation is expressed in most patients, which is thought to reflect UV damage[6]. In UM tumors, anterior UM (such as that of iris) have been shown to harbor V600E mutations, but V600E detection is negligible in posterior UM tumors[6]. This correlation can be attributed to the protection of posterior eye to UV exposure compared to the anterior[6]. Since most UM arises in the posterior uveal tract, UV exposure is likely not an important contributor to UM oncogenesis. Moreover, molecular data has not shown a typical UV-associated mutational profile, as is seen in skin melanoma, with no enrichment for typical C<T transitions at dipyrimidine sites.

Further evidence against a significant role of UV exposure in UM development involves the properties of our lens and cornea. It has been shown that adult crystalline lens and cornea jointly offer protection for the eye for wavelengths below 400nm[38].

3.2. Effect of blue light exposure

Compared to UV light which has been extensively studied for its biological effect, the role of visible light has been less studied. Blue light (BL) is generally defined as wavelengths between 400nm and 500nm. Being on the shorter-wavelength portion of the visible spectrum, BL exposure is thought to have higher energy that may have the potential to exert biological damages or effects. BL is emitted from various sources in our daily lives, including from the natural sun light, as well as artificial light sources. With recent developments, light-emitting diodes (LED) lights have become a substitution for various light sources, and the peak emission of LED lights lies in the 400nm-490nm range[39]. LED lights also make up the screen light that come from numerous electronic devices that are increasingly more prevalent in our lives. Welders are especially subjected to occupational exposure of blue light[40].

Studies of *in vitro* and *in vivo* effects of BL have been recorded for different types of cells. Hockberger *et al*. have demonstrated that light exposure in the

violet/blue wavelength ranges induces H_2O_2 production in mammalian cells (mouse fibroblasts, monkey kidney epithelial cells, human foreskin keratinocytes) and exerts cytotoxic effects[41]. Interestingly, a biphasic effect on proliferation and metabolic activity was reported by Becker *et al.* on HaCaT human keratinocyte cell line[42].

The effects of BL have been documented for human skin cells. Liebmann *et al.* demonstrated BL effects on human keratinocytes and skin endothelial cells[43]. According to their study, light of 412-426nm showed cytotoxic effects, and while wavelength of 453nm had no cytotoxic effect below 500J/cm^2 it reduced proliferation in a dose dependent manner. Liebmann's group showed a cytotoxic mechanism dependent on generation of nitric oxide (NO). The mechanism underlying the observed reduction in proliferation was attributed to increased differentiation of the irradiated cells[43]. It has also been shown that BL had an inhibitory effect on mouse melanoma cell lines[44]. Results such as these provide support of the use of blue-light therapy to treat hyperproliferative skin conditions. Currently, BL is known to be effective for treatment of neonatal jaundice[45], and its efficacy is under investigation for conditions such as acne and psoriasis[46, 47].

Godley *et al.* showed that exposure to blue light (390-550nm) induced mitochondrial DNA damage through production of reactive oxygen species (ROS) in primary retinal epithelial cells[48]. ROS can be generated when light excites molecules referred to as photosensitizers[48]. Examples of ROS include singlet oxygen, hydroxyl radical, or superoxide anions[48]. Photosensitizer molecules in pigmented cells include melanin, lipofuscin, and retinoids; however, it remains unclear which molecules act as photosensitizers in non-pigmented cells[48]. The mechanism in which ROS damages cells include damage through lipids, proteins, and DNA[48].

In the eye, retinal pigment epithelial (RPE) cells have been shown to increase apoptosis and ROS production upon exposure to BL emitted by screens[49]. Another group also showed RPE cells of the rat undergoes apoptosis in moderate intensity of BL, and necrosis in higher BL intensity[50]. Sparrow *et al.* demonstrated the ability of blue-light-absorbing intraocular lens (IOL) to reduce death of RPE cells after exposure to light of blue, green, and white wavelengths. Blue light has also been shown to decrease secretion of angiogenin by RPE cells[51].

3.2.1. Blue light and UM

Although epidemiological studies have not been able to conclusively draw a correlation between UV exposure and UM, a prominent correlation has been reported between arc welding and UM incidence[52]. Since welding can be a strong source of both UV and blue light[40], it led to the suspicion of a role of BL in UM.

Several studies have reported an effect of BL on UM *in vitro* and *in vivo*. Exposure to BL at 475nm on UM cell lines (92.1, MKT-BR, OCM-1, SP6.5) led to an increase in proliferation rate[53]; however, the mechanism underlying this observation was not elucidated.

In vivo evidence of a role of BL in UM came from a reported case of ocular tumor in a Long Evans rat following BL exposure in 434-475nm range, with a combination of antiapoptotic treatment[54]. Furthermore, when UM cell lines are inoculated into eyes in a rabbit model, exposure to BL increased proliferation of grafted cells upon reculture[55].

Further evidence of a role of BL in UM involves an epidemiology study that found neonatal blue-light phototherapy (used to treat neonatal jaundice) to be linked to melanocytic nevi development in the skin and eye[56]. Dysplastic nevus development is in turn linked to increased risk of developing melanoma[6]. A twin study also suggests neonatal blue-light phototherapy to be a risk factor for the development of melanocytic nevi[57].

The specific mechanism of action in the BL spectra is not clear. It is hypothesized that blue light may act biologically similarly to UV-A, due to the adjacent wavelength ranges of the two[6]. BL may thus contribute to the development of UM by triggering ROS production and leading to mutations in uveal melanocytes[6].

BL has also been explored in the context of neovascularization, which is of interest due to the role of neovascularization in tumor development. Vascular endothelial growth factor (VEGF) is a promoting factor for angiogenesis. In UM, VEGF is known to be induced by hypoxia[58], and high levels of VEGF are found in aqueous and vitreous humor of UM patients[59, 60]. BL exposure of RPE cells has been correlated to VEGF production[61].

With age, the human lens becomes progressively more yellow, potentially via progressive accumulation of yellow chromophore deposits, primarily 3-hydroxykynurenine glucoside derivatives, and is therefore better able to filter BL from entering the eye[62]. When patients undergo cataract surgery, the original lens is removed and replaced with an artificial intra-ocular lens (IOL). Most IOLs have UV-filtering capabilities, but many are not equipped to filter other wavelengths, such as BL. As such, the removal of the aged lens during cataract surgery is accompanied by the loss of the natural ability to filter BL. Given the known role of BL in age-related macular degeneration and potentially in UM, the use of BL-filtering IOLs may be warranted.

While having a rare incidence, UM has a high mortality rate. Given the lack of effective treatments for metastatic disease, discovery of preventative care would be greatly beneficial. Hence it is important to search for environmental factors that may exist that contributes to the development of UM in order to create corresponding preventative care. Especially considering the majority age of onset of around 60-74 years of age, which coincides with the age range of cataract surgeries and IOL implantations, clarifying the need for BL-filtering ability in IOLs could make a great difference in preventative care of intraocular malignancy.

Research aims and relevance

While rare, UM is a deadly malignancy. Moreover the survival rate of this disease has been unchanged in decades, despite major advances in primary tumor control and in our understanding of the mutational landscape. Importantly, no environmental factor has been definitely attributed to UM development, unlike CM in which UV light is a known contributor to disease. Several hypotheses exist, with a particular focus on BL. With no effective treatments for metastatic UM, finding preventative measures would greatly impact patient care. As there still exists ambiguity in the etiology and risk factors of UM, there is a need to further explore the underlying risks and uncover the biological processes that lead to transformation of uveal melanocytes. *GNAQ* mutations are an established initiating/early event in UM. However, no commercially available or widely used *GNAQ*-mutant system exists to study UM.

As such my first aim is to establish a human choroidal melanocytes model through which to study initiating mutations of UM, which would also involve developing our own cultures of human choroidal melanocytes (NCM) since no commercial purchase of these cells are available.

Aim1: Characterize *GNAQ*-mutant cells by:

- Establishing *GNAQ*-mutant human primary and immortalized choroidal melanocytes
- Utilize murine *GNAQ*-mutant melanocytes as a validation model
- Characterize the behavior of *GNAQ*-mutant and WT NCMs (NCM^{mGNAQ}, NCM^{WT}) via functional cellular assays
- Explore the proteomic changes that occur upon *GNAQ*-mutagenesis in NCMs

We hypothesize that a *GNAQ* mutation would result in altered behavior and proteomic profile of NCMs. In particular we believe that *GNAQ*-mutant cells would exhibit higher proliferation and migration abilities than the WT counterparts, and we expect quantitative proteomics profiles to present two distinct protein signatures that may reveal key mediators of oncogenesis in UM.

In the pathogenesis model proposed by Sodhi *et al.* (Figure 1), there is a second oncogenic hit needed to transform *GNAQ/11* mutated cells to UM. The exact

identity of this second hit is still unknown, however the potential role of BL in UM pathogenesis has recently been highlighted. We hypothesize that BL could potentially act in a secondary event to drive malignancy, and will explore its effect in the second aim of my project.

Aim2: Determine whether BL exposure acts as second event to drive the development of UM

- Establish model to study BL effects in cultured cells
- Perform functional assays on cells with and without BL exposure
- Compare proteomic profiles of BL-exposed vs. control cells
- Compare activation of major signaling pathways with and without BL exposure

Our hypothesis for Aim2 is that BL exposure could potentially act as a second oncogenic hit in addition to the initiating mutation of *GNAQ/11*, and *GNAQ*-mutated melanocytes after BL exposure would exhibit increased proliferation and migration potentials, possibly even at levels comparable of UM cell lines.

While UV protection of the skin and eyes has been widely accepted to be needed, there remains uncertainty in the need to protect against shorter wavelength regions of the visible light spectrum, namely the blue-light region. One clinical implication lies in the use of BL -filtering IOL. While UV-filtering property is standard now for IOLs, there remains debate on the necessity of the addition of BL-filtering property[6]. IOLs implants are involved in medical procedures such as cataract surgeries. Compared to our natural lens, which accumulates yellow chromophore deposits gradually[63], the IOL implant does not have the same property. Further studies suggesting a role of BL in the development of UM would provide a clinical rational for adding blue-light filtering property to standard IOLs.

Materials and methods

1. Cell culture

Uveal melanoma cell lines used (MP46, 92.1) were purchased from ATCC, and were maintained in culture medium of RPMI 1640 supplemented with 10% fetal bovine serum (FBS), 0.1% 10U/ml penicillin and 10 µg/ml streptomycin, 4mM L-glutamine, 10µg/ml insulin (Wisent, Canada), and 1mM NaPyruvate. Media components were purchased from Corning.

Melan-A cells stably transduced with either mutant or wildtype *GNAQ* plasmids were kindly gifted to us by Dr. Boris C. Bastian's lab (Department of Dermatology and Comprehensive Cancer Center, University of California, San Francisco)[10]. Melan-A cells were grown in RPMI 1640 media supplemented with 200nM tetradecanoyl phorbol acetate (TPA)(Sigma-Aldrich, 79346)[64], 4mM L-glutamine, 0.1% 10U/ml penicillin and 10 µg/ml streptomycin, and 10% FBS.

Normal choroidal melanocytes (NCM) extracted from donor eyes were cultured in Melanocyte Growth Medium (M2 medium) (Promocell, Germany), and 50µg/ml Geneticin/G418 (Sigma).

Frozen vials of human choroidal melanocytes were also gifted to us from Dr. Solange Landreville's lab (Centre de Recherche du CHU de Québec-Université Laval). Cells were thawed and cultured using media the cells were previously grown in: DMEM/Ham's F12 (1:1) (Thermofisher) with 10% FBS, 50µg/ml Gentamicin (Sigma), 50µg/ml Geneticin/G418, and 100nM TPA[65].

2. Establishing cell lines

2.1. Extracting human choroidal melanocytes from donor eyes

Informed consent from donor's next to kin was obtained, according to protocol (IRB #2019-5314) approved by Institutional Review Board (IRB) of MUHC-RI. Three donor eyes were obtained from Centre Universitaire d'Ophtalmologie (Centre Hospitalier Universitaire de Québec, Canada).

To extract choroidal melanocytes from the eyeballs, cornea, lens, vitreous humor and iris were first removed. Four incisions were made towards the optical nerve to obtain a petal-like shape. The choroid (with attached RPE cell layer) was detached from the sclera with forceps, then incubated in 0.02% disodium ethylenediaminetetraacetic acid (EDTA) for 30 minutes at 37˚C, followed by

incubation in trypsin (Sigma, 0.5mg/ml) with collagenases IA and IV for 1 hour at 37˚C, in order to remove RPE cells. The choroid was then incubated in dispase II (Boehringer Ingelheim, Germany) and diluted in M2 medium for 18 hours at 37˚C. Complete Protease Inhibitor Cocktail (Roche Diagnostics, Germany) was used to stop the dispase reaction. To obtain single cell suspension, digested tissue mixture was shaken, then passed through 40μm cell strainer. Cells were then spun at 100*g* for 5 minutes to obtain a pellet, and resuspended in M2 media and cultured on FNC (0407, Athena)-coated T25 tissue culture flasks. Culture medium was changed every three days. Geneticin/G418 (Sigma) was added to culture medium at concentration of 100μg/ml to diminish contamination with RPE cells or fibroblasts for 7 days prior to sub-cultivation. Confluent flasks were cryopreserved in liquid nitrogen using cryo-SFM (Procell).

2.2. Plasmid cloning and purification

All plasmids were purchased from Addgene and received as bacteria stab cultures. Psd44-GqQL was a gift from Agnese Mariotti (Addgene plasmid # 46826 ; RRID:Addgene_46826)[66, 67]. pLOX-TERT-iresTK was a gift from Didier Trono (Addgene plasmid # 12245 ; RRID:Addgene_12245)[68]. pMD2.G was a gift from Didier Trono (Addgene plasmid # 12259 ; RRID:Addgene_12259). psPAX2 was a gift from Didier Trono (Addgene plasmid # 12260 ; RRID:Addgene_12260).

Agar plates were made from 25g lysogeny broth (LB) powder per liter of autoclaved water, containing 10 μg/ml concentration of ampicillin for selection. Single colonies on agar plates were picked to be grown in 2ml starting culture of ampicillin-containing liquid LB and allowed to grow for 8hrs. Then 1ml of starting culture was spun at 5000rpm for 5 mins and expanded to a volume of 100ml for plasmid purification. The 100ml cultures were incubated at 37˚C with shaking of 150rpm overnight.

Plasmids were then purified from the bacteria culture with the GeneJET Plasmid Midiprep Kit (ThermoFisher, K0481) according to manufacture instructions, using low speed centrifugation. Briefly, bacterial cultures were centrifuged for 10min at 5000 *g*, bacteria pellet was then resuspended in 2ml of resuspension solution with RNase A solution added. 2ml of lysis solution was then added and incubated for 3min in room temperature. 2ml of neutralization solution, 0.5ml

endotoxin binding reagent, followed by 3ml 96% ethanol were then added before 40min centrifugation at 4000 *g*. Supernatant was transferred to supplied columns, centrifuged for 3 min at 2000 *g*, then washed with wash solution I and II. Finally 0.35ml elution buffer was added and purified plasmid DNA was collected. Purified plasmid products were quantified with Qubit 4 fluorometer (ThermoFisher) and stored in -20˚C.

2.3. Plasmid verification

Plasmids were verified for their identity after purification with restriction enzyme cutting followed by gel electrophoresis, along with uncut plasmids.

Plasmid psd44-GqQL was cut with restriction enzymes BamHI and Nhel, pLOX-TERT-iresTK with BanHI and Nhel, pMD2.G with HindIII and Xcml, and psPAX2 with Xcml and Nhcl (restriction enzymes from New England Biolabs). Expected fragment sizes were calculated with information of total plasmid size and restriction enzyme cutting location as indicated on Addgene.

Briefly, ~80ng of plasmid DNA was incubated with corresponding restriction enzymes in their respective buffer for 1hr at 37˚C, then separated on 1% agarose gel.

Psd44-GqQL plasmid was further verified with Sanger sequencing to verify presence of A>T substitution at c.206. Primers specific for the plasmid were designed with IDT PrimerQuest Tool (Table 1) and used to prepare the PCR product, which were then sent to Genome Quebec for analysis. PCR product was prepared using the MyTaq HS Red Mix (bioline). For each reaction, 40ng of plasmid DNA was utilized, with addition of 12 µl HS Red Mix, 1 µl of 10 µM forward and reverse primer. PCR cycling conditions used were: 95˚C (1min) initial denaturation , 95˚C (15s) denaturation, 55˚C (15s) annealing, 72˚C (10s) extension, for 35 cycles.

The sequencing reaction was done using BigDye® Terminator v3.1 Cycle Sequencing RR-2500 from Applied Biosystems. Sequencing reaction cleanup was done using PureSEQ from Aline Biosciences. The sequences were read on a 3730xl DNA Analyzer from Applied Biosystems.

Table 1: Primer sequence for psd44-GqQL plasmid

	Primer sequence	Length	T_m	GC%
Forward	CACCACAGGGATCATCGAATAC (sense)	22	62	50
Reverse	AGCCTTGCTTTCCTCCATTC (antisense)	20	63	50

2.4. Lenti-virus Production

Human embryonic kidney 293 cells (HEK293T) (gifted by Dr. Livia Garzia's lab, MUHC) were grown in T75 flasks till confluent (in DMEM high glucose media, 0.1% 10U/ml penicillin and 10µg/ml streptomycin, 10% FBS, 4mM L-glutamine), then plated in 15x15cm plates till 70% confluency, after which media was changed to antibiotics-free medium. A mixture of: 54µl Xtremegene9 (sigmaaldrich), 1.5ml Opti-Mem (Thermofisher), 34µl pMD2.G, 67µl psPAX2, and 65ul psd44-GqQL or 77ul pLOX-TERT-iresTK purified plasmid DNA (calculated to be equal molar based on molecular weight) was gently mixed and incubated in room temperature for 20mins, then added dropwise to each plate of HEK293T.

After incubation overnight at 37˚C, media for transfected HEK293T cells was renewed and reduced to 10ml each plate (without antibiotics). 48hrs after, supernatant from plates was collected and passed through 0.45µm filters (Millipore, SLHP033RS). Supernatant was mixed with Lenti-X concentrator (Takarabio) in 3:1 ratio and cooled at 4˚C for 1hr to overnight. The virus mixture was then spun at 1500*g* at 4˚C for 45min before used fresh or resuspended in 1/10 volume of PBS and aliquoted for storage in -80˚C.

2.5. Transduction

300µl from frozen viral suspension was added to each 6well of NCMs, then media was topped off to a final volume of 1.5ml. 1.5µl of polybrene (8mg/ml stock) was added to each well to increase transduction efficiency. NCMs were incubated with the virus for 48hrs, followed by PBS wash twice and refreshment of media.

2.6. Verification of Transduction

Genomic DNA was isolated from the transduced cells with the QIAamp DNA Mini kit (Qiagen) following the manufacturer's instructions. Briefly, collected cell pellet was

suspended in 200µl PBS in 1.5ml Eppendorf tube. 20 µl proteinase K and 200 µl buffer AL was added, followed by 15s pulse vortexing and incubation in 56˚C for 10min. 200 µl of 100% ethanol was added before transferring to a spin column and spinning for 1min at 6000*g*. Filtrate was discarded before adding 500 µl washing buffer 1 (AW1), followed by 1min of 6000*g* spin. Similarly, 500 µl washing buffer 2 (AW2) was added, followed by 3mins of 20000*g* spin. Finally 40 µl of elution (AE) buffer was added, incubated at room temperature for 1min before spinning for 1min at 6000*g*.

GNAQ-mutant transduction was verified with digital droplet PCR (ddPCR) using the QX200 PCR platform (BioRad, Irvine, CA, USA). Custom primers, probes, and gBlocks (positive control) were designed by IDT (Integrated DNA technologies, Coralville, Iowa)(Table 2). For each ddPCR reaction, ~5ng DNA was used, with 10µl supermix, 1.8µl of 10µM forward and reverse primers, and 0.5µl 10µM probes A and T. Positive controls have 0.5µl G-block A or G-block T added in 1:1000000 concentration. Thermocycler conditions were: 95˚C 10mins, 50 X (95˚C 30sec, 56˚C 1min, 72˚C 30sec), 98˚C 10min, and 12˚C hold. The results were analyzed using the QuantaSoft software (BioRad).

Table 2: Primer, probes, and gBlock sequences for GNAQ

Forward Primer	CTTGCAGAATGGTCGATGTAG
Reverse Primer	GCGCTACTAGAAACATGATAGAG
A allele Probe (WT)	5HEX/CCT+T+T+G+GCCC
T allele Probe (Q209L mutation)	56-FAM/CCT+T+A+G+GCCC
A allele gBlock	TATGAGTATTGTTAACCTTGCAGAATGGTCGATGTAGGGGGCC AAAGGTCAGAGAGAAGAAAATGGATACACTGCTTTGAAAATGT CACCTCTATCATGTTTCTAGTAGCGCTTAGTGAATATGATCAAG TTCTCGTGGAGTCAGACAATGAGGTA
T allele gBlock	TATGAGTATTGTTAACCTTGCAGAATGGTCGATGTAGGGGGCCT AAGGTCAGAGAGAAGAAAATGGATACACTGCTTTGAAAATGTC ACCTCTATCATGTTTCTAGTAGCGCTTAGTGAATATGATCAAGT TCTCGTGGAGTCAGACAATGAGGTA

Immortalization of NCM was verified by PCR. Primers were designed with IDT PrimerQuest Tool for hTERT plasmid obtained. PCR reactions each contain ~6ng

DNA, 0.75µl 10µM forward and reverse primer, and components of the KAPA HiFi PCR Kit (KapaBiosystems): 5µl 5X buffer, 0.75µl 10µM dNTP mix, and 0.5µl polymerase. PCR conditions were: 95˚C 3mins, 35 x (98˚C 20sec, 65˚C 15sec, 72˚C 60sec), and 72˚C 1min. The amplified PCR product was separated on 1% agarose gel, ran at 120V.

	Table 3: Primer sequence for pLOX-TERT-iresTK plasmid				
		Primer sequence	Length	Tm	GC%
Primer set1	Forward	CTGCGTTTGGTGGATGATTTC	21	62	47.6
	Reverse	CTTGGCTTTCAGGATGGAGTAG	22	62	50
Primer set2	Forward	GACCAAGCACTTCCTCTACTC	21	61.6	52
	Reverse	CGTGGTCTCCGTGACATAAA	20	61.7	50
Primer set3	Forward	GGTGAACTTCCCTGTAGAAGAC	22	61.9	50
	Reverse	GGTTCTTCCAAACTTGCTGATG	22	62	45

3. Blue light exposure

3.1. Fiber-optic illuminator

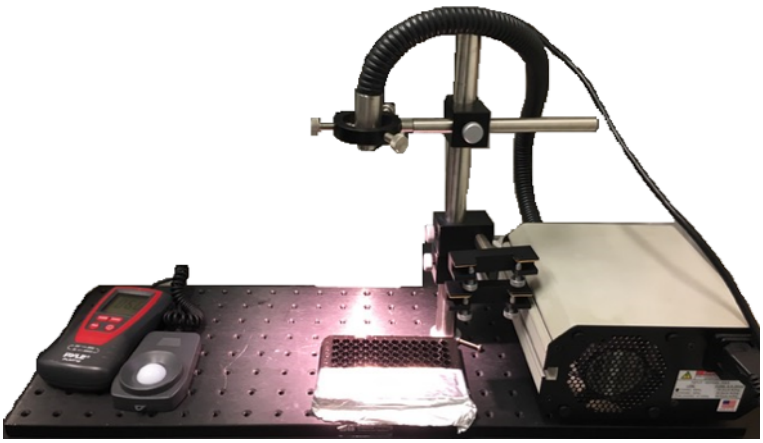

Figure 3: BL Exposure using Fiber-Optic Illuminator set-up (showing Luxmeter on the left, sample 96-well plate with foil covering control wells)

A 150-watt fiber-optic illuminator (Model: 21AC, Edmond Industrial Optics, Barrington, NJ, USA) connected to a fiber-optic light guide was used for light exposure for the first parts of the project. The light was adjusted to be at the desired

height above the surface where cell plates were placed to receive light directly below the light bulb. A radiospectrophotometer shows that although there is emission in the BL spectrum, the peak wavelength emitted is around 600nm.

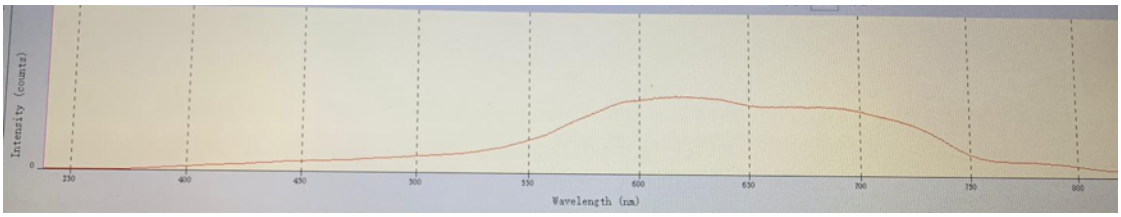

Figure 4: Wavelength range of light emitted from fiber-optic illuminator measured with radiospectrophotometer.

3.2. Solar simulator

Solar simulator (OAI, Tri-Sol Solar Simulator Model TSS-208) which projects light in the spectrum of 400nm to 1100nm, was used as a more defined source of BL. The solar simulator provides a controlled laboratory testing environment that mimics the natural sunlight.

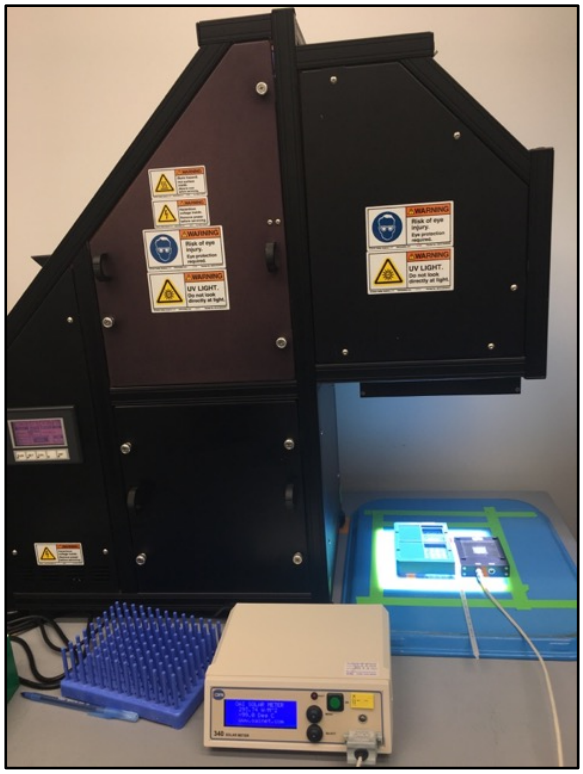

Figure 5: Experimental set up for Solar Simulator, with a 96-well plate with filter holder.

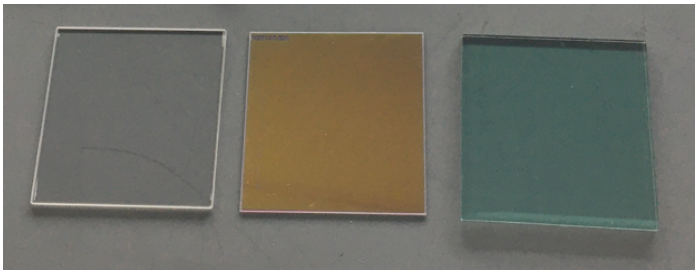

Figure 6: filter1 (left), filter2 (middle), filter3 (right) dimensions 50x50mm

Filters were ordered from OAI that would allow selected exposure of cells to BL of the range 400nm-500nm. Filter 1 (400nm steep-edge long pass filter, 400SC-01-50) blocks wavelengths below 400nm, Filter 2 (500nm short wave pass edge filter, 500FL07-50S) blocks wavelengths >500nm, and Filter 3 is an infrared (IR) filter.

Radiospectrophotometer readings with and without the filters show that the use of filters effectively produces a more restricted wavelength spectrum in the 400nm-500nm range. Cells were plated in plates and a holder is used to place the filters between the solar simulator and the cells.

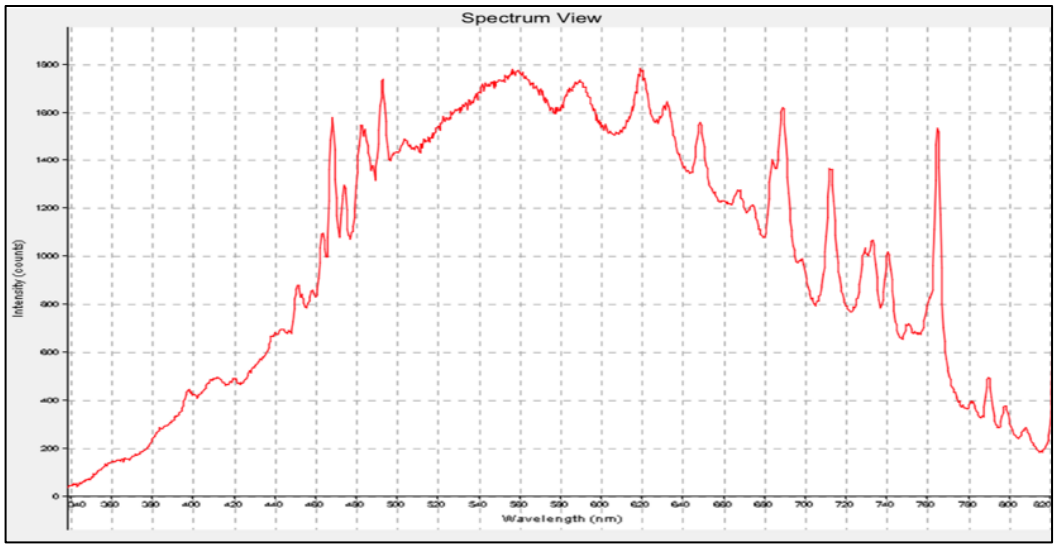

Figure 7: Radiospectrophotometer reading of solar simulator light at 0.3sun intensity without any filters.

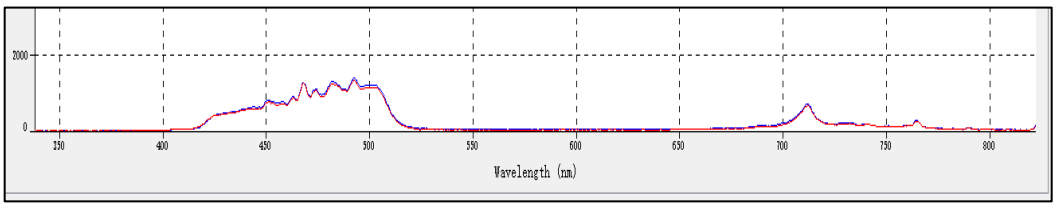

Figure 8: Radiospectrophotometer reading of solar simulator at 0.3Sun with combination of 400nm, 500nm, and IR filters.

4. Functional assays

4.1. Cell counting kit 8 (CCK8)

Cells were seeded in 96-well plates (Sigmaaldrich, CLS3603) at a density of 15000 cells/well. The light-protected control cells were covered with tin foil, and the plate was exposed to BL emitted from the fiber-optic illuminator for a range of exposure times (1hr/day, 2hrs/day, 3hrs/day repeated over 4 days). Media was changed to that not containing phenol-red prior to BL exposure.

Metabolic activity was measured after BL exposure with the Cell Counting Kit 8 (CCK8) assay (Dojindo), and was seen as an indirect indication of proliferation rate of the cells. 10µl of CCK8 reagent was added to each 96-well and incubated at 37˚C for 1hr. Absorbance results were read after with microplate reader (Tecan).

4.2. Incucyte

Incucyte (Essen BioScience) is an instrument that allows automatic real-time image-taking within a tissue culture incubator, with quantitative analysis. It can be used with a variety of function cell assays such as proliferation and migration assays, as well as assays with a fluorescent end-point reading.

For proliferation assay in Incucyte, cells were seeded in 96-well plates (Nunc, 167314) at density of 15000 cells/well. Cells were exposed to BL from the solar simulator. A filter-holder was designed that fits over the plates, and where the 3 filters in Figure 6 could be layered between the light source and cells. Starting from Day1 of BL exposure, cells were incubated in IncuCyte. Phase contrast images were scheduled to be taken every six hours using the 10x objective lens, 5 images taken per well. Cell confluency was analyzed using IncuCyte.

4.3. Scratch wound healing assay

Migration was assessed using the scratch wound healing assay[69]. Cells were seeded in 96-well plates and allowed to grow to 100% confluency in a monolayer of cells. Cells were starved 4hrs in serum-free media before a 200µL pipette tip was used to create a vertical scratch across the center of the well. After scratching, the wells were washed twice with PBS (Corning) to remove detached cells and replenished with fresh media with 1% serum. Pictures of cells at hour 0 and every 6 hours after were taken with Incucyte for 24hrs at 4x magnification under phase contrast. The measurement of the migration area was analyzed with ImageJ software (National Institute of Health). The migration rate was calculated by: % wound healing = (wound area at 0 h – wound area at 24 h / wound area at 0 h) × 100.

4.4. EthD-1 Assay

Cells were seeded in 96-well plate and exposed to BL for 3days/day over 4 days, then cell death was assessed using ethidium homodimer-1 (EthD-1) reagent from the LIVE/DEAD® Viability/Cytotoxicity Kit (Thermofisher), according to manufacturer's instructions. Briefly, 20µL of supplied 2mM EthD-1 stock solution (Component B) was added to 10ml of DPBS, to give a 4µM EthD-1 working solution. 100µl of EthD-1 working solution was added to each of 96wells and incubated in

room temperature for 40min. Cells permeated with 70% ethanol for 30min were used as positive control. EthD-1 positivity was then visualized and analyzed using Incucyte with its red fluorescence detection channel.

4.5. Terminal deoxynucleotidyl transferase dUTP nick end labeling (TUNEL) Assay

Cells were seeded in 96-well plate and exposed to BL for 3days/day over 4 days, TUNEL-positive cells were then measured using the *In Situ* Cell Death Detection Kit, Fluorescein (Roche). The kit detects and quantifies apoptosis at the single-cell level, based on labeling of DNA strand breaks (TUNEL technology); analysis by fluorescence microscopy or flow cytometry. Briefly, cells were fixed in 4% paraformaldehyde, then permeabilized in 0.1% Triton-X-100 in 0.1% sodium citrate. TUNEL reaction mixture is prepared according to kit manual and incubated in dark with cells for 60 mins at 37˚C.

TUNEL signals were visualized and analyzed using Incucyte in the detection range of 515-565nm (green).

4.6. Reactive Oxidative Species (ROS) Assay

Cells were seeded in 96-well plate and exposed to BL for 3days/day over 4 days, then level of ROS was measured with MitoSOX™ Red Mitochondrial Superoxide Indicator (Thermofisher). Briefly, 5mM MitoSOX reagent stock solution was made according to manufacturing instructions, and diluted in HBSS/Ca/Mg buffer to 5μM working solution. 100μl of working solution was added to each 96well and incubated with cells for 10mins at 37˚C in dark. Fluorescent signal was visualized and analyzed using Incucyte with the red detection channel.

4.7. Soft Agar Assay

A two-layer soft agar assay was used to test ability of cells to grow anchorage independently[70]. A bottom layer consisted of 0.8% agarose which did not contain cells. The upper layer of 0.35% agarose contained cells in concentration of 5000 cells/ml in each well of a 6well plate. 1ml of feeding media was then added on top of the upper agarose layer and refreshed every other day. Cells were kept in agar for up to 60 days. UM cell lines (92.1 and MP46) were used as positive controls.

Experiments were done in at least duplicates. Colonies were monitored and imaged using the EVOS imaging system.

4.8. Cell-free DNA (cfDNA) Assay

Cells were plated in 48well plates at density of 4 x 10^4 per well and exposed to BL from the solar simulator at 0.3sun intensity for 3hrs/day over 4 days. Circulating DNA (cfDNA) was isolated from supernatant using QIAamp Circulating Nucleic Acid kit (Qiagen) following the urine protocol. Briefly, 1ml of supernatant was collected from cells and centrifuged at 1000rpm for 5mins. Carrier RNA was prepared in Buffer ACL according to manual and number of samples. 125µl of proteinase K, 1ml of supernatant sample, 1ml of carrier RNA in ACL, 250 µl Buffer ATL were added to a 15ml tube. The mixture was vortexed and incubated in 60˚C water bath for 30mins. 3.6ml of Buffer ACB was added, pulse-vortexed and incubated on ice for 5mins. Samples were loaded to the QIAvac 24 Plus vacuum system, connected to QIAamp Mini columns. 600µl Buffer ACW1, 750µl Buffer ACW2, then 750 µl 100% ethanol were sequentially loaded and drawn through the columns. The columns were placed in collection tubes and spun at 20000*g* for 3 min, then dried on 56˚C heating block for 10min. Finally, 20µl of Buffer AVE was added to center of the column and spun at 20000 *g* for 1min, collected in a new 1.5ml Eppendorf tube.

Isolated cfDNA was then quantified with Qubit 2.0 (Thermofisher Scientific). Briefly, working solution was prepared by diluting Qubit reagent in 1:200 ratio with Qubit buffer. Each assay tube contains 1µl of cfDNA sample and 199µl working solution and then was read for DNA concentration.

ddPCR was performed to quantify copy numbers of both WT and mutant *GNAQ* in BL-exposed and non-exposed cells. Each ddPCR reaction had 5ng of cfDNA. Using primers, probes, and gBlocks designed by IDT (Table 2), using same ddPCR conditions as described in *GNAQ* transduction verification methodology, then analyzed using QuantaSoft.

5. Western Blot Analysis

Cells were trypsinized and washed with PBS twice (centrifuged at 1500rpm 5mins). 10-50µl of RIPA buffer is added according to cell numbers. RIPA buffer is made with 150nM sodium chloride, 1% TrionX-100, 0.1% SDS, 0.5% Sodium

Deoxycholate, and 50nM Tris at pH7.4, supplemented with Complete™ mini protease inhibitor (Sigma). Cells were lysed in RIPA buffer at 4˚C for 30mins before pulse sonicated and centrifuged at 13000*g* for 10mins.

20µg of protein extracted from cells were loaded to 12% precast polyacrylamide gel, then transferred to polyvinylidene fluoride (PVDF) membrane (BioRad). Membranes were blocked in 5% blocking buffer or milk for 1 hour. B-actin (1:10000) (A2228-200ul, Sigma) was included as a loading control. Blots were developed using ECL prime western blot detection (GE healthcare) and visualized using the ChemiDoc™ XRS+ System.

Table 4: Antibodies and concentrations for western

Antibody	**Company**	**Catalog number**	**Concentration**
GNAQ	Santa Cruz	136181	1:500
MAPK (ERK1/2)	Cell Signaling	4695	1:1000
p-MAPK (ERK1/2)	Cell Signaling	4370	1:1000
AKT	Cell Signaling	9272	1:1000
p-AKT (Thr308)	Cell Signaling	4056	1:1000
Active YAP	Abcam	205270	1:1000
β-actin	Sigma	A2228	1:10000

6. Proteomics

Cell lysate samples were prepared in identical manner as for western blotting.

Proteomic samples were assessed in the Clinical Proteomics Platform of RI-MUHC by bottom-up mass spectrometry (OrbiTrap) in duplicate protein samples per condition. Peptides were analyzed using a Thermo Orbitrap Fusion mass spectrometer operating at 120,000 resolution (FWHM in MS1) with linear ion trap CID sequencing at top speed for all peptides with a charge of 2+ or greater. The raw data was then converted into *.mgf format (Mascot generic format) for searching using the Mascot 2.5.1 search engine (Matrix Science) against mouse protein sequences (Uniprot 2018) The database search results was then loaded onto Scaffold Q+ Scaffold_4.4.8 (Proteome Sciences) for statistical analysis and data visualization. Filters were applied to data within Scaffold, including protein threshold greater than 99.0%, and peptide threshold greater than 95.0%. Analysis was

performed using t-test to identify proteins differentially expressed between to condition groups (ie. Mutant vs. WT). The identified up-regulated/down-regulated protein lists in Scaffold were exported to Microsoft Excel and uploaded into the DAVID Bioinformatics database (Database for Annotation, Visualization and Integrated Discovery version 6.8) or Reactome.org for functional annotation.

7. Statistical Analysis

Statistical analysis was performed using Graphpad Prism software (GraphPad Inc, San Diego, CA, USA). Significance was determined using student's t- tests, with p-values <0.05 being considered significant. Where multiple student's t-tests were used, the Holm-Sidak method was used to correct for multiple comparisons. Unless otherwise specified, results and error bars are representative of experimental triplicates.

Results Chapter 1: Establishment of model system to study initiating mutations in uveal melanoma

Introduction and rationale:

Melanomas arise from malignant transformation of normal melanocytes, most commonly in skin melanocytes found in the deep layer of the epidermis between the layer of basal cells. After cutaneous melanoma, uveal melanoma (UM) is the most common type of melanoma, and stems from transformation of melanocytes in the uveal tract, most commonly in the choroid. While UV plays a role in the development of cutaneous melanoma, the role of visible light exposure remains under debate in UM[4].

The pathogenesis of UM is characterized by early mutations in genes encoding G-protein coupled receptors, specifically *GNAQ* and *GNA11*. These mutations are thought to be the first step towards malignant transformation of uveal melanocytes, acting as oncogenes[5]. Analogous to the *BRAF* mutation in cutaneous melanoma, mutations in *GNAQ/11*, and less commonly *PLCB4* and *CYSLTR2*, are found in almost all UM patients. *GNAQ/11* mutations are the most common initiating events in UM[36], and are known to play an essential role in the development of these tumors. In fact, >80% of clinical cases of UM have been shown to harbor one of these two mutations[10]. Interestingly, mutations in these oncogenes have also been found in benign nevi of the choroid[10].

UM can develop *de novo*, but less commonly also could develop from pre-existing choroidal nevi. Choroidal nevi have a much higher prevalence rate than UM, ranging from 4.6% to 7.9% reported in the US[16]. Since they are less observable than cutaneous nevi, and are generally asymptomatic, they are often only found during ophthalmic exams for other reasons and the true incidence rate is likely higher. Moreover, while skin biopsies are straightforward procedures, intraocular biopsies are invasive and can incur rare but serious complications. Since nevi generally remain stable over time[71], choroidal nevi are not usually biopsied and are instead clinically followed for signs of growth or malignant transformation[17]. Several factors have been described to be predictive of malignant transformations, including tumor thickness greater than 2 mm, subretinal fluid, symptoms, orange pigment, tumor

margin within 3 mm of the optic disc, ultrasonographic hollowness, and halo absence[17].

Further understanding of the etiology of UM is needed in order to develop new treatment or preventative approaches to this disease. It is important to assess the role of intrinsic genomic factors (e.g. initiating mutations) as well as extrinsic factors (e.g. environmental exposures) that may lead to tumor development in the eye. While several UM cell lines exist to study the disease *in vitro*, pre-malignancy models are lacking to study the development of UM. Here we sought to develop an *in vitro* system of normal and oncogene (*GNAQ*)-mutated choroidal melanocytes that could be used to study the etiology of UM.

Results:

Viable cultures of choroidal melanocytes were established from donor eyes and verified for melanocyte-specific markers

We sought to understand the oncogenic role of initiating UM mutations in melanocytes in the uveal tract. Since the most common mutations occur in *GNAQ* or *GNA11* at hotspot c.626, we aimed to engineer normal choroidal melanocytes (NCMs) to express mutant GNAQ. However, while normal skin melanocyte cell lines can be purchased, no commercially available melanocyte cell line from the uveal tract exists. To address this need, we first aimed to establish a NCM cell line from donor eyes obtained through the Centre Universitaire d'Ophtalmologie eye bank.

Using eyes from 17 donors, we extracted melanocytes from the choroid layer of the posterior part of the eye. Donor characteristics can be found in Table 5. To do so, we adapted a protocol previously described[65] (Figure 9).

Table 5: Characteristics of donors and corresponding NCM culture

Code	#dossier	Date of death (dd/mm/yyyy)	Sampling Date	Cause of Death	Culture Outcome
2G-PPecF1968Y	201793	03/06/2019	04/06/2019	Hepatocellular carcinoma	Successful
2G-PPddF1983X	201735	02/06/2019	04/06/2019	Neo of pancreas	Contaminated
2G-PPiF1971X	202734	23/06/2019	25/06/2019	Cancer	Unsuccessful

2G-PpiF1970X	202727	23/6/2019	25/06/2019	Neo of metastatic endometrium	Unsuccessful
2G-PPjF1976Y	202706	22/06/2019	24/06/2019	Neo of colon with metastasis	Unsuccessful
2G-PPxG1981Y	203189	08/07/2019	09/07/2019	Severe cervical myelopathy	Successful
2G-PPjD1982X	199746	22/04/2019	23/04/2019	Abdominal hemorrhage	Contaminated
2G-PprE1972X	200834	14/05/2019	14/05/2019	Pulmonary Adenoma	Successful
2G-PPsH1982Y	204908	13/08/2019	14/08/2019	Probable Myocardial Infarction	Unsuccessful
2G-PpoH1972Y	205043	17/08/2019	19/08/2019	Neo of the stomach	Unsuccessful
2G-PpoH1977X	205043	17/08/2019	19/08/2019	Rectal cancer	Unsuccessful
2G-PeeF1984Y	N/A	N/A	N/A	N/A	Did not survive transduction
2G-PPpD1968Y	199530	16/04/2019	18/04/2019	Pulmonary Neo	Successful
2G-PPnC1984X	N/A	18/03/2019	20/03/2019	Infarction/ pulmonary embolism	Unsuccessful
2G-PPwC1963Y	N/A	09/03/2019	N/A	Infection, sécrétions vertes, pneumonie non tx.	Successful
2G-PPuB1961Y	N/A	11/02/2019	N/A	Respiratory insufficiency	Unsuccessful
2G-PPaE1974X	N/A	N/A	N/A		Viable but poor growth

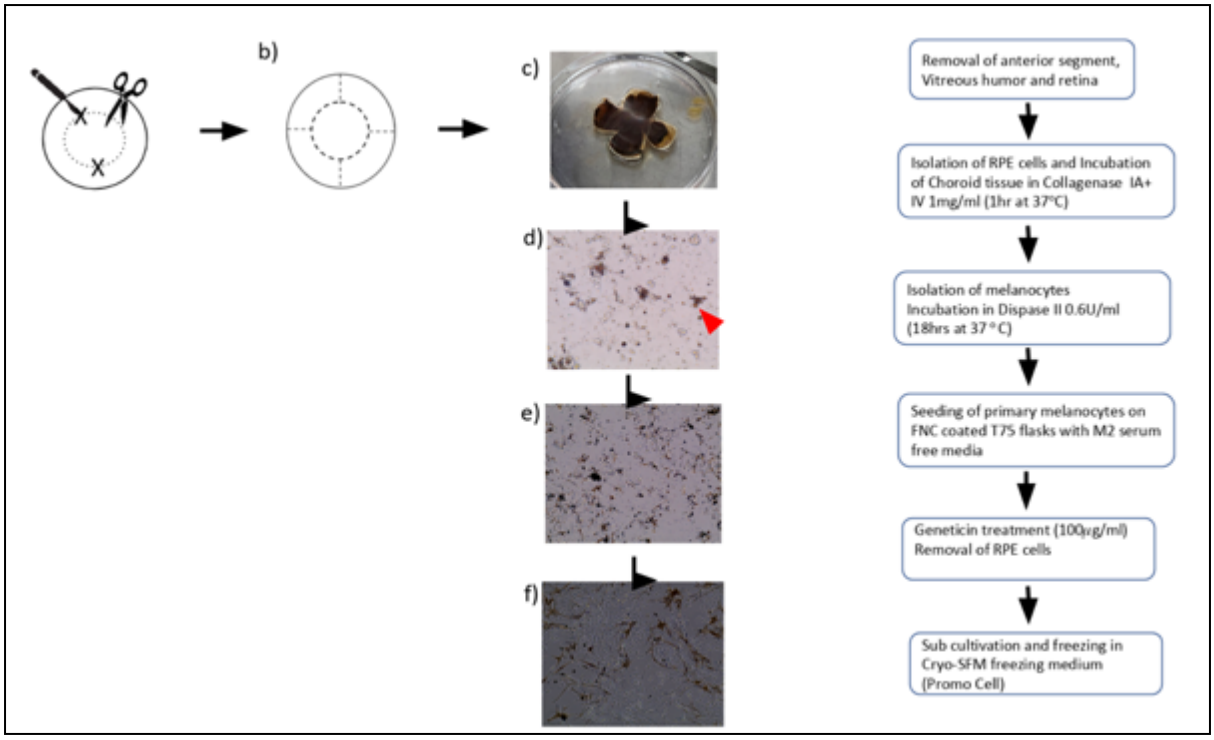

Figure 9: Schematic of NCM culture protocol. Donor eyes were cut (b) and anterior segment, vitreous humor, retina were removed (c). Isolated melanocytes were seeded (d) followed by geneticin treatment (e) and sub-cultivation (f). (schematic made by Thupten Tsering M.Sc.)

As shown in Figure 10, morphological characteristics were monitored during culture to confirm cellular viability. Initially, the NCM culture grew alongside retinal epithelial cells and fibroblasts. To ensure purity of the NCM culture, geneticin treatment (100µg/ml) was used to suppress growth of these other cell populations[72]. At earlier passages of NCM culture (Figure 10C), cells within close vicinity grew in colonies, and the majority of cells did not express much melanin and appeared clear in color. It was observed that with further passages, more pigmentation can be visualized in the NCM culture (Figure 10E). It is unclear what increased pigmentation signifies for our cell culture biologically, but it could be correlated to slowed proliferation as reported by another group, who observed more diluted pigmentation in more proliferative cells[73].

Over all, we established successful NCM cultures from 6 of the 17 donor eyes (35.3%), with the unsuccessful culture attempts resulting from either poor growth, no cell attachment, or contamination of culture as summarized in Table 5.

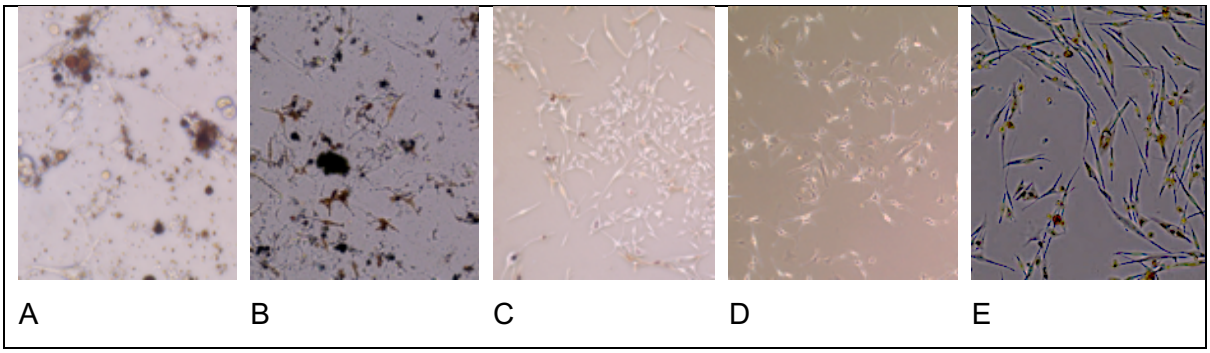

Figure 10: Progression of NCM morphology through culture time and passage. (A) 2 days in culture. (B) 5 days in culture, following treatment of geneticin (C) NCM culture at passage 2. (D) NCM culture at passage 5. (E) NCM culture at passage 6 and after prolonged culture time. Phase contrast image, 10X magnification.

Immunofluorescence staining was performed to ensure presence of a homogeneous, melanocyte population. Various melanocyte markers were chosen to be tested. Vimentin, an intermediate filament expressed by mesenchymal and neuroectodermal cells and that is used as a marker for melanoma[74], was positive in the NCM cultures (Figure 11). Similarly, expression of Melan-A was seen, a protein with unclear function related with melanocyte-specific expression[75]. Other markers expressed included S100, a calcium-binding protein expressed by neuroectodermal cells[76], and human melanoma black (HMB45) which has also been considered a marker for melanoma and certain nevi[77]. Expression of these four markers confirms our NCM cultures as melanocytes.

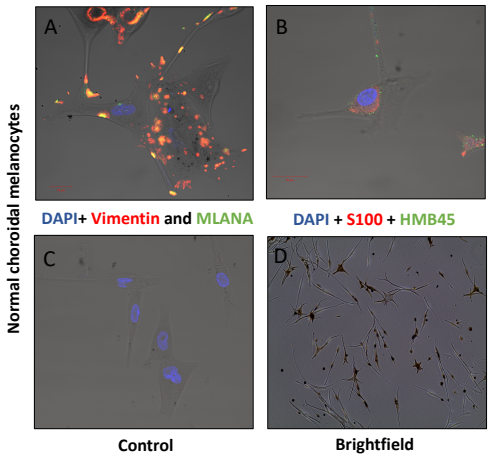

Figure 11: Immunofluorescence staining of NCM at passage 2 for melanocytic markers. (A) anti-MLANA (green), Vimentin (red), DAPI (blue). (B) S100 (red), HMB45 (green) Magnification 40X. (C) Negative control. (D) phase contrast image at magnification 20X. Scale bar of 20µm.

MLANA: Melan-A. HMB45: human melanoma black. DAPI is used to stain the nuclei. (Figure by Thupten Tsering M.Sc. as part of manuscript submitted)

Growths of NCM cultures match rates previously reported

Amongst the hallmarks of cancer cells are uncontrolled proliferation and escape from senescence. Primary cells on the other hand, are limited by a number of replications before senescence and eventually lose capability to further proliferate. Previous studies working with primary melanocytes have reported proliferation rates of their cultures[65, 78], and we sought to check the proliferation of our NCM cultures in comparison to those reported levels.

Our NCM cultures were observed to proliferate readily when freshly cultured from donor eyes, with an estimated doubling time of 3-5 days (data not shown).

A proliferation assay done after thawing of NCMs from cryopreservation however showed a markedly slower proliferation. Doubling time for our NCM culture was estimated from proliferation rate of four replicate wells of NCM culture, with confluency measured using the Incucyte Live Cell Imaging system over 48hrs (Figure 12). The calculated doubling time for the selected culture of NCM gives an estimation of 30 days, which is extensively longer than the 84-96hrs doubling time reported by other groups[65, 78]. However it was also described in literature that cryopreservation was found to extend doubling times of NCMs by up to 10 folds[78]. Since NCMs used in our proliferation assay had already undergone cryopreservation, this may explain the discrepancy of proliferation rates from other groups.

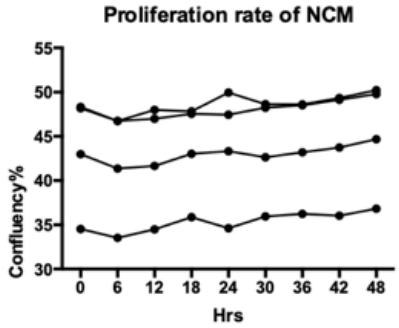

Average %confluency increased in 48hrs	Average Growth Rate per 48hrs	Projected doubling time
1.87%	4.47%	30days

Figure 12: Proliferation rate assessed in NCM cultures using Incucyte over 48 hours. Average % confluency increased= Final %confluency at end of 48hr culture - Starting %confluency. Average growth rate = Average %confluency increased / Starting %confluency. Projected doubling time

was estimated using the principles from the Rule of 70[79], designed to estimated doubling time of exponential growth.

Cultured NCMs were engineered to express mutant GNAQ via lentiviral transduction

To create a system to study UM development, we aimed to engineer NCMs that express one of the initiating mutations responsible for UM development. To do so, we created *GNAQ*-mutant NCMs (NCM^{mGNAQ}) with an A>T base substitution at codon 626, resulting in Q to L amino acid transformation at position 209. As shown in Figure 13, a psd44-GqQL plasmid from Addgene containing our mutant gene of interest was used.

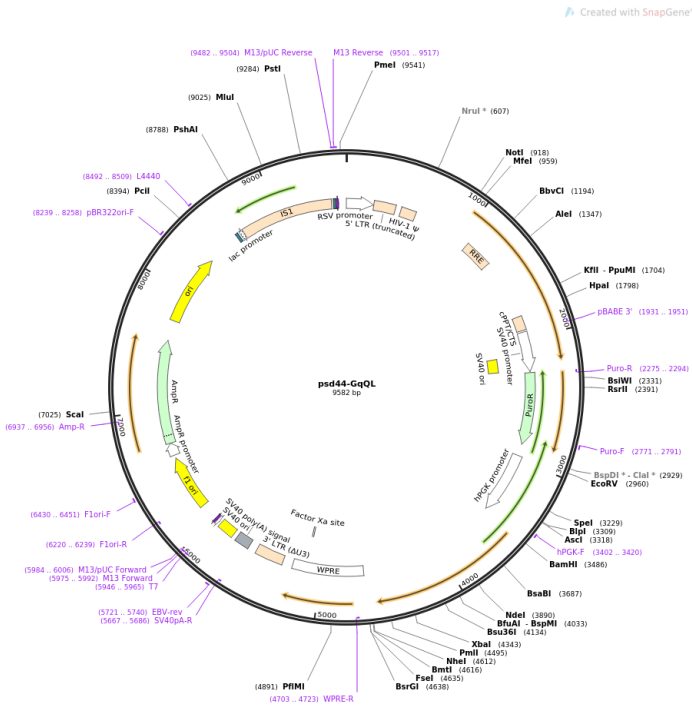

Figure 13: Schematic of the GNAQ-mutant Plasmid: (sequenced by AddGene). The psd44-GqQL plasmid from AddGene contains our mutant gene of interest - human *GNAQ*^{Q209L}. The other elements of interest contained in the plasmid are ampicillin resistance gene for selection of plasmid-containing bacteria colonies, and puromycin resistance gene for post-transduction selection.

Obtained plasmids were verified with restriction enzyme digestion and showed bands at expected fragment sizes (Figure 14). The gene-of-interest plasmid of psd44 was digested at 5' and 3' ends respectively with restriction enzymes BamHI

and NheI, and gel electrophoresis results post-restriction enzyme digestion resulted in two bands both at roughly the expected band sizes (3211bp and 10121bp). In comparison, the uncut plasmid showed only one band at a higher molecular weight. This served as a rough confirmation of the identity of our gene-of-interest plasmid, demonstrating it has the right total plasmid size as well as inserted gene (*GNAQ*^{Q209L}) size.

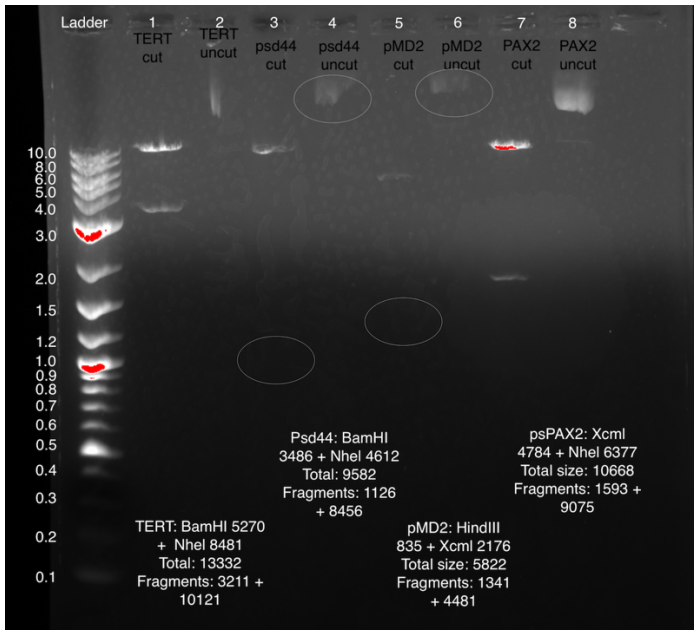

Figure 14: Plasmids after restriction enzyme digestion separated on gel. DNA Ladder in kb. Lanes (1,2) TERT plasmid cut and uncut. (3,4) GNAQ-mutant plasmid cut and uncut. (5,6) envelope plasmid cut and uncut. (7,8) packaging plasmid cut and uncut.

Although gel electrophoresis verified grossly the size and identity of the psd44 plasmid, due to the single base mutation profile of our gene-of-interest *GNAQ*^{Q209L}, we conducted Sanger sequencing to verify the exact mutation. Sanger sequencing verified that *GNAQ*-mutant plasmid contained the expected A>T substitution mutation at position 626.

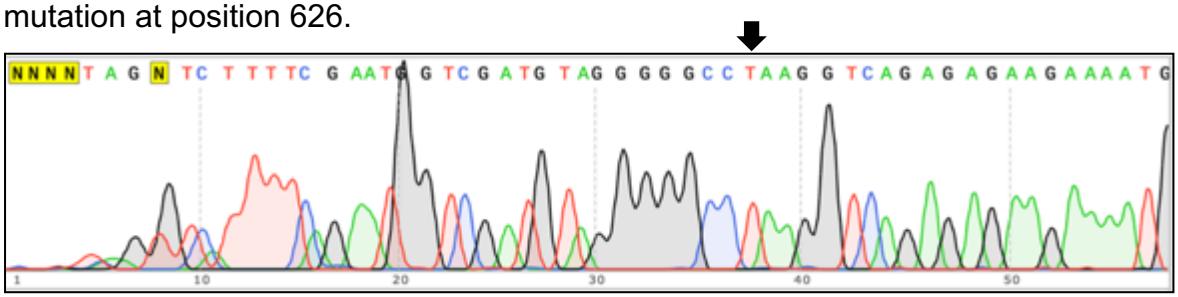

Figure 15: Sanger sequencing result of bases surrounding the mutation site of *GNAQ*-mutant plasmid psd44. Arrow specifies the location of A>T mutated base.

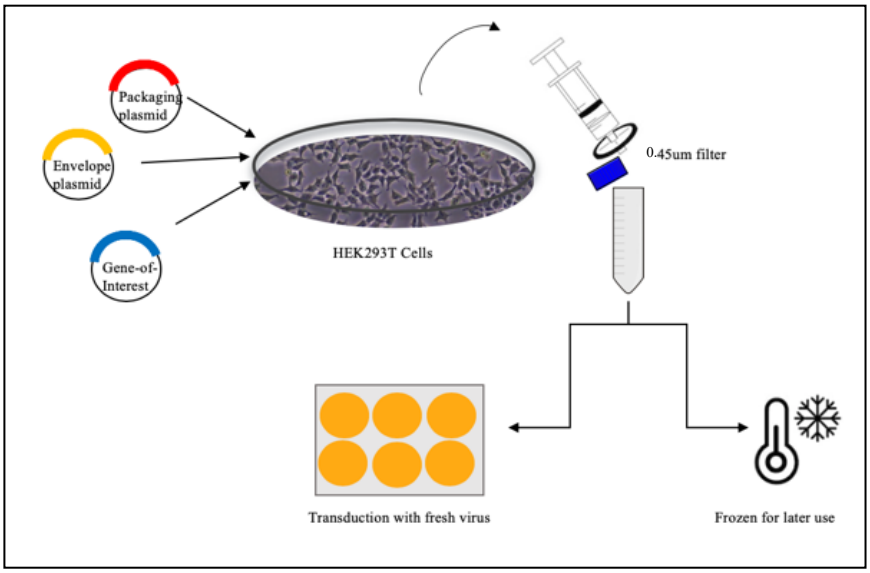

Figure 16: Schematic for viral transduction: Equal molar ratios of packaging, envelope, and gene-of-interest plasmids were added to 15cm^2 plates of HEK293T cells. Supernatant of HEK293T was collected after 48hrs of incubation and passed through 0.45µm filters. After a cooling step in Lenti-X concentrator and centrifugation at 1500*g*, virus can either be added to cells of interest directly or resuspended in PBS for storage in -80˚C.

Puromycin is an antibiotic that exerts toxicity by acting as a protein synthesis inhibitor. Plasmids used in lentiviral transduction often contain a puromycin resistance cassette that allows the use of puromycin-containing media to select for survival of successfully transduced cells[80]. In order to establish a more homogenous population of NCM^{mGNAQ} cells, we included a puromycin selection step in our transduction protocol. Toxicity testing of varying doses of puromycin on non-transduced NCM demonstrated a high sensitivity of NCMs to puromycin toxicity. As shown in Table 6, non-transduced NCMs could withstand a puromycin concentration of 0.05µg/ml for 6 days, but higher dosages resulted in cell toxicity as seen by a rounding morphology.

NCMs successfully transduced with *GNAQ*^{Q209L}-containing plasmid should gain a resistance to puromycin. However, through our repeated attempts at culturing NCM^{mGNAQ} cells in various concentrations of puromycin (1µg/ml, 0.5µg/ml, 0.1µg/ml), although toxicity was not seen past 6 days of exposure, we were not able to maintain the cells in culture for prolonged periods (>2weeks) (Figure 17C). In order to maintain a viable post-transduction culture of NCMs long enough for further

experiments, the protocol was adapted to exclude the puromycin-selection step and instead cells were transduced, verified with ddPCR, and immediately used for experiments.

Table 6: Puromycin toxicity on NCM at various dosages

24hr exposure					
0µg/ml	1µg/ml	2µg/ml	3µg/ml	4µg/ml	5µg/ml
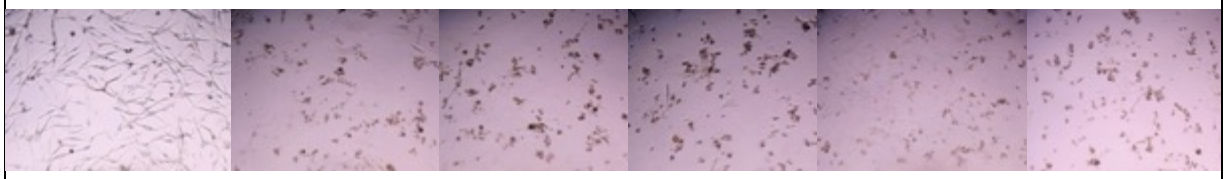					
6 day exposure					
0.05 µg/ml	0.1µg/ml	0.2µg/ml	0.3µg/ml	0.4µg/ml	0.5µg/ml
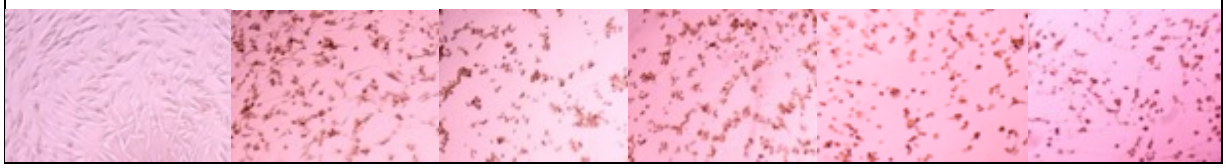					

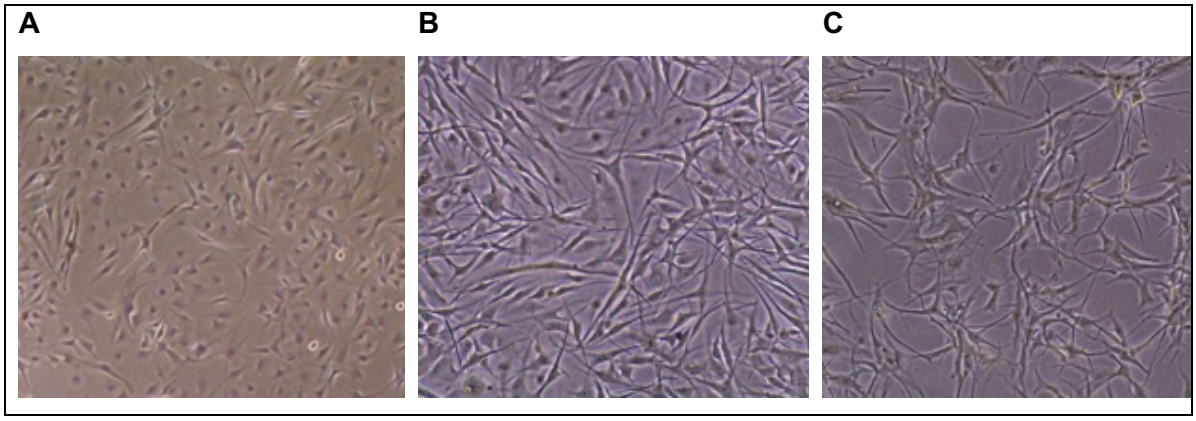

Figure 17: Morphology of NCMs pre- and post-transduction of GNAQ. (A) NCM prior to transduction. (B) Day 4 post-transduction. (C) Post-puromycin selection.

Since we have excluded the puromycin-selection step from our transduction protocol, we could not ensure that our NCM^{mGNAQ} population was homogenously mutant, as transduction efficiency is not 100% and not all NCMs would have incorporated the $GNAQ^{Q209L}$ gene. Thus we aimed to optimize our transduction protocol to have a higher transduction efficiency and hence result in a more representative population of NCM^{mGNAQ} cells.

Figure 18A shows ddPCR results following an early transduction attempt using frozen vials of lentivirus. As seen, the copies of *GNAQ*-mutant-positive droplets (blue) were far fewer than GNAQ-WT-positive droplets (green). This indicates that the NCM^{mGNAQ} population seen here contains extensively more NCM^{WT} than NCM^{mGNAQ} cells.

Lentivirus is known to be sensitive to freeze-thaw cycles[81], thus to increase transduction efficiency, instead of using stored frozen virus, virus was freshly made prior to transduction and used immediately. Polybrene is a cationic polymer that helps to enhance transport and binding of virus to target cell membrane[82]. Polybrene toxicity was tested on NCMs at concentrations of 8μg/ml and 4μg/ml, and results showed that no visible toxicity was seen after 2 days of exposure. Both polybrene concentrations were tested in the following transductions.

ddPCR (Figure 18B) showed that with polybrene addition to media and usage of fresh virus, transduction efficiency improved, as there was an increase in the ratio of *GNAQ*-mutant-positive droplets (blue) to GNAQ-WT-positive droplets (green).

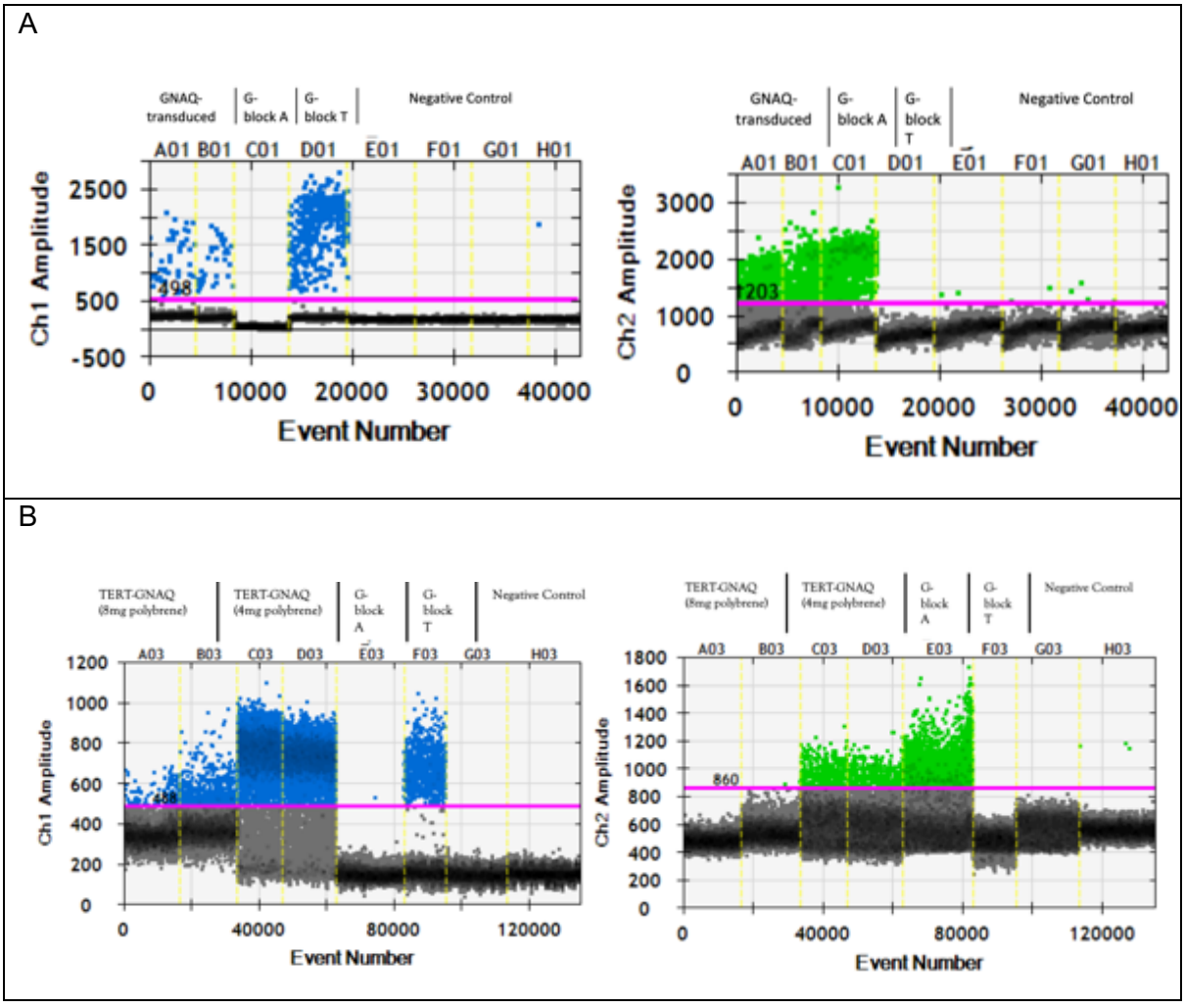

Figure 18: ddPCR of mutant and WT *GNAQ* copies in NCMs post-transduction. (A) Transduction without addition of polybrene. (B) Transduction with addition of 4µg/ml or 8µg/ml polybrene. Green: $GNAQ^{WT}$ droplets. Blue: $GNAQ^{Q209L}$ droplets. TERT-GNAQ: immortalized NCM^{mGNAQ} cells. GNAQ-transduced: NCM^{mGNAQ} cells. G-block A/T: positive control for $GNAQ^{WT}$ and $GNAQ^{Q209}$ respectively.

The *TERT* gene was used to generate immortalized NCM^{mGNAQ} cells

Primary cells such as NCMs are limited by a certain number of replication cycles before reaching senescence. To establish a NCM culture that could be maintained for prolonged periods, we sought to surpass that replication limitation by immortalizing cells by expressing exogenous *TERT*. *TERT* codes for telomerase which functions to extend the telomere tail of cells that otherwise would get progressively shorter through each replication cycle, until senescence is eventually reached[83].

We used a pLOX plasmid (Addgene) containing the human TERT gene (Figure 19) to be expressed in NCM cells. After verification of the plasmid by restriction enzyme digestion (Figure 14), lentivirus containing the plasmid were produced and used fresh for transduction of NCMs.

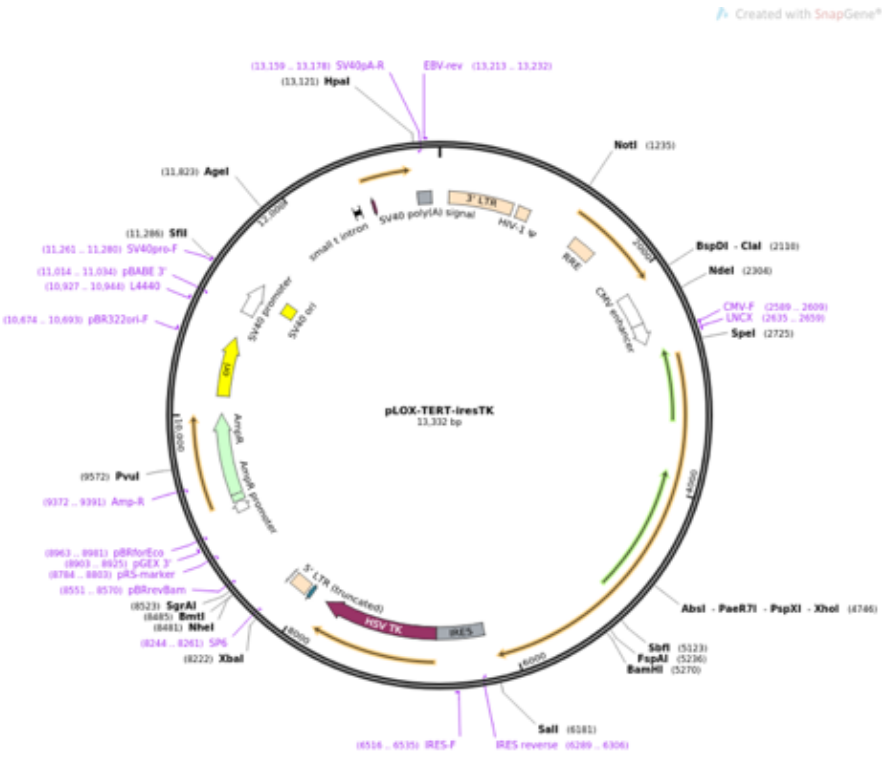

Figure 19: Diagram of *hTERT*-containing plasmid (sequenced by AddGene). The pLOX-TERT-iresTK plasmid from AddGene contains inserted gene of *hTERT*. The plasmid contains ampicillin

resistance gene for selection of plasmid-containing bacteria colonies, but does not contain a resistance gene for post-transduction selection.

Unlike the *GNAQ*^{Q209L} plasmid, the *hTERT* plasmid did not contain a post-transduction selection gene such as puromycin resistance. Hence after two days of incubation with *hTERT*-containing virus, hTERT-NCM were grown directly in non-selective medium, and sub-cultivated when ~70% confluency is reached.

As shown in Figure 20, the morphology of *hTERT*-NCM was unchanged post-immortalization and sub-cultivation. Compared to NCM culture prior to immortalization, there seem to be a reduction in pigmentation in the culture. The immortalized cells were in good health and remain proliferative in culture.

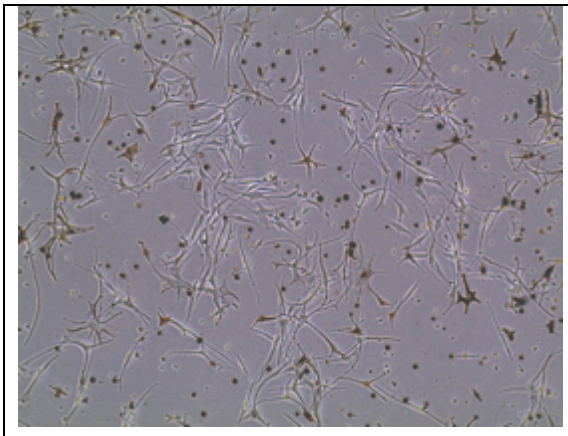

A NCM pre-immortalization

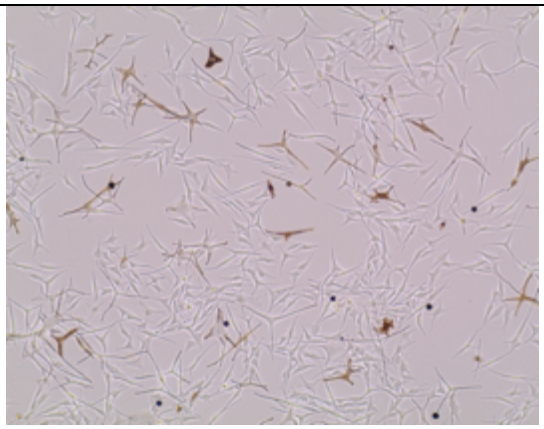

B NCM post-immortalization (P1)

Figure 20: Morphology of NCMs pre- (A) and post-(B) immortalization. P1: Passage 1, one sub-cultivation after transduction. 10X magnification.

Immortalization of NCMs was verified by PCR and gel electrophoresis, with designed primer specific for the TERT sequence contained in the transduction plasmid (Figure 21) . The same sample was used for three different primer sets (Table 3). In all three primer sets, a visible band was seen for *TERT*-transduced NCMs (faint for primer set 2 due to sample loss during loading). No band was seen for non-transduced NCMs or the negative control. Although not informative quantitatively of the proportion of cells immortalized, it was confirmed that at least some cells have been immortalized in our sample.

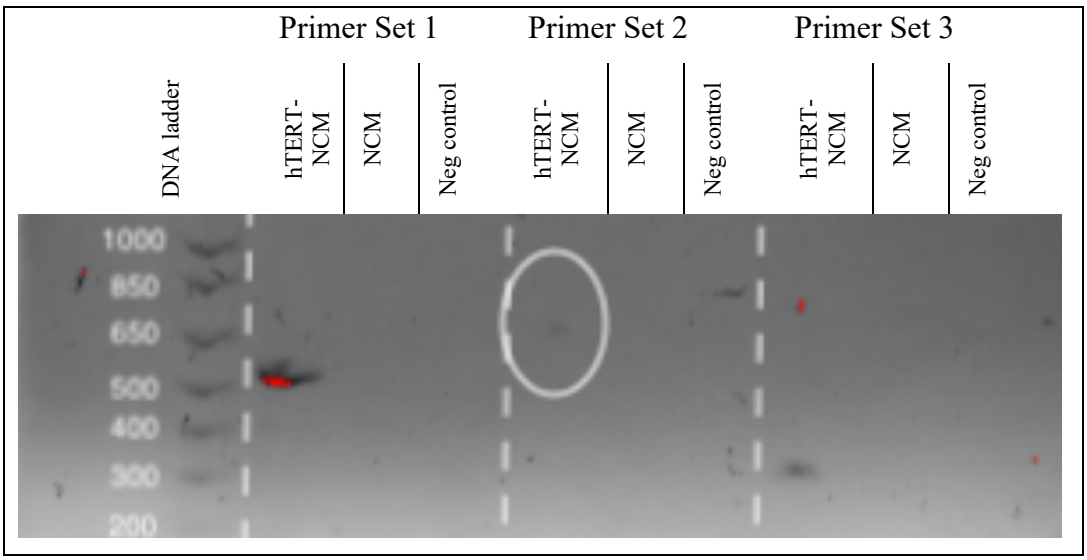

Figure 21: Verification of *TERT* transduction by PCR followed by electrophoresis. Lanes from left to right: DNA ladder; TERT-transduced NCM; Non-transduced NCM, Negative control (repeated for 3 different sets of primers)

Murine melanocyte cell line expressing mutant and wildtype GNAQ was used as a comparative system

In order to test our data in a second system of *GNAQ*-mutant melanocytes, we utilized a previously established murine melanocyte model. Melan-A cells harbouring mutant or wildtype *GNAQ* were gifted to us by Dr. Boris Bastien (University of San Francisco)[10]. The expressed mutation was confirmed by ddPCR, showing that the GNAQ-mutant cells expressed both WT and mutant GNAQ copies, GNAQ-WT cells did not express any mutant copies (Figure 22). Although the human NCM system would be a more suitable model to study the disease, the murine model has the advantage of having a much shorter doubling time and are used to complement some experiments.

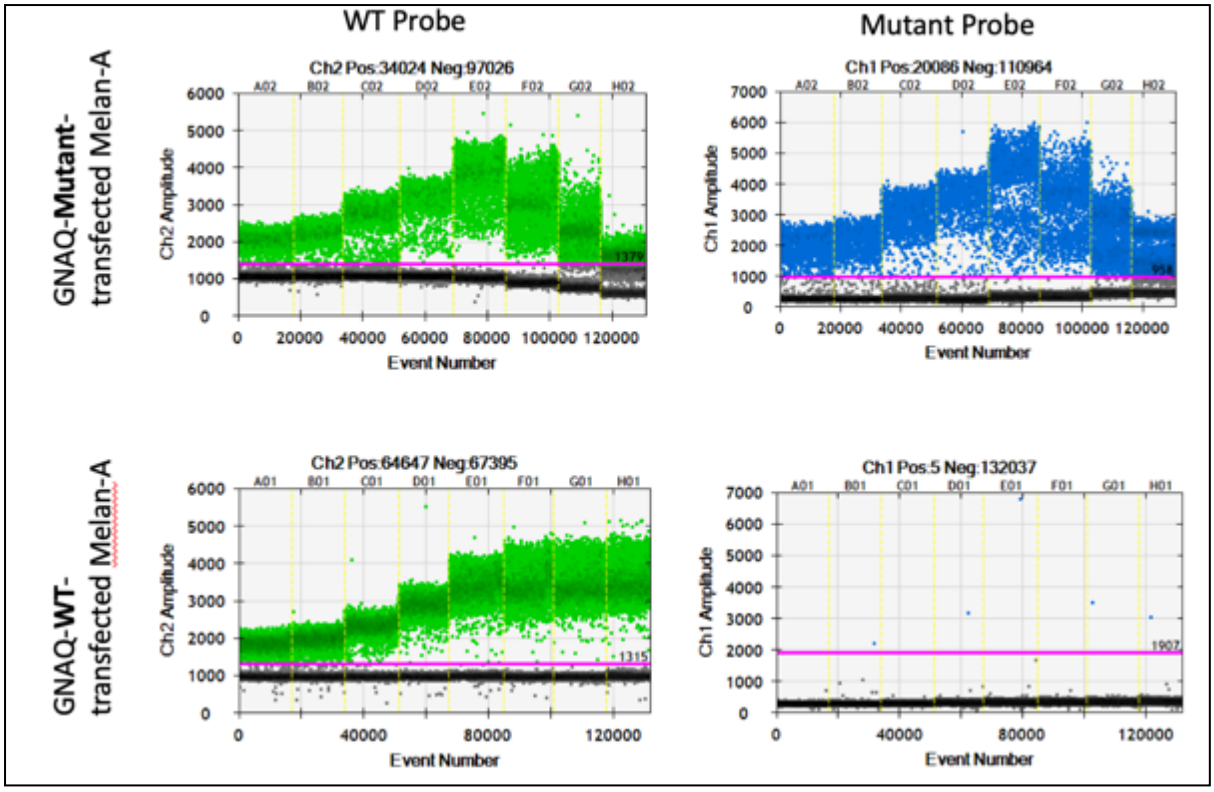

Figure 22: Verification of *GNAQ* A>T mutation in murine Melan-A cells by ddPCR on a temperature gradient. Lanes represent different temperatures. Green: WT GNAQ copies. Blue: mutant GNAQ copies.

The morphology of the Melan-A mutant and wildtype cells are shown in Figure 23. Compared to the morphology seen in human NCM cells, the murine melanocytes had a more dendritic rather than spindle morphology.

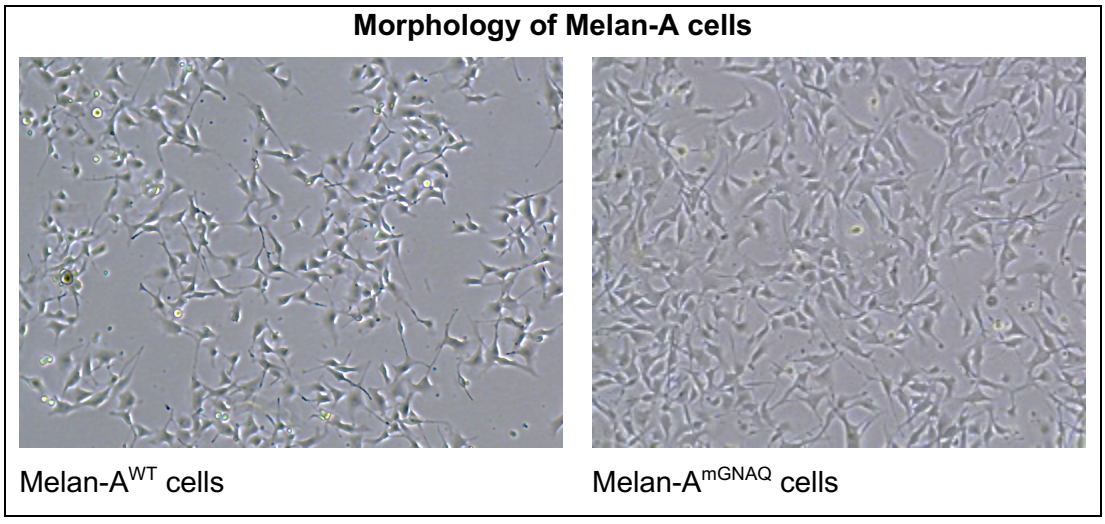

Figure 23: Morphology of murine melanocytes, transduced with wildtype and mutant plasmids of GNAQ respectively.

Although the focus of the experiments would be on WT and *GNAQ*-mutant melanocytes as a pre-malignant model of UM, UM cells were included in certain experiments for comparison. 92.1 and MP46 are two UM cell lines that contain a mutation in *GNAQ*, specifically that of A>T base substitution at codon 626, which is identical with the mutation of the *GNAQ* mutation contained in the purchased plasmid that will be used for transduction of the NCMs. For this reason, 92.1 and MP46 will be the UM cells used as comparison with the human transduced and NCMs.

Table 7: Selected UM cell lines and their characteristics

UM Cell Line	Morphology (spindle, epithelioid, mixed)	GNAQ mutation	GNA11 mutation	SF3B1 mutation	EIF1AX mutation
MP46[84]	Mixed	c.626 a > T	None	None	None
92.1[85]	Mixed	c.626 A>T	None	None	c.17G/A

Discussion

Despite both arising from melanocytes, cutaneous and uveal melanoma are diseases that differ in many important aspects, including pathogenesis and response to treatment[86]. Hence although many *in vitro* studies use dermal melanocytes to study melanoma, it is important to use uveal melanocytes to understand the pathogenesis of UM. To this end, we spent the first part of this project establishing immortalized NCM^{mGNAQ} cells to build a model system for studying UM development. To the best of our knowledge, this is the first comprehensive human NCM system to study initiating mutations in UM.

Although commercial uveal melanocyte cell lines are not available, other groups have isolated and cultured melanocytes from the choroid of donor eyes[65, 87]. We have adapted previous protocols to establish the model system here. Our NCM culture had the same spindle morphology as previously reported[88], and we verified the NCM culture for melanocyte-specific markers.

Doubling times of specific NCM cultures have been reported by different groups to range in approximately 84-96hrs[65, 78]. However, a previous group also reported that generation time of NCMs was markedly increased after cryopreservation[78]. While non-cryopreserved NCMs had generation time of 3.5 days, that of cryopreserved NCMs markedly increased to 37.8 days[78]. Our NCM culture prior to cryopreservation also doubled approximately every 3-5 days. The proliferation rate of cryopreserved NCMs in another group[78] mirrors the slow proliferation rate of our NCM cultures post-cryopreservation, which had been estimated to have a doubling time of 30 days.

Through verification of our transduction plasmids, and optimization of our transduction protocol, we have established a reliable *in vitro* model to study the initiating UM mutation of *GNAQ*. In the following chapters, this model will be used in studying the biological effects of mutant GNAQ protein on normal melanocytes, and later to study an effect of BL as an environmental factor.

Results Chapter 2: Phenotypic and proteomic assays characterize *GNAQ* to be a weak oncogene conferring growth advantage and anchorage-independent growth

Introduction and rationale:

As aforementioned, the importance of early mutations in the *GNAQ/11* G-protein coupled receptor signaling pathway has been well observed in UM patients, as almost all UM tumors harbor a mutation in either *GNAQ*, *GNA11*, *PLCB4* or *CYSLTR2*[3]. Although thought of as an activating mutation, *GNAQ* mutation status does not appear to have prognostic significance, as they cannot predict UM disease progression and do not correlate with disease-free survival (DFS)[24]. Similarly, *GNAQ* mutations did not correlate with clinicopathological parameters such as age, gender, largest tumor diameter, and scleral extension[35, 36]. These evidence in combination with the presence of *GNAQ/11* mutations in benign blue nevi suggest that despite its wide presence in UM, mutations in the GNAQ pathway alone may be insufficient for malignancy.

Following the establishment of NCMs harboring the *GNAQ*^{Q209L} mutation, we aimed to understand the effect of this initiating mutation on otherwise healthy cells. Here, we use functional cellular assays as well as high throughput quantitative proteomics to characterize human and murine *GNAQ*-mutant cells.

Results:

GNAQ mutation confers a growth advantage in human NCMs and murine melanocytes

In order to understand the growth characteristics of mutant and wildtype cells *in vitro*, we conducted a viability assay through analysis of CCK8. Although CCK is a direct measure of metabolic activity, we are using it here as an indirect indication of proliferation. Melan-A^{WT} and Melan-A^{mGNAQ} cells were seeded at 15000cells/well in 96-well plates and cultured under the same conditions. By Day 4 in culture, the metabolic activity of Melan-A^{mGNAQ} cells was significantly higher than in Melan-A^{WT} cells ($p=0.0086$) (Figure 24). This result indicates that the *GNAQ* mutation has given transduced cells a proliferative advantage.

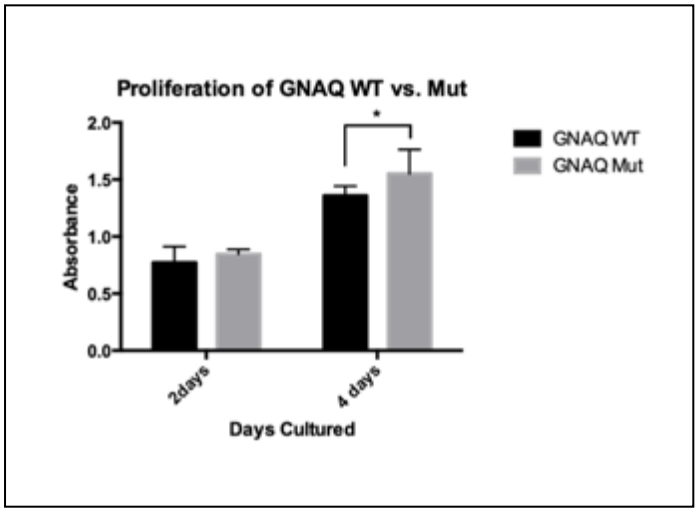

Figure 24: CCK absorbance of Melan-A^{WT} and Melan-A^{mGNAQ} cells after 2 days and 4 days of culture. *p-value<0.05. GNAQ WT: Melan-A^{WT}, GNAQ Mut: Melan-A^{mGNAQ}. Error bars represent experimental triplets.

To confer the results we saw in the murine mutant cells, we also conducted a proliferation assay on human mutant and wildtype cells using a more direct approach via cell confluency as visualized by Incucyte. The UM cell line MP46 (GNAQ-mutant) was included for comparison. By 120hrs of culture, the UM cell line MP46 showed increased confluency by approximately 60%, and growth has been continual in a roughly linear manner (Figure 25). In contrast, lower proliferation rates are seen across the NCMs, with wildtype (non-transduced) NCMs showing the lowest level of proliferation. In comparison, NCM^{mGNAQ} show a slightly steeper growth curve (difference was significant at four time points indicated by *)(Figure 25), confirming that mutant GNAQ similarly confers growth advantage to human NCMs as seen in the murine model.

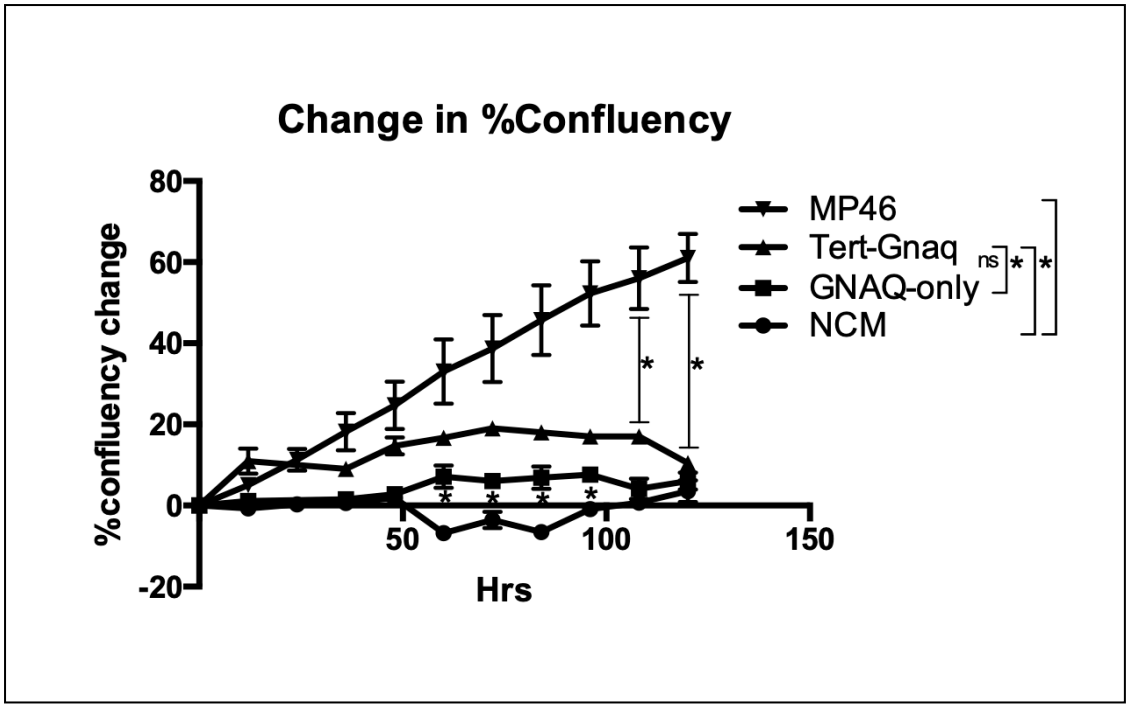

Figure 25: Change in % confluency of transduced and non-transduced NCM over 5 days measured in Incucyte, compared to UM cell line MP46. *p<0.05 indicates significance calculated by multiple t-tests followed by Holm-Sidak correction. Error bars representative of experimental triplicates. NCM: normal choroidal melanocyte; GNAQ-only: NCM^{mGNAQ}; Tert-Gnaq: immortalized NCM^{mGNAQ}. Ns: not significant across all time points. Difference between Tert-Gnaq, MP46 with NCM was significant at all time points.

No difference in migratory capacity was seen following *GNAQ*-mutant transduction

Migratory capacity is an important attribute of carcinogenesis and an essential process in the formation of metastasis[89]. In UM where the metastatic disease is the key to its high mortality, it would be interesting to understand more about migration potential of UM cells.

We hypothesized that a mutation in *GNAQ* would confer a greater cell migration ability in our model. To test this hypothesis, we conducted a wound healing assay to compare the ability of mutant and wildtype cells to migrate to fill the wound following a scratch *in vitro*. After 24hrs, both mutant and wildtype murine Melan-A cell lines were able to close the majority of the wound, with no significant difference between the % migration between the WT and mutant cells (Figure 26).

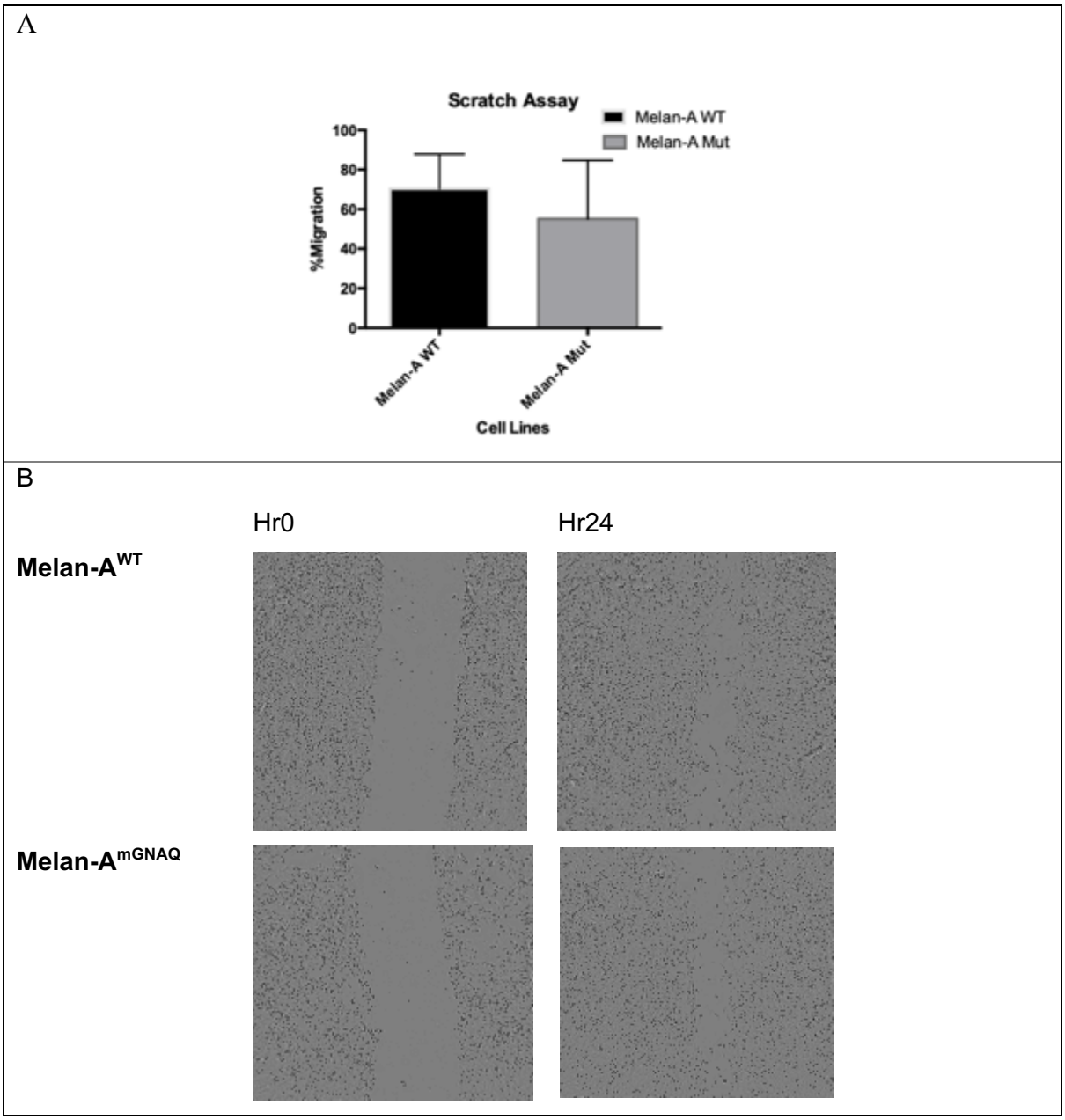

Figure 26: Wound healing assay. (A) Percent migration of Melan-A cells after 24hrs. Error bar represents four experiment replicates. (B) Representative wound healing pictures at Hours 0 and 24 for $GNAQ^{Q209L}$ and WT Melan-A cells. Phase contrast image, 4X magnification.

NCM^{mGNAQ} cells show an increased ability to grow in an anchorage independent manner

Adhesion to extracellular matrix is a requirement for many cell types to proliferate and survive. The ability of a cell to proliferate in an anchorage-independent manner is a frequent characteristic of transformed cells, correlating with tumorigenic phenotype[90].

Here, we aimed to assess the ability of mutant and wildtype cells to grow in anchorage independence using a soft agar cloning assay[70]. In order to compare our findings with malignant cells, we used the UM cell lines 92.1 and MP46. Both of these cells express mutations in *GNAQ*.

When grown on soft agar, both 92.1 and MP46 readily formed colonies within one month of culture (Figure 27). As early as day 6 of soft agar culture (image not shown), colonies of three and more cells were detectable under the microscope at 10X magnification.

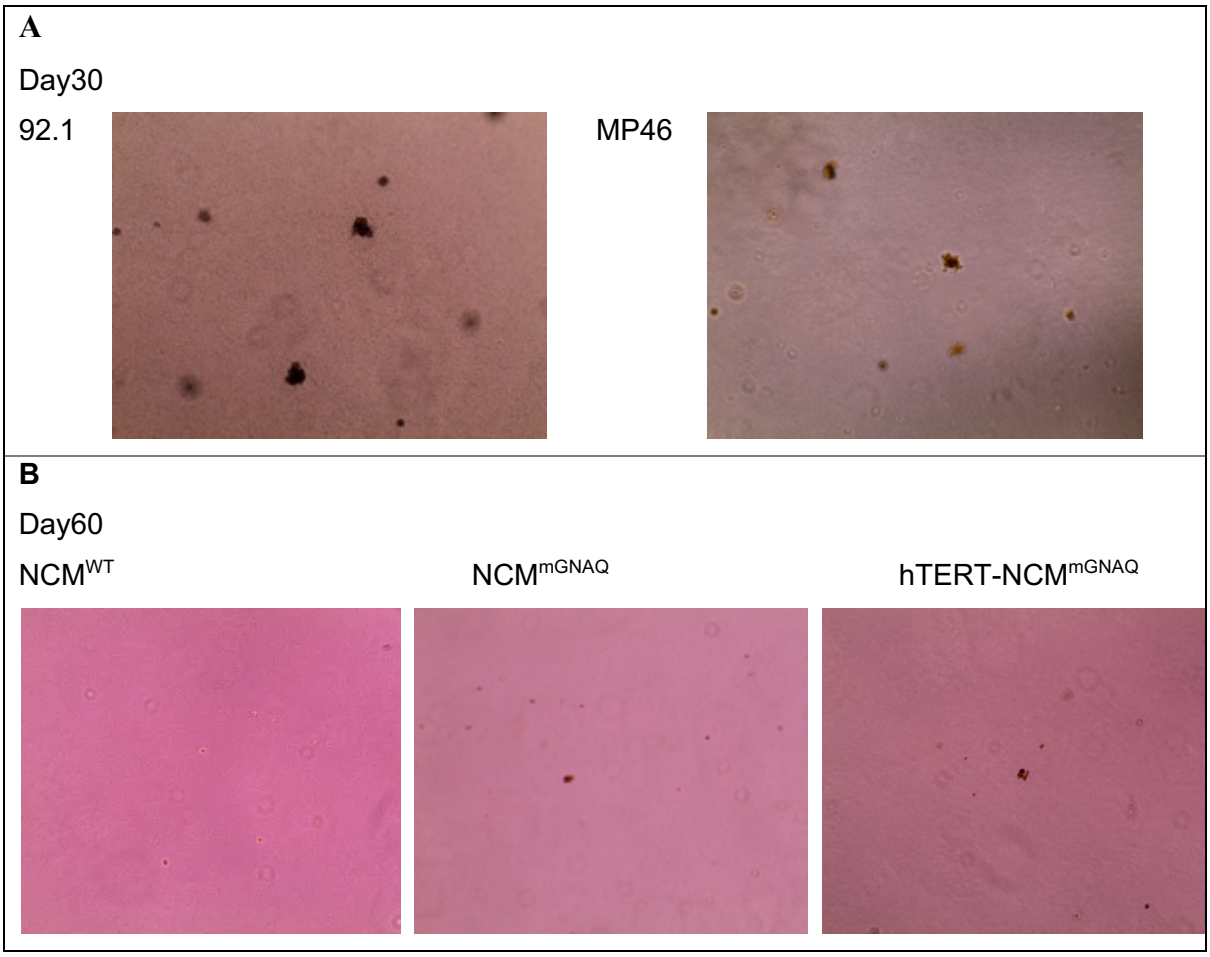

Figure 27: Soft agar colony growth of UM and NCM cells. (A) UM cells 92.1 and MP46 colonies at Day30. (B) NCM cells at Day60. Images taken at 10X magnification.

In contrast to the UM cell lines, by day 30 of soft agar culture, none of the human NCMs (transduced and non-transduced) showed colony formation (image not shown). However, while NCM^{WT} did not show evidence of colony formation even at 60 days post seeding, colonies were seen for both immortalized and non-

immortalized NCM^{mGNAQ} (Figure 27B). The much slower proliferation rate of the NCM cells may explain the slower growth of colonies in agar. The results suggest that *GNAQ* mutation, and thus GNAQ protein signaling, may render cells ability to grow independent of anchorage.

When we compare the average colony size between UM cells and *GNAQ*-mutant cells, we can see that colonies of UM cells are visibly larger and more abundant than *GNAQ*-mutant cells (Figure 27). This observation shows that although GNAQ mutation confers a change in growing capacity, the effect does not reach that of malignant cells.

NCM^{mGNAQ} cells demonstrate contact-uninhibited growth in culture

Normal cells when grown in culture would grow in a monolayer until confluency when contact inhibition halts their proliferation. In cancer cells however cells often escape from contact inhibition and are able to grow in an overlapping way that form what is referred to as a focus[91]. Foci-forming ability is considered to be a hallmark of transformation.

In our culture of NCM^{mGNAQ} cells, we observed disruptions of the monolayer growth as observed in NCM^{WT} cells, and saw cells growing in overlapping manner that formed small foci (Figure 28), this further confirms that GNAQ^{Q209L} has a transforming effect on the NCM cells.

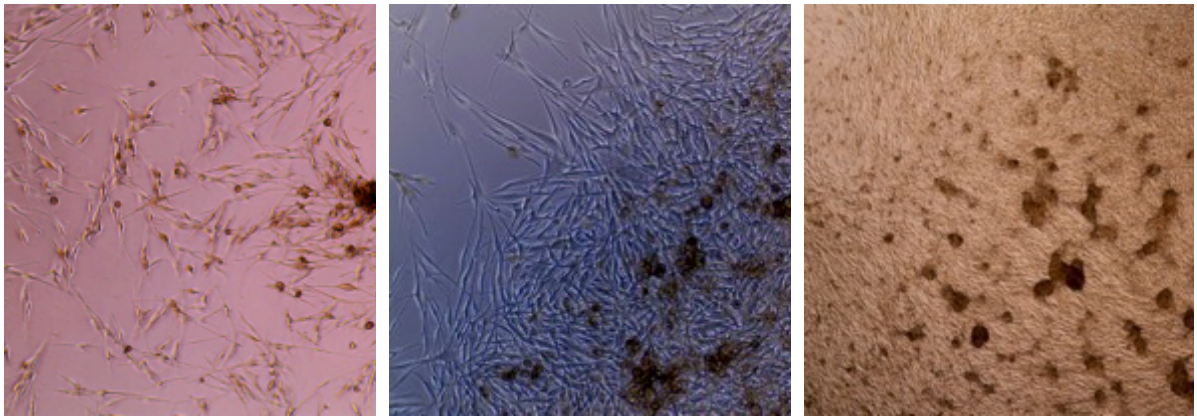

Figure 28: NCM^{mGNAQ} showed occasional growth in foci. Each image represents a different culture. Images taken under 10x magnification.

Quantitative mass spectrometry analysis reveals differences in the proteomic profiles of Melan-A^{WT} and Melan-A^{mGNAQ} cells

Enhanced GNAQ signaling is associated with activation of important pathways that lead to cellular proliferation, migration and survival[92]. Previously, transcriptomic analysis comparing UM cells with normal uveal melanocytes showed differential expression of proteins in the pathways of MAPK signaling, cell cycle, melanogenesis, p53 pathway, and apoptosis[93]. To our knowledge, few studies have compared proteome expressions between normal and *GNAQ*-mutant melanocytes in a non-biased high throughput manner, and we aimed to do so using our murine Melan-A model.

To determine what protein changes occurred following transduction with a *GNAQ*^{Q209L} mutation in healthy melanocytes, we conducted quantitative mass spectrometry on Melan-A^{WT} and Melan-A^{mGNAQ} cells (each sample in duplicates) and compared their proteomes based on significance by the t-test built in Scaffold. P-value <0.05 was considered significant. Protein expression profiles between the two cell types are shown in Venn diagrams (Figure 29) according to either quantitative profiles based on t-test significance (Figure 29A), or based on presence or absence of proteins in each sample (Figure 29B). As shown, while the majority of proteins were common to both mutant and wildtype cells, we identified 93 upregulated proteins in Melan-A^{mGNAQ} cells, and 85 were uniquely found in these cells.

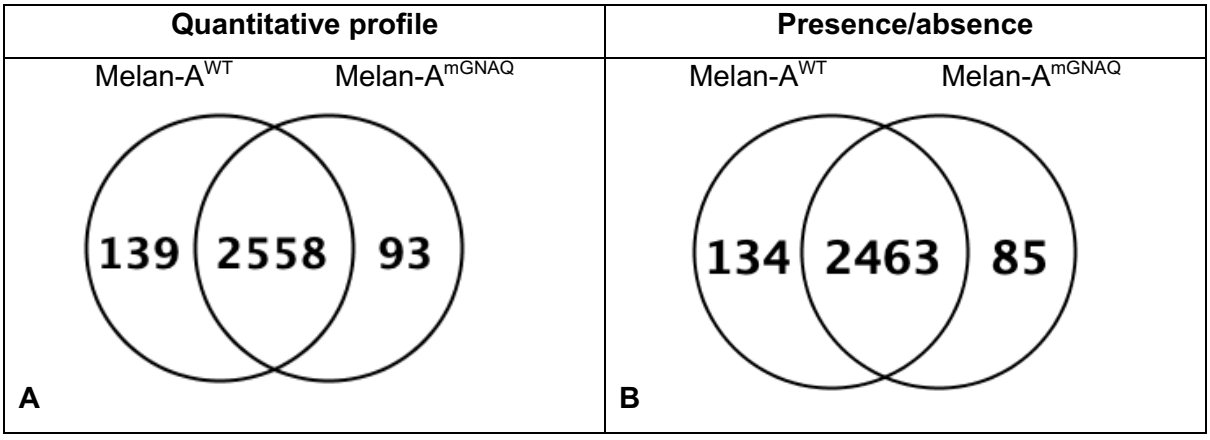

Figure 29: Venn diagram showing (A) number of proteins significantly upregulated in Melan-A^{WT}(139) or Melan-A^{mGNAQ}(93) cells (p<0.05). (B) number of unique proteins only expressed in Melan-A^{WT}(134) or Melan-A^{mGNAQ}(85) cells.

Proteins up-regulated in Melan-A^{mGNAQ} cells show enrichment in metabolism and translation pathways

To understand the significance of our data, we sought to group the up-regulated proteins in the Melan-A^{mGNAQ} cells by common pathways. Using Reactome pathway enrichment analysis (version 72), 61 of the 93 upregulated proteins in the Melan-A^{mGNAQ} cells were matched in the software and therefore included in the analysis. The results were represented in a Reactome over-representation map, which indicates whether the up-regulated proteins are statistically over-represented or enriched in particular biological pathways (Figure 30). The map indicates that *GNAQ*-mutant cells are enriched for proteins in metabolism (categories "metabolism", “metabolism of proteins”, and “metabolism of RNA”) and disease.

Figure 30: Reactome overrepresentation map analyzing proteins significantly up-regulated in Melan-A^{mGNAQ} cells. Branches with darker color represent sub-pathways more significantly overrepresented /enriched.

More details of the enriched pathways are summarized in Table 8 below. The most enriched pathway based on protein abundance was Metabolism (40/3650), and a very high enrichment significance (p-value=1.45e-05) was seen in the Translation pathway.

Table 8: Selected most enriched pathways of Melan-A^{mGNAQ} (by p-value)

(pathways including overlapping proteins are excluded)

Reactome Pathway	**Found protein entities**	**p-value**	**Proteins**

Translation	11/339	1.45e-05	Eif4a2, Rl13a, Rps5, Srp54, Nars, Rpl24, Rps7, Yars, Ppa2, Rpl7, Sec61a1
Metabolism	40/3650	2.24e-04	Acaa2, Acot2, Aldh1l2, Acat2, Acsl3, Asl, Acot1, Acsl4, Atp5me, Cpt2, Eci2, Glrx5, Gys1, Pkm, Psat1, Rlp24, Rps7, Decr1, Eif4a2, Got1, Hmgcl, Plin2, Rfc1, Rpl7, Slc24a1, Dld, Fdps, Gstp1, Ppa2, Rpl13a, Rps5, Uqcrb, Cpt2, Hmgcs2
Peroxisomal protein import	4/67	0.001	Acot2, Ech1, Eci2, Hmgcl
Regulation of lipid metabolism by PPARα	6/176	0.001	Cpt2, Hmgcs2, Plin2

Proteins with significantly higher expression ($p<0.05$) as identified by Scaffold t-test, but which also has high expression fold changes (>2) were selectively included in Table 9. These identified proteins and other proteins of interest in the data set were searched for their function and description in literature.

Overall, the upregulated proteins reveal a particular focus on lipid metabolism. For instances, these proteins include those involved in lipid biosynthesis (HMGCS2), beta oxidation (CPT2, ACAA2), ketone body formation (HMGCL), and accumulation of lipid droplet (PLIN2) (Table 8). Dysregulation in lipid metabolism has been implicated in cancer[94], thus it is plausible that a change in metabolism regulation plays a part in malignant transformation related to *GNAQ* mutations.

There is also an overall enrichment of upregulated proteins in the translation pathway, including transcription initiation factors (EIF4a2) and ribosomal proteins (RL13a, RPs5, RPl24, RPs7, RPl7). This enrichment corroborates with the increased proliferation observed in our functional assays of Melan-A^{mGNAQ} and supports the characterization of mutant GNAQ as an oncogene[95].

We also noticed dual specificity protein phosphatase 3 (DUS3) (Table 9) to be notably up-regulated in Melan-A^{mGNAQ} cells ($p=0.017$, fold change 2.9). DUS3 is thought to function as negative regulation of MAPK pathway, and a human protein with similar function, dual specificity phosphatase 6 (DUSP6), has been reported to have high basal levels in *GNAQ*-mutant UM cell lines[96]. This was thought to reflect an induced negative regulation of a high level of MAPK activity in *GNAQ*-mutant cells[96].

Table 9: Selected markedly up-regulated proteins in Melan-A^{mGNAQ} (p<0.05, fold change >2)	
Abbreviation	**Protein name**
PGAM5	Serine/threonine-protein phosphatase PGAM5, mitochondrial
SRP54	Signal recognition particle 54 kDa protein
SKT	Sickle tail protein
RL24	60S ribosomal protein L24
QCR7	Cytochrome b-c1 complex subunit 7
DUS3	Dual specificity protein phosphatase 3
MAP4	Microtubule-associated protein 4
ECI2	Enoyl-CoA delta isomerase 2
SLIRP	SRA stem-loop-interacting RNA-binding protein, mitochondrial
ATP51	ATP synthase subunit e, mitochondrial

Proteins down-regulated in Melan-A^{mGNAQ} cells reveals enrichment in cell cycle-related pathways

Proteins up-regulated in Melan-A^{WT} cells can similarly be interpreted as being down-regulated in Melan-A^{mGNAQ} cells. In the list of proteins significantly down-regulated in Melan-A^{mGNAQ} cells, 93 of the 139 proteins (Figure 29A) were matched to Reactome pathways. From the Reactome over-representation graph below, it can be seen that enriched pathways are located mostly under the main pathways of "cell cycle", "DNA repair", as well as "programmed cell death" (Figure 31).

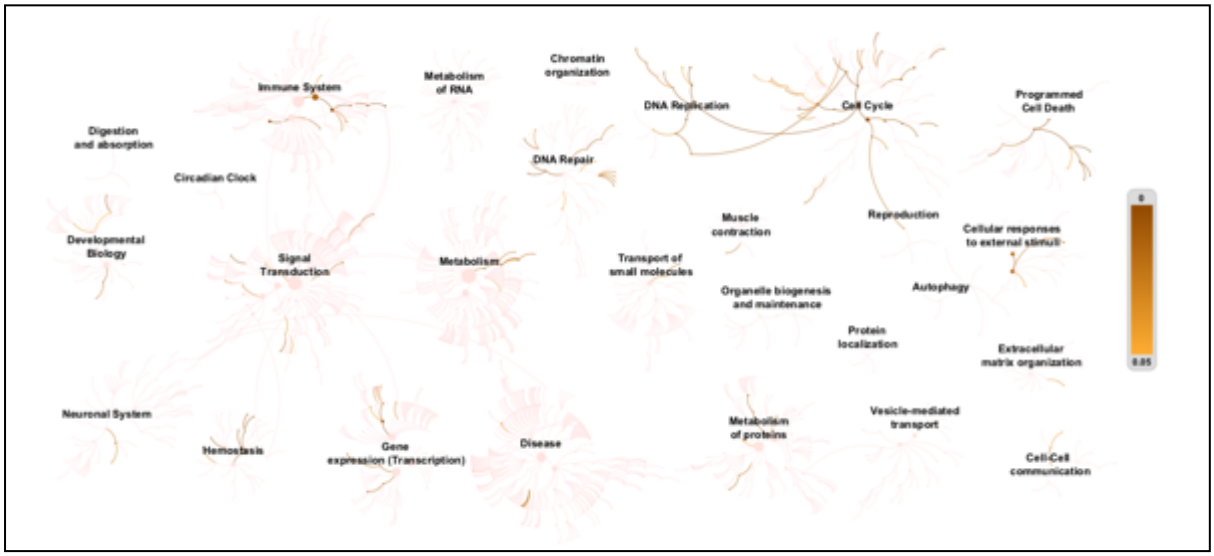

Figure 31: Reactome overrepresentation map analyzing proteins significantly down-regulated in Melan-A^{mGNAQ} cells / up-regulated in Melan-A^{WT}. Branches with darker color represent sub-pathways more significantly overrepresented /enriched.

In the analysis of individual proteins that were more abundant in the Melan-A^{WT} cells, we found proteins involved in: proteasome/ ubiquitination (PSMA6, CUL1), DNA replication (RPA1, PCNA), DNA damage response (RPA1), as well as apoptosis (CASP3,CASP6) (Table 10).

Table 10: Selected most enriched pathways of Melan-A^{WT} (by p-value)
(pathways including overlapping proteins are excluded)

Reactome Pathway	Found protein entities	p-value	Proteins
G1/S Transition	10/150	5.21e-06	Cdk1, Mcm7, Rpa1, Cul1, Pcna, Mcm2, Psma6
Apoptosis	10/189	3.71e-05	Casp3, Casp6, Hmgb1, Hmgb2, Lmna, Mapk3, Psma6, Stat3, Stk24, Ywhah
Cell cycle	19/715	2.07e-04	Anapc5, Hsp90ab1, Mcm2, Psma6, Smc3, Cdk1, Lmna, Mcm7, Rcc2, Sun2, Cul1, Mapk3, Pcna, Rpa1, Ywhah

While inferring from the proliferation results, we would expect a lower expression level of replication-related proteins in GNAQ-WT cells, interestingly we noted several cell cycle progression proteins such as CDK1, MCM, PCNA. However, we also saw a higher level of apoptosis proteins. This suggests the possibility that compared to GNAQ-mutant cells, the WT cells for some reasons undergo a higher level of cell turnover.

Analysis of proteins comparatively more abundant in wildtype cells revealed an enrichment of the cell-cell adhesion pathway, for example cell adhesion molecules (CADM4, NCAM1). A difference in expression levels of adhesion components may similarly explain the loss of contact-inhibited growth and anchorage independent growth that were observed in our human GNAQ-mutant NCMs (Figure 27,Figure 28).

Additionally, individual protein entities of interest have emerged from our analysis. For example, 5,6-dihydroxyindole-2-carboxylic acid oxidase (TYRP1) is an enzyme involved in melanin biosynthesis has been observed to also be downregulated in Melan-A^{mGNAQ}. Its downregulation has been reported by other groups in different contexts of UM[93, 97].

In Table 11, we identified selected proteins with significantly higher expression ($p<0.05$) as identified by Scaffold t-test, but which also has high expression fold changes (>2). We found DNA mismatch repair protein (MSH2) to be significantly down-regulated in Melan-A^{mGNAQ} cells ($p=0.029$). It has been reported that in choroidal melanoma, DNA mismatch repair proteins including MSH2 were found to be insignificantly reduced in tumors with higher genomic instability[98]. Hence an increase in genomic instability may be implicated in progression from pre-malignancy to malignancy in UM.

Unexpectedly, amongst the proteins in Table 11 was protein GNAQ itself and its largely homologous protein GNA11. The level of GNAQ detected here is total GNAQ level and gives no information to its activation level nor its mutation status. Amongst the proteins upregulated in Melan-A^{mGNAQ} cells, we mentioned the identification of protein phosphatase DUS3, which was thought to be induced as a negative regulation pathway of a high level of MAPK activity in *GNAQ*-mutant cells[96]. Although the mechanism is uncertain, it is plausible that because of the constitutively active mutant GNAQ protein, the cell has induced compensatory mechanisms to downregulate the expression of signal proteins. Hinting support of this theory was a study that reported GNAQ signaling to induce internalization of upstream GPCR[99]. Furthermore, this finding corroborates with a similar finding previously reported in transfected NIH cells, where the cells transfected with $GNAQ^{WT}$ showed an overexpression of GNAQ proteins in western blot compared to the mutant cells[100].

Table 11: Selected markedly up-regulated proteins in Melan-A^{WT}
($p<0.05$, fold change >2)

Abbreviation	Protein name
PLXB2	Plexin-B2
MSH2	DNA mismatch repair protein 2
EGFM	Elongation factor G, mitochondrial
CASP6	Caspase-6
GNAQ	Guanine nucleotide-binding protein G(q) subunit
GNA11	Guanine nucleotide-binding protein subunit α11
CADM4	Cell adhesion molecule 4
CRKL	Crk-like protein
RCN1	Reticulocalbin-1

PARP1	Poly (ADP-ribose) polymerase 1

Discussion:

This chapter of results addresses our aim of characterizing GNAQ-mutant cells. We accomplished this using the human and murine models we described in the previous chapter. Our functional and proteomic results compared *GNAQ*-mutant cells with WT cells, demonstrated and confirmed the general characterization of GNAQ as a weak oncoprotein shown in previous studies[10, 100].

GNAQ/11 gained attention as activating oncogenes in melanocytes following a genetic screen in mice showing hypermorphic mutations in *GNAQ/11* to increase intradermal proliferation of melanocytes[101]. Another study later demonstrated that *GNAQ/11* mutations were able to transform hTERT/CDK4^{R24C}/p53^{DD} melanocytes, which are immortalized melanocytes with deficient p53 and p16/CDK4/RB pathways[10, 102]. Their results showed that hTERT/CDK4^{R24C}/p53^{DD} cells transduced with *GNAQ*^{Q209L} produced colonies in soft agar assays. In contrast, transduction of primary melanocytes with *GNAQ*^{Q209L} was not sufficient to produce colonies in soft agar. In our experiments, NCM cells were immortalized with *hTERT* alone. While we agree no colonies grew for primary melanocytes, our results produced soft agar colonies for both immortalized and non-immortalized NCMs transduced with *GNAQ*^{Q209L}. However, this discrepancy could be a difference in experimental methods, where we had a longer period of soft agar culture (60 days) compare to the previous group (28 days)[10].

The transforming ability of mutant GNAQ has also been demonstrated in murine cells NIH 3T3, a fibroblast cell line, where cells transfected with mutant *GNAQ* exhibited foci formation and anchorage-independent growth[100]. The tumorigenic ability of *GNAQ*-mutant NIH 3T3 cells was further demonstrated *in vivo* on nude mice. Foci formation, though not explicitly measured with a staining assay, had been observed in our NCM^{mGNAQ} cultures as well, confirming *GNAQ* has transforming effect in human uveal melanocytes.

To the best of my knowledge, previous reports of bottom-up mass spectrometry proteomic analysis of *GNAQ*-mutant melanocytes are lacking. In this study, we performed an unbiased analysis and comparison of global protein expressions between Melan-A^{WT} and Melan-A^{mGNAQ} cells. We discovered an overall

up-regulation of proteins involved in lipid metabolism in Melan-A^{mGNAQ} cells. This could point to future research venues for knock-out or knock-down studies targeting specific lipid metabolic enzymes to confirm whether changes in metabolism play a vital role in the down-stream effects of aberrant GNAQ signaling.

Further studies in the future could be added to strengthen and clarify some of the results shown in this chapter. The scratch wound-healing assay was used here and did not show significant difference in migratory potential between the cell lines. While it is an acceptable migration assay, an addition of a transwell migration assay would be able to further confirm the results. Proteomics results showed an enrichment for apoptotic and cell cycle proteins in Melan-A^{WT} compared to Melan-A^{mGNAQ} cells, thus it would be interesting to explore this finding through functional assays that study apoptosis, such as an annexin V assay.

Results Chapter 3: Blue light exposure results in decreased proliferation and protein expression in melanocytes

Introduction and rationale:

While UV exposure has been linked with cutaneous melanoma development, evidence has been inconclusive regarding the role of UV exposure on UM carcinogenesis[103, 104]. Amongst various plausible environmental risk factors of UM, welding appears to be strongly associated with UM development[52]. While welding is a source of UV exposure, it is also a strong source of BL[105].

Recently, it was shown that BL increases the proliferation of UM cells both *in vitro*[53] and *in vivo* in a xenograft model[106]. While the exact mechanism underlying the relationship between BL and UM cells remains unknown, shorter wavelengths of light have been shown to induce retinal pigment epithelial cell death by mitochondrial-derived ROS production[107].

With age, the human lens becomes progressively more yellow, potentially via progressive accumulation of yellow chromophore deposits 3-hydroxykynurenine glucoside derivatives, and is therefore better able to filter BL from entering the eye[62]. When patients undergo cataract surgery, the original lens is removed and replaced with an artificial intra-ocular lens (IOL). Although most IOLs have now UV-filtering capabilities, many are not equipped to filter other wavelengths such as BL. As such, the removal of the aged lens during cataract surgery is accompanied by the loss of the natural ability to filter BL. Given the known role of BL in age-related macular degeneration[108] and potentially in UM, the use of BL-filtering IOLs may be warranted as preventative measures.

Welders are subjected to occupational exposure of blue light[40], but other everyday sources of BL affect the general population. Important sources of BL include natural sun light, LED lights, and, importantly in today's era, light from screens of numerous electronic devices. Such chronic exposure of low levels of BL can lead to accumulation of damage to various structures. The role of such exposure on ocular cells is largely unknown.

Following establishment of our *in vitro* model of NCM^{mGNAQ} and demonstrating $GNAQ^{Q209L}$ as a weak oncogene in melanocytes, there still remains the question of the identity of additional events that alongside the GNAQ mutation result in full malignancy. We wished to therefore investigate the effect of BL exposure on GNAQ-

mutant cells, and determine whether BL has the potential of acting as an additional oncogenic stimulus. Two set-ups of BL sources were used in our experiments, a fiber-optic illuminator and a solar simulator. Cells were subjected to BL under these BL sources and in various doses for analysis of subsequent biological effects.

Results:

Murine melanocytes show reduced metabolic activity after BL exposure

Our first goal was to establish an appropriate dose of BL that would represent low exposure over time. In the first experiment, Melan-A^{WT} and Melan-A^{mGNAQ} cells were exposed to BL via a fiber-optic illuminator setup (Figure 3) for various time periods of: 1hr/day over 2days, 1hr/day over 4 days, 2hrs/day over 4 days, and 3hrs/day over 4 days, as a dose-response experiment. The maximal dosage of 3hrs/day for 4 days was determined based on a previous study on UM cells which utilized the same BL set-up[109].

To assess the effects of BL exposure on melanocytes, we conducted a CCK8 viability assay. Although CCK is a direct measure of metabolic activity, we are using it here as an indirect indication of proliferation. When exposed to BL for 1hr/day over 2 days, no significant difference in CCK absorbance was seen before and after BL exposure in either cell line (Melan-A^{WT} and Melan-A^{mGNAQ}) (Figure 32), suggesting this exposure level was not enough to incur a biological response. However, when we continued low dose (1hr/day) exposure over 4 days, we began to see significant changes in proliferation (Figure 32B).

While we expected BL to act as a stressor which would inhibit proliferation in $GNAQ^{WT}$ cells, we hypothesized that BL might act in cooperation with the *GNAQ* mutation in $GNAQ^{Q209L}$ cells to further transform the mutant cells. While BL did not have a pro-proliferation effect on $GNAQ^{Q209L}$ cells, mutant cells showed a resistance (though inconsistent) to the anti-proliferative effect of BL, compared to WT cells which consistently showed a reduced proliferation (Figure 32B,C,E). This suggests that the *GNAQ* mutation might confer cells a survival advantage when exposed to BL through an unclear mechanism.

The UM cell line 92.1 was also included for comparison, since UM cell lines have been previously reported to show increased proliferation after BL exposure[109].

Amongst the experimental repeats done, the effect of BL on 92.1 cells was varied, with a range of effects seen (Figure 32). Increased CCK absorbance was evident in one experiment post-BL, but this effect was not reliably captured in repeats. Nevertheless, it serves as indication that UM cells respond to BL differently compared to non-cancer cells.

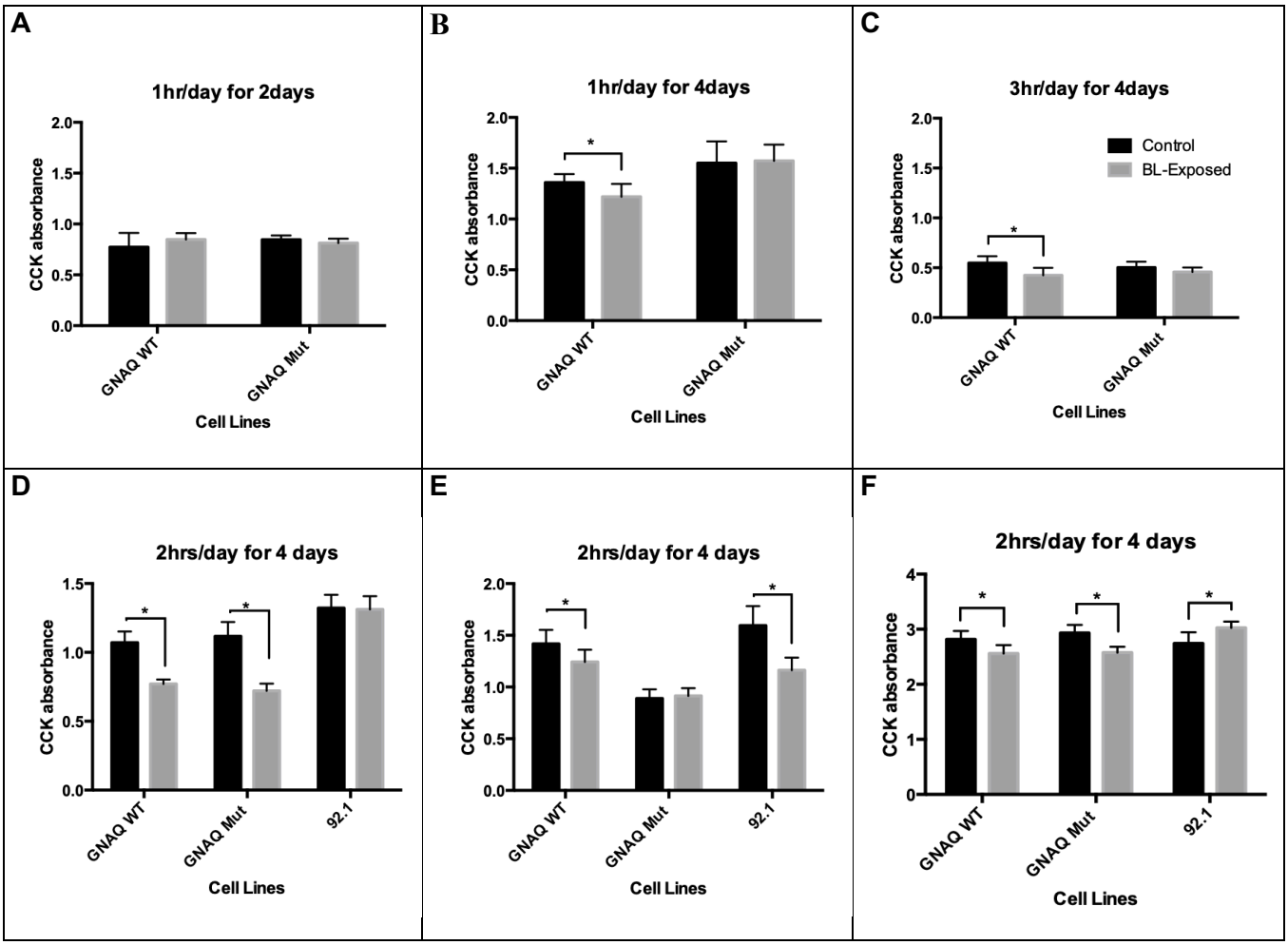

Figure 32: CCK absorbance for Melan-A^{WT} and mutant cells at different exposure times with comparison of UM cell (92.1) *p-value<0.05. (A) BL dosage 1hr/day x 2. (B) BL dosage 1hr/day x4. (C) BL dosage 3hrs/day x4. (D,E,F) Three separate experimental repeats of BL dosage 2hrs/day x4.

Real time tracking reveals reduced proliferation of human NCMs after BL exposure via a solar simulator

Next, we set up a solar simulator as a more reliable BL source (Figure 5), with more precise control of the wavelengths and intensities the cells were subjected cells to, reducing the confounding factors of UV, other visible light exposure, and temperature.

Prior to our functional assays using the solar simulator, we tested BL exposure on cells at various intensities. At intensity of 1sun (1000 W/m^2), after only an exposure time of 2hrs, the exposed melanocytes had rounded morphology which suggests a cytotoxic response. Moreover, cytotoxicity was also felt by the light-protected controls, suggesting it was likely result of the high heat generated from the solar simulator at high intensities. After testing with intensities of 1sun, 0.5sun, and 0.3sun, we ultimately chose 0.3sun for our BL exposure experiments. After 3hrs of exposure at 0.3sun, melanocytes maintained healthy morphology, a thermometer ascertained that the temperature of cells did not exceed 32˚C in the exposure duration.

We also switched to a realtime imaging quantification of cell proliferation via Incucyte, which in comparison with CCK8 would directly measure proliferation, and able to adjust for any differences in starting seeding density.

We exposed cells to BL under the solar simulator for 3hrs/day for 4 days, while monitoring cell confluency through the Incucyte. Our results showed that while both immortalized and non-immortalized GNAQ-mutant NCMs showed significantly reduced proliferation after BL, human UM (MP46) cells were not affected (Figure 33). This differential response of UM cells towards BL mirrors the CCK results above.

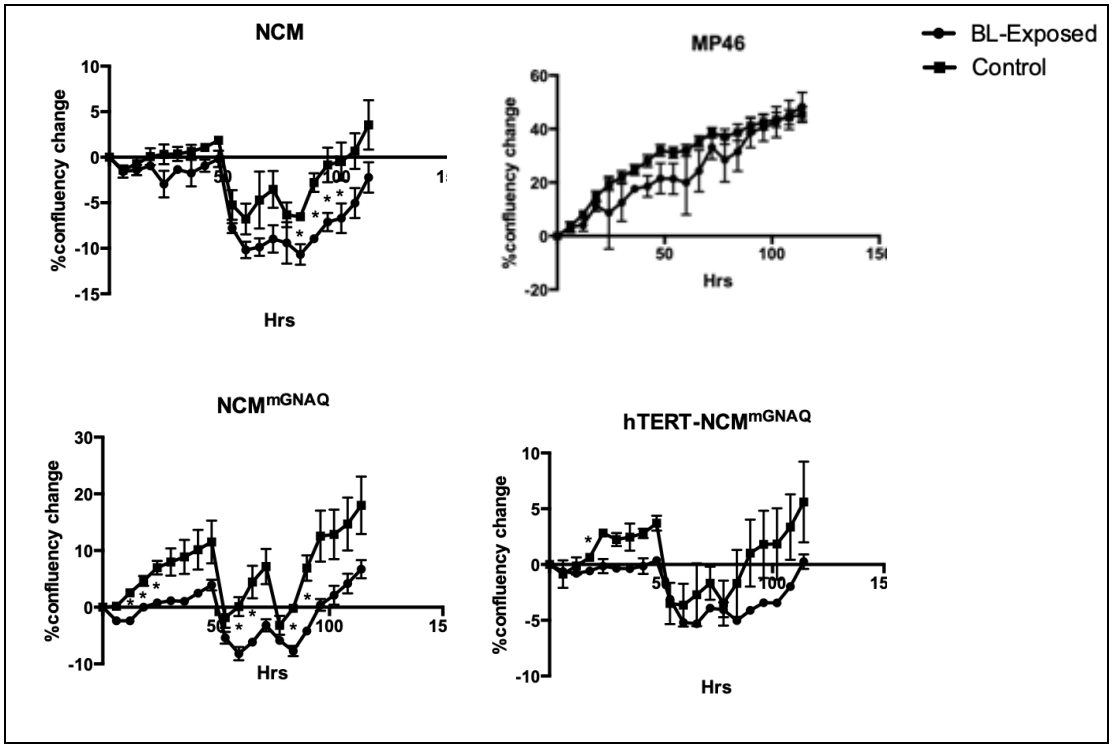

Figure 33: Change in confluency of NCMs and MP46, with and without BL exposure of 0.3 sun of 2hrs/day x 4 days. Cell confluency measured by Incucyte. %confluency change = absolute %confluency - starting confluency. Results representative of 3 individual experiments. Error bars represent sample triplicates. *p<0.05, multiple t-tests.

BL exposure did not lead to consistently significant cellular damage and apoptosis in melanocytes or UM cells.

In an attempt to elucidate the mechanisms behind the observed reduction in proliferation, we then wanted to assess cellular damage resulting from light exposure. We exposed our melanocyte and UM cell lines to BL under the solar simulator for 3hrs/day for 4 days, before subjecting them to assays characterizing cell death including ethidium homodimer (EthD-1) and TUNEL assay.

To measure damage to the plasma membrane, we quantified EthD-1 in the murine and human melanocytes and UM cell lines following BL exposure to assess cell membrane disruption. EthD-1-positive cells indicate damage of plasma membrane and therefore cell death. Our results showed hTERT-NCM^{mGNAQ} cells to have a lower base level of EthD-1-positive cells compared to NCM^{WT} (Figure 34). Exposure to BL resulted in a higher or unchanged level of mean EthD-1 positivity in all cell lines, but the results were not significant (Figure 34).

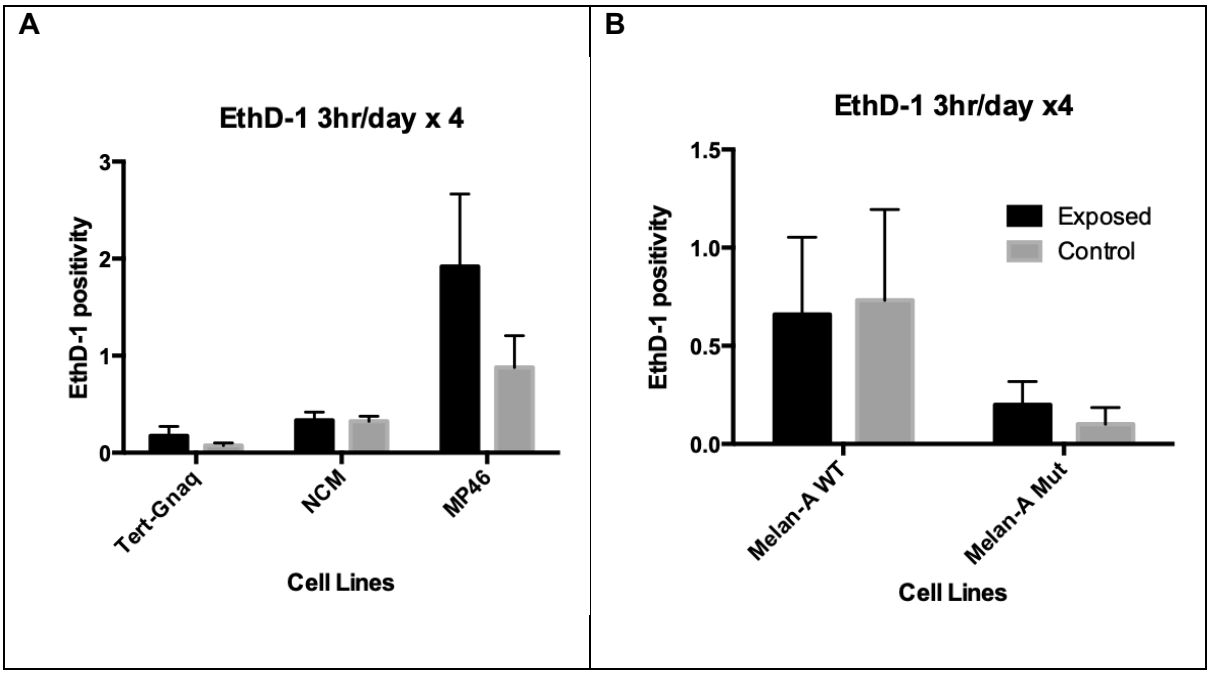

Figure 34: EthD-1 positivity of cells after BL exposure and light-protected control (A) human NCMs and UM cells (B) murine Melan-A cells. Error bars represent experimental triplicates.

EthD-1 positivity calculated by number of EthD-1 signals / cell confluency. Error bars represent sample triplicates.

To clarify the results from the EthD-1 assay, we used a different approach to monitor cytotoxicity and resulting cellular death through a TUNEL assay, which quantifies late stage apoptosis. After BL exposure for 3hrs/day for 4 days, we did not see a statistically significant difference in TUNEL positivity in exposed vs. nonexposed cells (Figure 35). While the TUNEL results show that the exposed cells in all cell lines have a higher median level of TUNEL positivity, the difference was not statistically significant due to a high standard deviation in the BL-exposed cells. While TUNEL positivity in GNAQ-WT vs. Mut cells are similar, it was notable that UM cells (MP46) had evidently lower base level of TUNEL-positivity compared to Melan-A cells, and TUNEL-positivity post-BL exposure did not increase by a great amount compared to MP46 control cells.

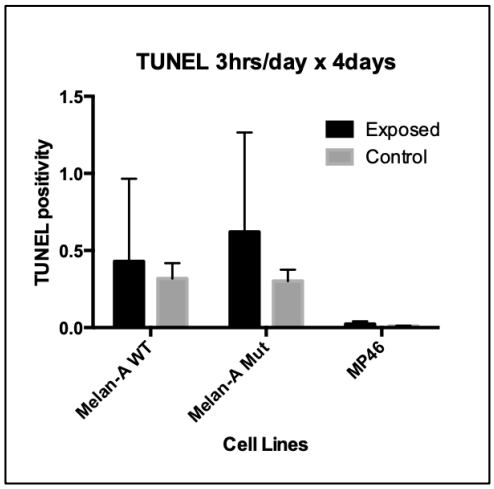

Figure 35: TUNEL assay on Melan-A and MP46 cells. TUNEL positivity measured as the number of TUNEL signals / %confluency of cells. Error bars represent sample triplicates.

No significant difference in emission of cell-free DNA (cfDNA) following BL exposure in NCM^{WT} verses NCM^{mGNAQ}

Cell-free DNA (cfDNA) are short fragments of DNA that are released by cells during cell death[110], associated with extracellular vesicles and through cellular secretion. cfDNA is utilized in cancer research as a biomarker of disease through liquid biopsies[111]. We have previously utilized quantification of cfDNA to assess

response of UM cells to drug compounds, such as beta blockers[69]. Here we aimed to use a cfDNA assay to determine whether BL induces increased release of fragmented cfDNA.

Since we have observed UM cells to be resistant to the anti-proliferation effects of BL in proliferation studies, we hypothesized that *GNAQ* mutation might confer a degree of protection from BL exposure in terms of cell death. Following our results from cell death assays that showed GNAQ-mutant cells did not significantly differ from GNAQ-WT cells, we wished to further confirm that result with a more sensitive method that allows distinction between WT and mutant GNAQ cells in a heterogenous transduced culture.

WT (Tert-only) and $GNAQ^{Q209L}$(Tert-GNAQ) NCM cells were exposed to BL for 3hrs/day over 4 days, and cell-free supernatant was collected at Day2 and Day4. As expected, the Tert-only NCMs did not express mutant GNAQ copies in cfDNA (Figure 36A). However, in the Tert-GNAQ NCMs, no significant difference was seen between the percentage of GNAQ-mutant vs. GNAQ-WT copies in total events, indicating both WT and mutant cells respond similarly to the cytotoxic effect of BL (Figure 36B).

A

Mutant-GNAQ-positive droplets

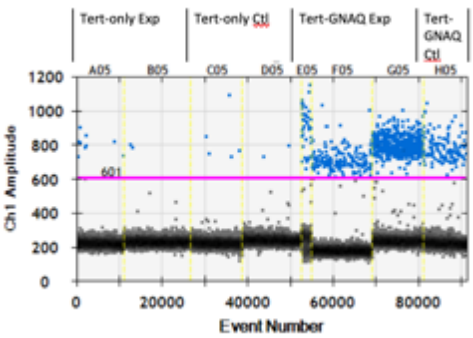

WT-GNAQ-positive droplets

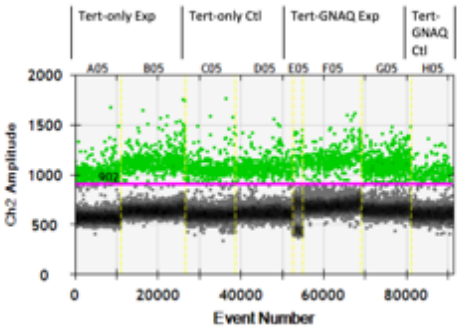

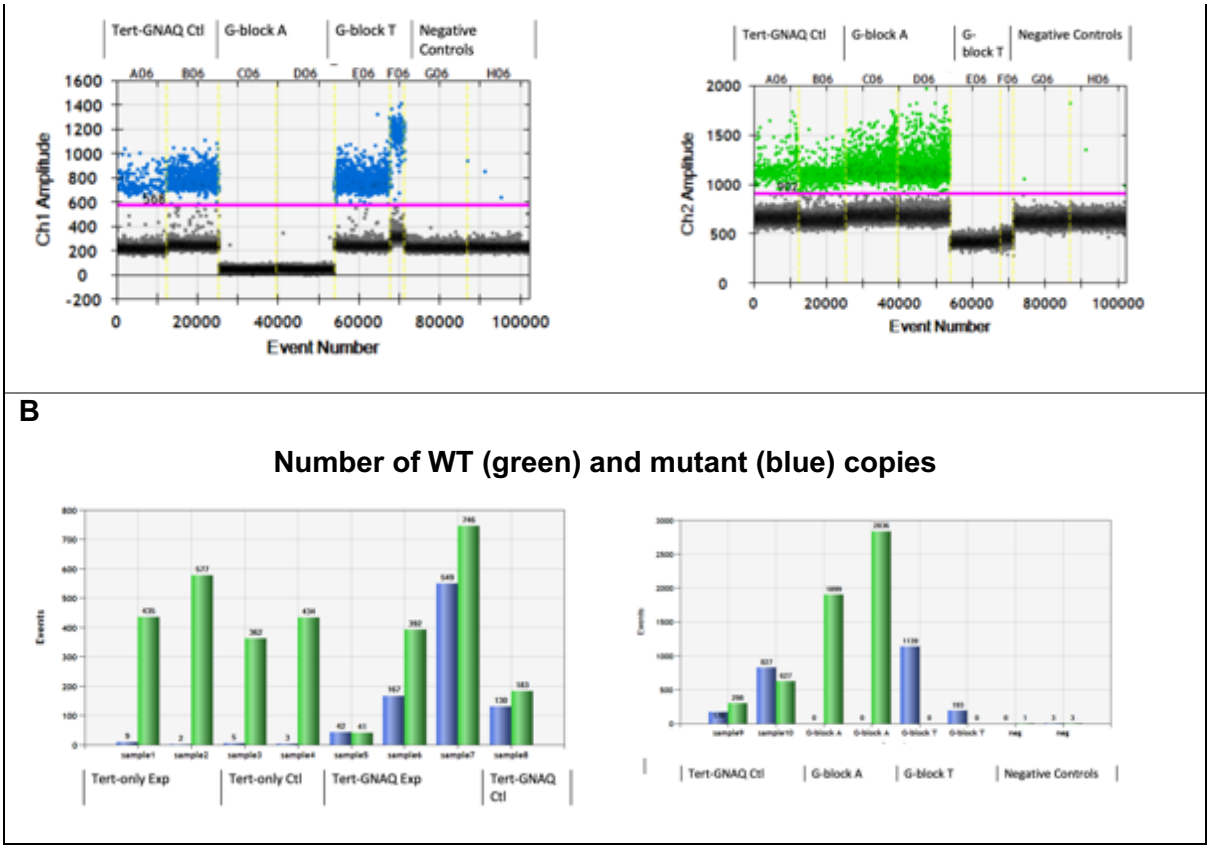

Figure 36: ddPCR results of mutant and WT NCM cells with and without BL exposure (A) positive droplets of ddPCR in each sample. Mutant droplets in blue, WT droplets in green. (B) Quantification of droplet copies in each sample.

A trend toward increased reactive oxidative species (ROS) is seen post-BL exposure

Although we demonstrated an anti-proliferative effect of BL on NCM and Melan-A cells, the biological mechanisms underlying this effect remained unclear. BL has been reported to increase intracellular ROS in literature[48]. We thus sought to investigate the role of ROS production as a plausible mechanistic link to the anti-proliferative effect of BL.

Melan-A^{WT} and Melan-A^{mGNAQ} and MP46 cells were exposed to BL for 3hrs/day x 4days via the solar simulator, and intracellular ROS levels were measured with MitoSOX Red indicator and compared to BL-protected control. As shown in Figure 37, the median ROS level has been elevated in all cell lines post-BL exposure. However, similarly to the TUNEL results, a high standard deviation in exposed cells renders the difference non-significant. It is important to note that GNAQ-mutant cells had a much lower base ROS level compared to WT cells. And interestingly, the highest level of ROS was seen in MP46 cells.

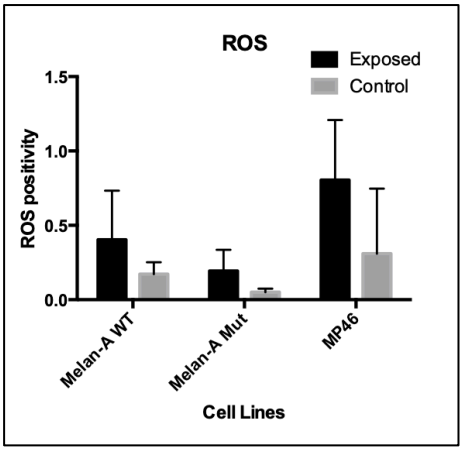

Figure 37: ROS assay on Melan-A and MP46 cells; ROS level is measured as the number of ROS fluorescent signals / %confluency of cells. Error bars represent sample triplicates.

Quantitative proteomics reveals a higher number of down-regulated proteins following BL exposure in Melan-A cells

In order to further understand the effects of BL on melanocytes, we conducted quantitative mass spectrometry on cell lysates from Melan-A^{WT} and Melan-A^{mGNAQ} cells following BL exposure (0.3sun, 3hrs/day x 4 days) (each sample in duplicates), and compared their proteomes with their respective light-protected controls using t-test analysis in Scaffold. $P<0.05$ was considered significant. Protein expression profiles between samples are represented in Venn diagrams according to either their quantitative profiles based on t-test significance (Figure 38A, Figure 39A), or based on their presence or absence in each sample (Figure 38B, Figure 39B).

When we compared the protein lists, we saw that the majority of proteins were shared between exposed vs. non-exposed cells. However, in both the wildtype and mutant cells, we saw a significantly higher number of proteins that were more abundant in the non-exposed cells, or downregulated in exposed cells (Figure 38A, Figure 39A). In fact, the number of proteins downregulated after BL exposure in Melan-A^{WT} cells were over six folds more than proteins up-regulated after BL (1009 vs. 148 proteins), and similar numbers are found for Melan-A^{mGNAQ} cells (935 vs 144 proteins).

Quantitative		Presence/Absence	
Melan-A^{WT}-control	Melan-A^{WT}-BL	Melan-A^{WT}-control	Melan-A^{WT}-BL

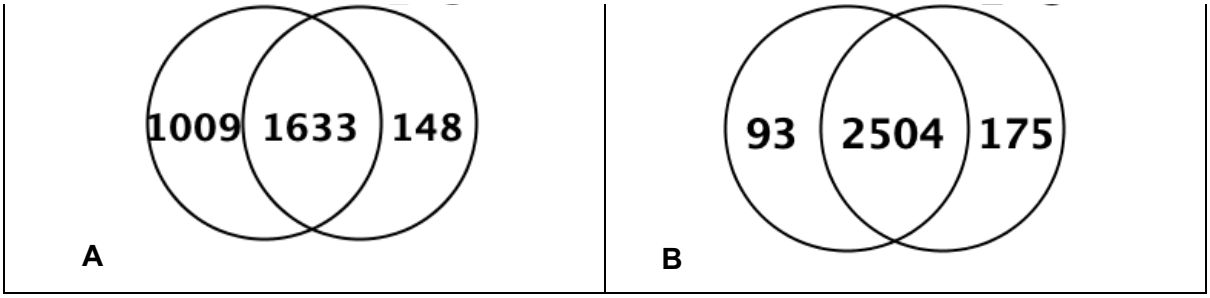

Figure 38: Venn diagram comparing Melan-A^{WT} BL-exposed with control A) number of proteins significantly upregulated in control (1009) or BL-exposed (148) cells ($p<0.05$). B) number of unique proteins only expressed in control (93) or BL-exposed (175) cells.

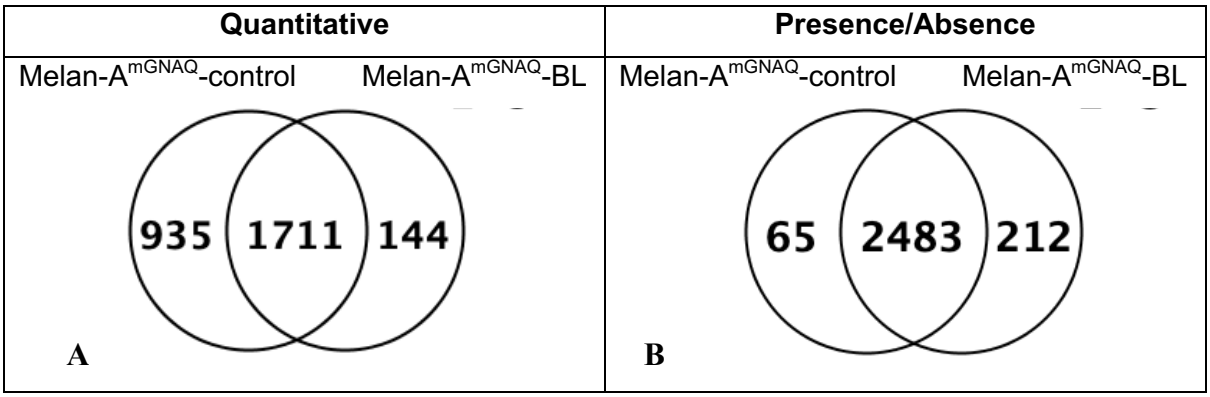

Figure 39: Venn diagram comparing Melan-A^{mGNAQ} BL-exposed with control A) number of proteins significantly upregulated in control (935) or BL-exposed (144) cells ($p<0.05$). B) number of unique proteins only expressed in control (65) or BL-exposed (212) cells.

We then to sought to understand which pathways may be implicated by protein expression changes following BL exposure. We therefore input the protein lists of differentially expressed proteins in the exposed vs. non-exposed groups in each cell line ($p<0.05$) into the DAVID program. Upon analyzing the DAVID biological pathways more abundant in control cells (or down-regulated post-BL), we identify pathways involved in: translational initiation, DNA replication, protein stabilization, mRNA processing (Figure 40). Decreased expression in these pathways coincides with the anti-proliferative phenotype seen after BL exposure in our functional assays.

In Melan-A^{mGNAQ} cells after BL exposure, it is worth noting the upregulation of pathways related to response to oxidative stress. This suggests that although the

increase in ROS level in our ROS assay was not significant, ROS may contribute to the effects of BL on cells.

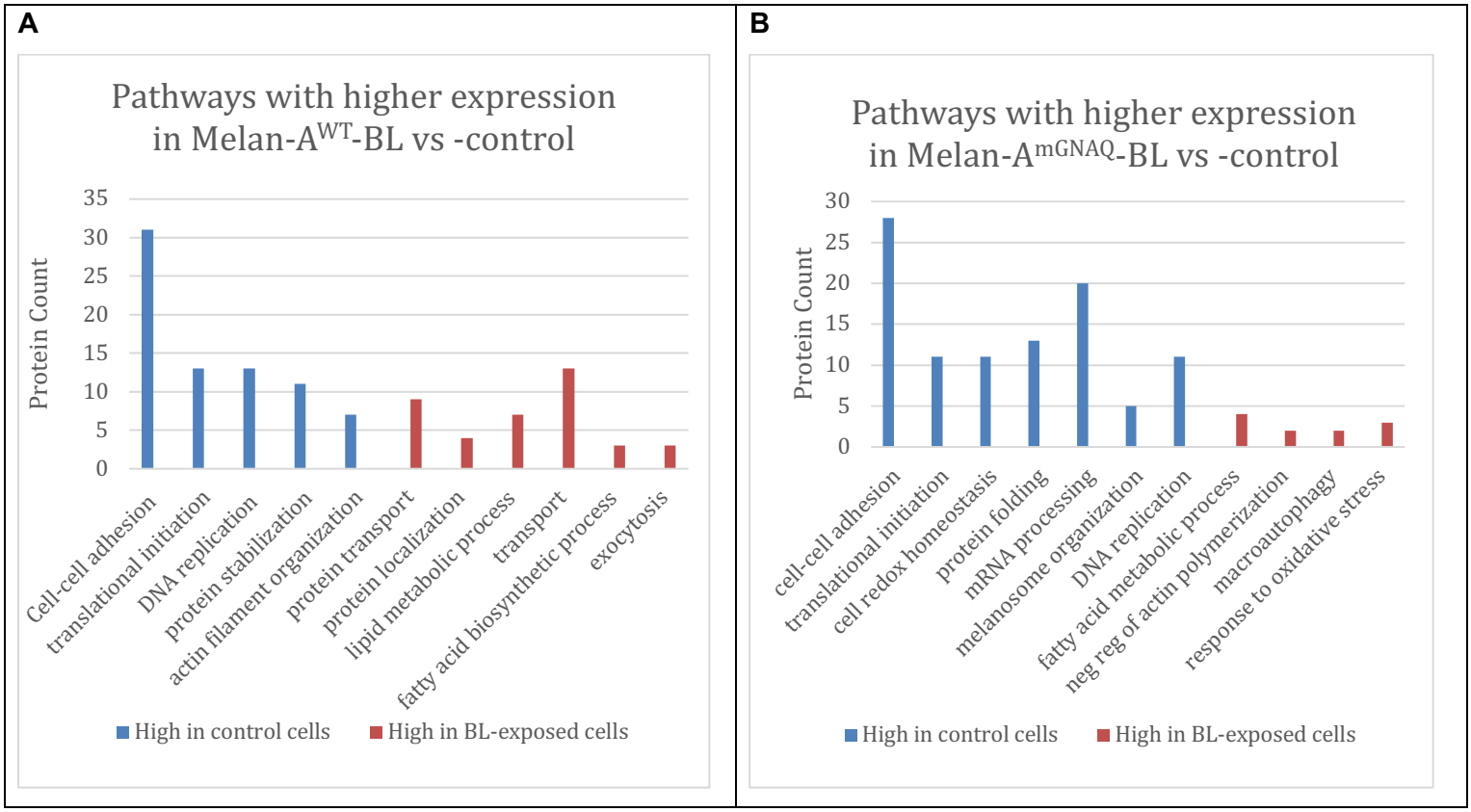

Figure 40: Graphs summarizing selected results (based on p-values) from DAVID analysis comparing up-regulated protein lists in control and BL-exposed cells of Melan-A^{WT} (A) and Melan-A^{mGNAQ} (B). P<0.05 considered significant. Proteomic samples were in duplicates.

We summarized proteins that were the most markedly (fold change >2) and significantly (p<0.05) differentially expressed in two tables below (Table 12,Table 13), and it was observed that the WT and mutant cells have proteins in common upregulated in each of BL-exposed and control conditions. This illustrates that on a proteomic level, GNAQ-mutant and WT cells respond in a similar manner to BL-exposure.

In a previous study, it has been shown that BL exposure impacted expression levels of inflammation genes in murine microglial cells, specifically inducing upregulation of COX2 expression[112]. COX2 expression was also found to be upregulated post-BL exposure (p=0.032, fold change= 1.2). COX2 expression has been related to poor prognosis in UM patients[113]. COX2 inhibitors have been

reported to show promise in both UM cell lines as well as in a rabbit animal model[114, 115].

In the list of proteins of Table 12, we identified UBR4 which is a E3 ubiquitin ligase. The ubiquitin-proteosome pathway has essential role in proteolytic processes, and its regulation and activity has been implicated in responding to oxidative stress and the regulation of oxidized proteins[116]. This further supports a role of BL in inducing oxidative stress. We also identified scaffold protein such as plectin (PLEC), which was upregulated post-BL in both cell lines. In normal cells PLEC has an important role in cytoskeleton organization, but PLEC has also been identified as a marker for pancreatic ductal adenocarcinoma, associated with tumor exosome transfer and enhancement of tumor growth[117].

Table 12: Selected markedly up-regulated proteins in BL-exposed cells
($p<0.05$, fold change >2)

Melan-A^{WT}		**Melan-A^{mGNAQ}**	
Abbreviation	**Protein Name**	**Abbreviation**	**Protein Name**
DYHC1	Cytoplasmic dynein 1 heavy chain 1	UBR4	E3 ubiquitin-protein ligase UBR4
UBR4	E3 ubiquitin-protein ligase UBR4	DYHC1	Cytoplasmic dynein 1 heavy chain 1
USP9X	Probably ubiquitin carboxyl-terminal hydrolase FAF-X	PLEC	Plectin
PLEC	Plectin	S12A2	Solute carrier family 12 member 2
RBP2	E3 SUMO-protein ligase RanBP2	ACACA	Acetyl-CoA carboxylase 1
ACACA	Acetyl-CoA carboxylase 1	INF2	Inverted formin-2
STRN3	Striatin-3	F1142	Protein FAM114A2
JIP4	C-Jun-amino-terminal kinase-interacting protein 4	HCFC1	Host cell factor 1
TECR	Very-long-chain enoyl-CoA reductase	CP4B1	Cytochrome P450 4B1
ABLM1	Actin-binding LIM protein 1	SMU1	WD40 repeat-containing protein SMU1

On the other hand, in the list of proteins up-regulated in control cells, we identify proteins involved in DNA replication and protein translation (RL35A, RFC2, CDK1, SMC2), which may explain a more active replication and growth activity in light-protected control cells. Another group of proteins upregulated in control cells compared to BL-exposed cells was cytoskeletal proteins such as keratin, and proteins of the cytoskeleton has been known to be implicated in responding to cellular stress[118].

Table 13: Selected markedly up-regulated proteins in control cells
($p<0.05$, fold change >2)

Melan-A^{WT}		**Melan-A^{mGNAQ}**	
Abbreviation	**Protein Name**	**Abbreviation**	**Protein Name**
GOLI4	Golgi integral membrane protein 4	K2C1	Keratin type II cytoskeletal 1
GFAP	Glial fibrillary acidic protein	ADAS	Alkyldihydroxyacetonephosphate synthase, peroxisomal
GLNA	Glutamine synthetase	CLPP	ATP-dependent Clp protease proteolytic subunit, mitochondrial
RL35A	60S ribosomal protein L35a	SPD2B	SH3 and PX domain-containing protein 2B
SYMPK	Symplekin	MTMR2	Myotubularin-related protein 2
RFC2	Replication factor C subunit 2	MGLL	Monoglyceride lipase
CDK1	Cyclin-dependent kinase 1	GLCNE	Bifunctional UDP-N-acetylglucosamine 2-epimerase
CRKL	Crk-like protein	NDUAA	NADH dehydrogenase (ubiquinone) 1α subcomplex subunit
SMC2	Structural maintenance of chromosomes protein 2	K2C1B	Keratin type II cytoskeletal 1b
NOLC1	Nucleolar and coiled-body phosphoprotein 1	AIFM1	Apoptosis-inducing factor 1, mitochondrial

BL may have an effect on activation of signaling pathways down-stream of GNAQ

The mechanisms underlying biological effects of BL remains largely unclear in literature. Light can directly induce signaling cascades through light-responsive opsin molecules, but could also indirectly trigger signaling cascades from generation of

oxidative species which in turn act as second messengers[119]. Melanocytes function in producing melanin in response to sun light, and murine melanocytes were recently shown to express light-responsive opsin molecules[120]. Additionally, ROS production has been implicated in BL exposure[48]. Hence we decided to investigate whether BL exposure has an effect on the downstream signaling pathways of GNAQ in melanocytes. Melan-A^{WT} and Melan-A^{mGNAQ} as well as MP46 cells were exposed to BL for 3hrs daily for 4days and compared with non-exposed cells for protein expression of AKT, MAPK, and YAP.

Shown in Figure 41, total AKT appears to be higher in WT compared to mutant cells, regardless of whether BL-exposed. AKT quantification was also shown to be higher in WT cells in proteomics data, but the difference was not statistically significant ($p=0.19$). The level of phosphorylated AKT (pAKT) allows observation of the activation level of AKT, and despite total AKT being lower in mutant cells, the level of phosphorylated AKT appears to be the same level with WT cells. This result suggests that $GNAQ^{Q209L}$ activates the AKT pathway, which is in concordance with what is suggested literature[3].

However, though a difference in AKT level was seen between WT and mutant cells, no perceivable difference was seen post-BL exposure in either cell lines. On the other hand, BL seem to have an effect on the MAPK pathway. Although total MAPK levels in both WT and mutant cells were higher for non-exposed cells, the level of phosphorylated MAPK (pMAPK) appeared higher in BL-exposed cells for both cell lines. This suggest that BL exposure had some degree of stimulatory effect on the MAPK pathway. A stimulatory effect of BL on MAPK is also evident in MP46 cells (Figure 41B).

Finally, we also included the YAP signaling pathway. Total YAP level was not included in western results, but as reflected in our mass spec proteomic data it did not show significant change between control and BL-exposed Melan-A cells. Meanwhile from our western results, level of active YAP in both mutant and WT cells seem be to markedly inhibited after BL exposure. The mechanism that could lead to this effect is unknown, and further experiments are needed to verify this effect.

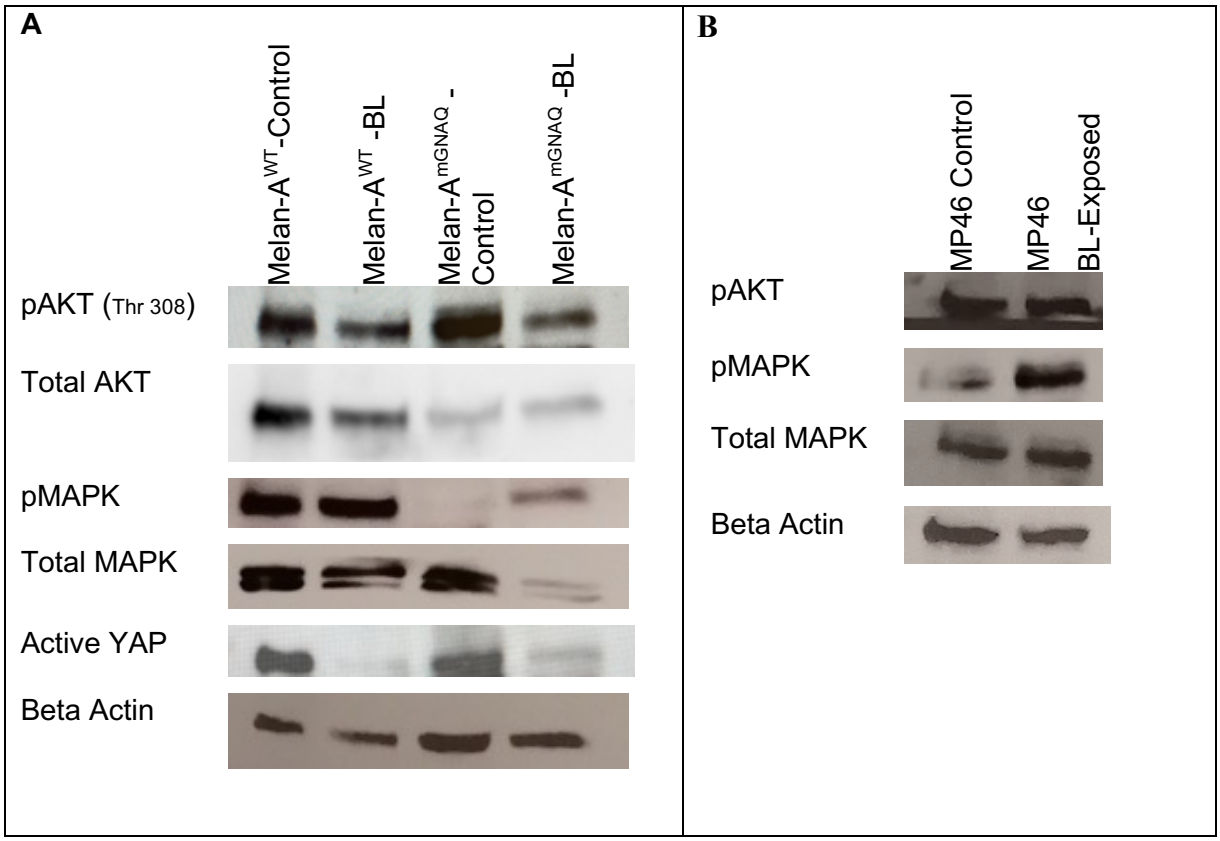

Figure 41: Western blot of major signaling pathways downstream of GNAQ (A) Melan-A cells with and without BL exposure; (B) MP46 cells with and without BL exposure; pAKT: phosphorylated AKT; pMAPK: phosphorylated MAPK; Thr308: threonine 308

Discussion

While the pathogenesis of cutaneous melanoma has been strongly linked to UV exposure, a similar environmental etiology has yet to be established in UM. Given the ease of protecting the eyes from light exposure, it is of paramount interest to understand whether light exposure plays a role in malignancies of the ocular tissues. Moreover, with increased use of artificial lighting in tablets and smartphones, understanding light effects is of clinical significance.

Previously, a link between BL exposure and UM development has been proposed[6]. Here we aimed to understand the effects of BL on premalignant cells related to UM. Since we have established an important human model of NCMs that harbor specific mutations that play a role in UM development, we wanted to test whether BL exposure would further push these cells towards a malignant phenotype. To do this we used dose exposure over several days to mimic chronic light exposure

and we then characterized the behavior, proteomes and signaling pathways. This is the first comprehensive analysis of BL exposure in a premalignant model of UM.

We have observed an anti-proliferation effect of BL exposure on melanocytes, which corresponds with previous studies done on other cell types. For instance, a cytotoxic effect has been documented on skin endothelial cells and in keratinocytes at high BL dosages, while an anti-proliferation effect was reported at low BL dosages[43]. An inhibition of metabolic activity was reported on human dermal fibroblasts[121], which corresponds to our CCK8 results post-BL exposure. Our results follow these observations and showed that BL also exerts an inhibitory effect on the proliferation of human NCMs. Additionally, we observed that countering our expectation of BL contributing to the transformation of *GNAQ*^{Q209L} mutant cells, the mutant cells were subjected to a similar anti-proliferative effect.

Our proteomic analysis shows a down-regulation of many proteins in melanocytes after exposure to BL, which agrees with previous studies reported. Proteomic changes following BL exposure had been reported in primary adult mouse dermal fibroblasts (AMDFs), which showed a suppressive effect on multiple pathways including those of carbon metabolism, amino acid biosynthesis and cell mobility[122]. Pathway analysis of our proteomic results similarly reflected downregulation of proteins of proliferation-related pathways.

Although BL has been reported to possess an inhibitory effect on the proliferation of human melanoma cells[123], a pro-proliferation effect has also been reported on UM cell lines[109]. Although our proliferation results with UM cell lines did not reflect a consistent pro-proliferation effect, it nonetheless supports that UM cells are at least more resistant to the anti-proliferation effect of BL compared to GNAQ-WT or even GNAQ-mutant cells. These results indicate that perhaps while NCMs undergo reduced viability, malignant cells may respond differently.

We did not record significant differences in cell death when comparing BL-exposed to non-exposed cells through EthD-1 and TUNEL assay. These data corroborate with studies that demonstrated anti-proliferative activity of BL but not cytotoxicity at certain light dosages[43].

Oxidative stress has been proposed to be a probable mechanism that relays the effects of BL exposure to cells, for instance mitochondrial ROS has been highlighted to mediate cytotoxicity of BL in RPE cells[107]. Our results suggest that ROS could mediate cellular changes of BL in melanocytes as well, although

statistical significance was not achieved in our model. Future studies looking at ROS production and mitochondrial DNA damage could elucidate some of these mechanisms. The ROS detection assay used in our study was specific to superoxide species. Since ROS includes a range of other species such as nitric oxide and H_2O_2 species, a more inclusive ROS assay would be helpful to include as a future experiment.

Regarding signaling pathways, BL has been previously shown in a phosphoproteomic analysis to suppress phosphorylation of ERK/mTOR substrates in primary adult mouse dermal fibroblasts[122]. However, it was also shown that in cortical neuron, BL exposure induced the expression of a range of neuron-activity-genes, and it was speculated to be through an induction of oxidative stress that in turn stimulate pathways including MAPK and NFkB[124]. Our western results showed BL being an activating stimulation for the MAPK/ERK pathway, while showing a suppressive effect in activation level of the YAP pathway. Further results would be warranted to confirm or elucidate this effect in melanocytes. Finally, our western results did not present with a role of *GNAQ* mutation in response to BL exposure, as both cells with and without mutant GNAQ showed similar changes (if any) in signaling molecules after BL exposure. A plausible future experiment to further explore whether there is interaction between GNAQ status and BL exposure could involve knockout / knockdown studies of GNAQ in a similar setup of BL exposure.

Conclusion

Uveal melanoma is a disease with a high mortality rate due to a lack in effective treatments for its metastatic disease. In recent years we have seen increasingly more studies that gradually uncover the genetic events underlying disease development and progression. Compared with many other cancers, UM has a relatively less mutation burden and a simpler genetic profile. However, while the identity of these genetic events has been uncovered, the mechanistic role of many of them in UM disease progression and development remains unclear. Thus a clearer understanding of the disease is key to finding ways to prevent and treat UM. One important genetic event that is an initiating early event in UM pathogenesis is a mutation in the genes involved in the GPCR pathway.

GNAQ/11 mutations have been found in up to 80% of UM but are also present in premalignant nevi. As such, while *GNAQ/11* mutations have been thought to be an early activating oncogenic event in the development of UM, they alone are not sufficient for full malignancy of the disease.

Although *GNAQ* and *GNA11* are highly analogous proteins, *GNA11* compared to *GNAQ* has been found to relate to some extent to prognosis of the disease, correlating more with disease metastasis. Although both are valuable candidates for further study, we have chosen to study *GNAQ* as we are most interested in the early development phase of the disease.

Knowing that *GNAQ* mutation is not enough for development of malignancy, we tested the hypothesis that it may interact with a second oncogenic event, and hypothesized that this event could be an environmental one – more specifically BL exposure. Environmental risk factors in UM are generally not well understood. For instance, while UV exposure has been clearly established as a risk factor for the development of cutaneous melanoma, literature in UM presents contradicting evidence for its role in UM[4]. However there seems to be a plausible role of BL in UM, as welding, a source of BL, had been shown to have a strong link with UM development[52]. Additionally, studies in recent years have suggested BL promotes UM growth in *in vitro* and *in vivo* models[53, 106].

To study whether BL interacts with initiating mutations of *GNAQ* in melanocytes, we established an *in vitro* model of transduced NCM cells and subjected them to controlled dosages of BL via a solar simulator.

Our study has resulted in three major novel findings:

1) Through a lentiviral transduction system of mutant-*GNAQ* on donor-derived human choroidal melanocytes, we established a viable and suitable system to study UM development.

2) We showed that the $GNAQ^{Q209L}$ mutation modifies the behavior and proteome of uveal melanocytes, suggesting its role as an oncogene in this system.

3) Our evidence indicates that BL acts as an environmental stressor to non-malignant melanocytes but not to UM cells.

General Discussion

Establishing a reliable model that is easy to work with *in vitro* or *in vivo* is important in research of diseases. In UM, a disease where there is a high and unimproved mortality rate over the years and where no efficient therapies exist for metastasis, there is a pressing need to uncover more about genetic and environmental events that contribute to disease development and progression. Using lentiviral transduction of NCM cells and a solar simulator, we sought to investigate the effect of *GNAQ*^{Q209L} as an initiating genetic event and BL as an environmental risk factor.

Melanocytes are the originating cells for both cutaneous and uveal melanoma, however the two disease differ greatly in genetic alterations, response to therapy, immune response and risk factors[86]. While melanocytes of the skin and uveal tract both derive from the neural crest, the two populations are thought to behave in very different ways[86]. For this reason, we sought to cultivate and use choroidal melanocytes in our experiments, even though cutaneous melanocytes were more available commercially. In Results chapter 1, we showed that we successfully developed a system to study human NCM derived from donor eyes. We demonstrated that we established viable cultures of primary and immortalized NCMs, and characterized the growth of these cells. Moreover, using lentiviral transduction, we successfully created *GNAQ*^{Q209L} cells that represent a premalignant model to study UM development. To the best of our knowledge, this is the first comprehensive human NCM system to study initiating mutations in UM. Through verification of genetic mutations of plasmids and immunofluorescent confirmation of melanocyte-specific markers, we have confidence in the reliability of our NCM cells cultured from donor eyes to be used as a model to study UM.

While the use of human NCMs and our model was preferable, we also used previously established murine Melan-A cell lines to complement a portion of our experiments. As reported in our proliferation results, our human NCM cultures proliferated at a much slower rate compared to Melan-A cells, hence they were not included in all experiments due to time constraints.

To overcome the lack of commercial uveal melanocyte cell lines on the market, we referenced and adapted protocols established previously by other groups[65, 87]. As reported in these studies, doubling times of NCM cultures have been

reported to be around 84-96hrs[65, 78]. On the other hand, one study that also reported the proliferation rate of NCMs after freeze/thaw cycles reported that cryopreservation of these cells greatly reduced the proliferation rate by as large as 10-fold[78]. In our study, proliferation rates of NCM culture were similar to those previously reported and reflected similarly the difference between proliferative potentials before and after cryopreservation.

Optimization of NCM culture growths are essential to reliably study intraocular diseases such as UM *in vitro*. Referencing other studies in literature, there appear to be several venues that could be adapted to our protocol in the future to increase proliferation ease of NCMs. Firstly, an obvious way of increasing proliferative potential of NCMs would be to avoid freeze/thaw cycles. As observed from our own experience and reported by others[78], as few as one freeze/thaw cycle greatly reduces the proliferation rate of NCMs. Additionally, another aspect of possible optimization addresses supplementary cell culture medium supplements. Various supplemented factors in culture medium have been proven beneficial to NCM growth, for instance it was reported that in addition to TPA or basic fibroblast growth factor (bFGF), and FBS, a cyclic adenosine monophosphate (cAMP) stimulator (such as cholera toxin) is needed for good growth of NCM[125]. In our culture medium for NCMs, we have supplemented FBS as well as TPA, but not cholera toxin. This work will be continued in the laboratory.

Other factors to consider include oxygen levels in the cell culture environment. While most cell culture incubators are set to atmospheric oxygen level of ~20%, uveal melanocytes *in vivo* are subjected to a lower physiological oxygen level of below 12%[126]. It has been reported that at 3% oxygen level, NCMs grew to a higher confluency compared to 21% oxygen, and had a shorter doubling time[65]. If we grew NCM cultures in low oxygen level incubators, we may be able to model the UM disease in a more physiologically accurate manner.

Upon establishing a viable NCM culture from donor eyes, we continued with introducing an UM initiating mutation $GNAQ^{Q209L}$ to complete a pre-malignancy model of UM. By utilizing a lentiviral transduction system, we aimed to create a stably-transduced immortalized NCM cell line harboring a mutation in *GNAQ*. Several optimizations of the transduction protocol were necessary, and from our experience, we have identified the need to utilize fresh virus batches and addition of polybrene at 4µg/ml for 2 days, as well as a non-compatibility of puromycin with the

NCM culture. Following the establishment of a NCM model that harbors *GNAQ* as an initiation mutation, we aimed to characterize *GNAQ*-mutant melanocytes via functional and proteomic assays. In Results chapter 2, we performed an in-depth functional and proteomic characterization of the human mutant and wildtype NCMs, with the aim of shedding light on the mechanisms underlying the development of UM.

Results of other groups have suggested *GNAQ/11* mutations to be weak oncogenes. A transforming ability of mutant *GNAQ* in murine cell line was first demonstrated in NIH 3T3 cells, which is a murine fibroblast cell line[100]. NIH 3T3 cells transfected with mutant *GNAQ* exhibited foci formation and were able to show anchorage-independent growth in soft agar culture[100]. The tumorigenic ability of mutant-GNAQ NIH 3T3 cells were then further demonstrated in nude mice[100].

GNAQ/11 mutations have also been reported in the context of forward genetic screening in mice, where hypermorphic mutations in *GNAQ/11* were found to increase intradermal proliferation of melanocytes[101]. In a study by Van Raamsdonk *et al.* it was demonstrated that *GNAQ/11* mutations were only able to transform hTERT/CDK4^{R24C}/p53^{DD} cells, which are immortalized melanocytes with a deficiency in the p53 and p16/CDK4/RB pathways[10, 102]. Their results showed that hTERT/CDK4^{R24C}/p53^{DD} cells transduced with GNAQ^{Q209L} produced colonies in soft agar. Interestingly, GNAQ^{Q209L} transduction to primary melanocytes were not enough to produce colonies in soft agar in that study.

Overall, our functional and proteomic results comparing GNAQ-mutant cells with WT cells demonstrated and confirmed the general characterization of GNAQ as a weak oncoprotein. For instance, our proliferation and soft agar assays showed mutant GNAQ to confer a growth advantage and anchorage-independent growth in NCMs, which correlated with a transforming property of mutant *GNAQ* gene as has been reported in studies mentioned above.

However, it remains unclear why nevi could harbor a mutation in *GNAQ* while remaining benign. While we would expect a fully transformative gene to confer an enhanced migratory potential to transformed cells, we did not capture a difference in migration between Melan-A^{WT} and Melan-A^{mGNAQ} cells. Hence further characterization assays such as tumorigenic assay in nude mice would help elucidate whether *GNAQ* truly has full transforming capacity in NCMs.

Existing proteomic studies have been conducted on UM cells, either comparing different UM cell lines[96], or comparing primary with metastatic UM tumors[127]. Fewer studies have focused on *GNAQ* mutations specifically, with only one study focused on UM cell lines that harbored *GNAQ* mutations. In that study, the authors demonstrated downregulation of several MEK-related proteins after exposure to a MEK inhibitor[96], showing an important dependence of MEK-related proteins on the *GNAQ* mutation.

A transcriptomic analysis compared protein expression differences between UM cells and normal uveal melanocytes, and highlighted differential expression of over 5,000 genes in MAPK signaling, cell cycle regulation, melanogenesis, p53 pathway, apoptosis[93]. However, to the best of our knowledge, no studies exist that report proteomic changes between *GNAQ*-mutant and -wildtype NCMs melanocytes.

In our study, we performed an unbiased analysis and comparison of global protein expression between Melan-A^{WT} and Melan-A^{mGNAQ} cells. We discovered an overall up-regulation of proteins involved in lipid metabolism in Melan-A^{mGNAQ} cells. This could point to future research venues for knock-out or knock-down studies targeting specific lipid metabolic enzymes to confirm whether changes in metabolism play a vital role in the down-stream effects of *GNAQ* mutations.

While initiating genomic events clearly play a role in UM development, other events appear to also be important. Amongst various plausible environmental risk factors of UM, welding has been shown to be strongly associated with UM development[52]. While welding is a source of UV exposure, it is also a strong source of blue light. Recently, it was shown that blue light increases the proliferation of UM cells both *in vitro*[53] and *in vivo* in a xenograft model[106].

It is important to elucidate the role of BL in UM development as it could potentially be an easy and effective preventative measure for ocular diseases including UM. With age, the human lens becomes progressively more yellow, and gradually gains the ability to filter BL from entering the eye[62]. Intra-ocular lens (IOL) replaces the patient's original lens during cataract surgeries, and although most IOLs now have UV-filtering capabilities, many are not equipped to filter other wavelengths. If BL was shown to contribute to ocular malignancy, it would serve as strong evidence to warrant BL-filtering ability as new commercial standard for IOLs.

Following establishment of our *in vitro* model of GNAQ-mutant NCMs and demonstrating $GNAQ^{Q209L}$ as a weak oncogene in melanocytes, there still remains

the question of additional oncogenic events that interact with the *GNAQ* mutation to result in full malignancy. We wished to therefore investigate the effect of BL exposure on *GNAQ*-mutant cells, and whether BL has the potential to drive malignant transformation. In Results chapter 3, we analyzed the effects of different doses of BL on NCMs as well as *GNAQ*-mutant cells.

Previous studies involving BL have been selectively summarized in Table 14 below based on relevance to our study. Overall, BL has shown a suppressive biological effect on processes such as proliferation, metabolic activity, and protein translation, and appear to act as a biological stressor that results in intracellular stress or damage[121, 123, 128]. In concordance with the literature, our study also demonstrated an anti-proliferative effect of BL exposure on melanocytes in both our human and murine models. Our results suggest that the anti-proliferation effect may be correlated to an increase in ROS production after BL exposure, supporting the characterization of BL as an environmental stressor on normal cells. Although statistical significance was not achieved in our model, future studies looking at ROS production and mitochondrial DNA damage could elucidate some of these mechanisms. BL has been associated to ROS stress in the literature, for instance mitochondrial ROS in RPE cells has been found to mediate cytotoxicity of BL[107].

We did not see major differences in cell death when comparing BL-exposed to non-exposed cells. These data corroborate with studies that demonstrated anti-proliferative activity of BL but not cytotoxicity at certain light dosages[43]. It is therefore plausible that although BL could induce oxidative stress, it does not always result in cell death. This is particularly important in the context of cancer, where the accumulation of damage within cells can contribute to oncogenesis.

Although BL has been reported to possess an inhibitory effect on the proliferation of human melanoma cells[123], a pro-proliferation effect has also been reported in UM cell lines[109]. This led to our hypothesis of characterizing BL as a second oncogenic hit in the *GNAQ*-mutant NCM model. However, our results did not convincingly confirm this hypothesis, as GNAQ-mutant melanocytes responded for the most part similarly to GNAQ-WT cells. Nevertheless, our assays involving UM cells confirmed that fully malignant UM cells are resistant to the effects of BL.

One of the major problems in the field of studies involving BL is a lack of standardization in experimental methods, and especially in the parameters of BL exposure such as light intensity and exposure times, which makes comparison of

results across studies difficult. In our model we tried BL exposure over several days to mimic a chronic exposure, after establishing a dose response. However, further studies looking at long-term exposure could help clarify the effects on ocular cells. Moreover, few studies have been done on normal uveal melanocytes. From the wide difference between behavior of cutaneous and uveal melanoma, it is reasonable to think that different cell types and origin could also respond in differently to BL. What is interesting is that a biphasic response of cells to BL has been reported[129], where cells may have a response at a very low and very high response but not dosages in between. If this effect is present, it would be even more crucial to standardize exposure parameters in BL studies. Further experiments using the same BL exposure parameters on human choroidal melanocytes are also warranted to compare and confirm findings in our study.

Table 14: Selected BL studies in literature

Study Title	Authors	Cell Type	BL Parameter	Main Findings
Blue light inhibits proliferation of melanoma cells[123]	Becker et al.	Human malignant melanoma cell line SK-Mel28		BL decreased cell proliferation and had no effect on cell death. BL downregulated anti-inflammatory genes and upregulated cytochrome P450 and steroid hormone biosynthesis genes.
Blue-light irradiation regulates proliferation and differentiation in human skin cells[43]	Liebman n et al.	Skin endothelial cells, Keratinocytes	453nm (>500J/cm2)	BL was cytotoxic for skin endothelial cells and keratinocytes. Non-toxic irradiation dosages reduced proliferation (due to initiation of differentiation). BL resulted in release of nitric oxide.
Photobiomodulatio n of human dermal fibroblasts in vitro: decisive role of cell	Mignon et al.	Human dermal fibroblasts	450nm (2 – 60 J/cm2)	BL inhibited cell metabolic activity.

culture conditions and treatment protocols on experimental outcome[130]				
Blue light is phototoxic for B16F10 murine melanoma and bovine endothelial cell lines by direct cytocidal effect[44]	Sparsa et al.	Murine melanoma cell line B16F10, endothelial cell line EJG	450nm (10J/cm2, 20J/cm2)	BL was phototoxic to both cell lines. No oxidative damage or difference in lipid peroxidation was found.
Enhanced proliferation inhibition of HL60 cells treated by synergistic all-trans retinoic acid/blue light/nanodiamonds[131]	Zhuang et al.	Human leukemia cell line HL60	456nm (0.25mW/cm^2, 12hrs)	BL reduced cell viability, increased apoptosis and increased ROS.
Effects of blue light emitting diode irradiation on the proliferation, apoptosis, and differentiation of bone marrow-derived mesenchymal stem cells[128]	Yuan et al.	Bone-marrow-derived mesenchymal stem cells (BMSCs)	470nm (20mW/cm^2, 1, 5, 10, 30, 60 mins)	BL decreased EdU staining, induced apoptosis, increased ROS production and led to DNA damage.

Future Directions

In this thesis, I have demonstrated *GNAQ*^{Q209L} to act as a weak activating oncogene in an *in vitro* model of NCMs. It would be interesting to follow up with an *in vivo* animal model and test whether *GNAQ*^{Q209L} mutated NCMs are capable of inducing tumors following intraocular injection.

Our proteomic analysis has shown up-regulation of different pathways in *GNAQ*^{Q209L} cells; however, one limitation of standard proteomic analysis is that it does not allow quantification of the activation status of proteins. In our proteomic results we encountered incidences of proteins that showed a paradoxical elevated expression level when its activity should have increased (GNAQ in WT cells where higher than mutant cells). Since a lot of proteins rely on phosphorylation for regulation of activation, a phosphoproteomic analysis could be useful for further analysis.

Since we have showed an anti-proliferative effect of BL on choroidal melanocytes, it would be valuable to test whether commercial IOLs with BL-filtering abilities can protect against this effect. This would allow further evidence to whether BL protection should be warranted as a standard for IOLs and other eye protections such as glasses.

Bibliography

1. Krantz, B.A., et al., *Uveal melanoma: epidemiology, etiology, and treatment of primary disease.* Clinical ophthalmology (Auckland, N.Z.), 2017. **11**: p. 279-289.
2. Jovanovic, P., et al., *Ocular melanoma: an overview of the current status.* International journal of clinical and experimental pathology, 2013. **6**(7): p. 1230-1244.
3. Yang, J., et al., *Treatment of uveal melanoma: where are we now?* Therapeutic Advances in Medical Oncology, 2018. **10**: p. 175883401875717.
4. Kaliki, S. and C.L. Shields, *Uveal melanoma: relatively rare but deadly cancer.* Eye, 2016. **31**: p. 241.
5. Sodhi, A. and S. Merbs, *Molecular Genetics of Choroidal Melanoma*. Vol. 3. 2012. 2247-2253.
6. Logan, P., et al., *Evidence for the Role of Blue Light in the Development of Uveal Melanoma.* Journal of Ophthalmology, 2015. **2015**: p. 7.
7. Singh, A.D., M.E. Turell, and A.K. Topham, *Uveal Melanoma: Trends in Incidence, Treatment, and Survival.* Ophthalmology, 2011. **118**(9): p. 1881-1885.
8. Smit, K.N., et al., *Uveal melanoma: Towards a molecular understanding.* Progress in Retinal and Eye Research, 2019: p. 100800.
9. Furney, S.J., et al., *SF3B1 Mutations Are Associated with Alternative Splicing in Uveal Melanoma.* Cancer Discovery, 2013. **3**(10): p. 1122-1129.
10. Van Raamsdonk, C.D., et al., *Frequent somatic mutations of GNAQ in uveal melanoma and blue naevi.* Nature, 2009. **457**(7229): p. 599-602.
11. Yavuzyigitoglu, S., et al., *Correlation of Gene Mutation Status with Copy Number Profile in Uveal Melanoma.* Ophthalmology, 2017. **124**(4): p. 573-575.
12. Singh, A.D., et al., *Uveal melanoma: genetic aspects.* Ophthalmol Clin North Am, 2005. **18**(1): p. 85-97, viii.
13. Santarpia, L., S.M. Lippman, and A.K. El-Naggar, *Targeting the MAPK–RAS–RAF signaling pathway in cancer therapy.* Expert Opinion on Therapeutic Targets, 2012. **16**(1): p. 103-119.
14. Cohen, Y., et al., *Lack of BRAF mutation in primary uveal melanoma.* Invest Ophthalmol Vis Sci, 2003. **44**(7): p. 2876-8.
15. Wong, C.W., et al., *BRAF and NRAS mutations are uncommon in melanomas arising in diverse internal organs.* J Clin Pathol, 2005. **58**(6): p. 640-4.
16. Singh, A.D., P. Kalyani, and A. Topham, *Estimating the risk of malignant transformation of a choroidal nevus.* Ophthalmology, 2005. **112**(10): p. 1784-9.
17. Shields, C.L., et al., *Choroidal nevus transformation into melanoma: analysis of 2514 consecutive cases.* Arch Ophthalmol, 2009. **127**(8): p. 981-7.
18. Eskelin, S., et al., *Tumor doubling times in metastatic malignant melanoma of the uvea: tumor progression before and after treatment.* Ophthalmology, 2000. **107**(8): p. 1443-9.
19. Diener-West, M., et al., *Development of metastatic disease after enrollment in the COMS trials for treatment of choroidal melanoma: Collaborative Ocular Melanoma Study Group Report No. 26.* Archives of ophthalmology (Chicago, Ill.: 1960), 2005. **123**(12): p. 1639-1643.
20. Logan, P.T., et al., *Single-cell tumor dormancy model of uveal melanoma.* Clin Exp Metastasis, 2008. **25**(5): p. 509-16.

21. Nichols, E.E., A. Richmond, and A.B. Daniels, *Micrometastatic Dormancy in Uveal Melanoma: A Comprehensive Review of the Evidence, Mechanisms, and Implications for Future Adjuvant Therapies.* International Ophthalmology Clinics, 2017. **57**(1): p. 1-10.
22. Chattopadhyay, C., et al., *Uveal melanoma: From diagnosis to treatment and the science in between.* Cancer, 2016. **122**(15): p. 2299-2312.
23. Shoushtari, A.N. and R.D. Carvajal, *GNAQ and GNA11 mutations in uveal melanoma.* Melanoma Research, 2014. **24**(6): p. 525-534.
24. Bauer, J., et al., *Oncogenic GNAQ mutations are not correlated with disease-free survival in uveal melanoma.* British Journal Of Cancer, 2009. **101**: p. 813.
25. Chen, X., et al., *RasGRP3 Mediates MAPK Pathway Activation in GNAQ Mutant Uveal Melanoma.* Cancer Cell, 2017. **31**(5): p. 685-696.e6.
26. Chen, X., et al., *Combined PKC and MEK inhibition in uveal melanoma with GNAQ and GNA11 mutations.* Oncogene, 2014. **33**(39): p. 4724-4734.
27. Wu, X., et al., *Protein Kinase C Inhibitor AEB071 Targets Ocular Melanoma Harboring GNAQ Mutations via Effects on the PKC/Erk1/2 and PKC/NF-κB Pathways.* Molecular Cancer Therapeutics, 2012. **11**(9): p. 1905-1914.
28. Harvey, K.F., X. Zhang, and D.M. Thomas, *The Hippo pathway and human cancer.* Nat Rev Cancer, 2013. **13**(4): p. 246-57.
29. Yu, F.X., et al., *Mutant Gq/11 promote uveal melanoma tumorigenesis by activating YAP.* Cancer Cell, 2014. **25**(6): p. 822-30.
30. Feng, X., et al., *Hippo-Independent Activation of YAP by the GNAQ Uveal Melanoma Oncogene through a Trio-Regulated Rho GTPase Signaling Circuitry.* Cancer Cell, 2014. **25**(6): p. 831-845.
31. Sato, T., F. Han, and A. Yamamoto, *The biology and management of uveal melanoma.* Current Oncology Reports, 2008. **10**(5): p. 431.
32. Boru, G., et al., *Heterogeneity in Mitogen-Activated Protein Kinase (MAPK) Pathway Activation in Uveal Melanoma With Somatic GNAQ and GNA11 Mutations.* Investigative Ophthalmology & Visual Science, 2019. **60**(7): p. 2474-2480.
33. Khalili, J.S., et al., *Combination Small Molecule MEK and PI3K Inhibition Enhances Uveal Melanoma Cell Death in a Mutant GNAQ- and GNA11-Dependent Manner.* Clinical Cancer Research, 2012. **18**(16): p. 4345-4355.
34. Griewank, K.G., et al., *Genetic and clinico-pathologic analysis of metastatic uveal melanoma.* Modern Pathology, 2014. **27**(2): p. 175-183.
35. Pópulo, H., et al., *Analysis of GNAQ mutations, proliferation and MAPK pathway activation in uveal melanomas.* British Journal of Ophthalmology, 2011. **95**(5): p. 715-719.
36. Onken, M.D., et al., *Oncogenic Mutations in GNAQ Occur Early in Uveal Melanoma.* Investigative Ophthalmology & Visual Science, 2008. **49**(12): p. 5230-5234.
37. Serrage, H., et al., *Under the spotlight: mechanisms of photobiomodulation concentrating on blue and green light.* Photochemical & Photobiological Sciences, 2019. **18**(8): p. 1877-1909.
38. Mainster, M.A. and P.L. Turner, *Ultraviolet-B phototoxicity and hypothetical photomelanomagenesis: intraocular and crystalline lens photoprotection.* Am J Ophthalmol, 2010. **149**(4): p. 543-9.
39. Tosini, G., I. Ferguson, and K. Tsubota, *Effects of blue light on the circadian system and eye physiology.* Molecular vision, 2016. **22**: p. 61-72.

40. Wolska, A., *[Occupational exposure of welders to ultraviolet and "blue light" radiation emitted during TIG and MMA welding based on field measurements].* Med Pr, 2013. **64**(1): p. 69-82.
41. Hockberger, P.E., et al., *Activation of flavin-containing oxidases underlies light-induced production of H2O2 in mammalian cells.* Proc Natl Acad Sci U S A, 1999. **96**(11): p. 6255-60.
42. Becker, A., et al., *Gene expression profiling reveals aryl hydrocarbon receptor as a possible target for photobiomodulation when using blue light.* Scientific Reports, 2016. **6**(1): p. 33847.
43. Liebmann, J., M. Born, and V. Kolb-Bachofen, *Blue-light irradiation regulates proliferation and differentiation in human skin cells.* J Invest Dermatol, 2010. **130**(1): p. 259-69.
44. Sparsa, A., et al., *Blue light is phototoxic for B16F10 murine melanoma and bovine endothelial cell lines by direct cytocidal effect.* Anticancer Res, 2010. **30**(1): p. 143-7.
45. McDonagh, A., L. Palma, and D. Lightner, *Blue light and bilirubin excretion.* Science, 1980. **208**(4440): p. 145-151.
46. Kleinpenning, M.M., et al., *Efficacy of blue light vs. red light in the treatment of psoriasis: a double-blind, randomized comparative study.* J Eur Acad Dermatol Venereol, 2012. **26**(2): p. 219-25.
47. Pei, S., et al., *Light-based therapies in acne treatment.* Indian dermatology online journal, 2015. **6**(3): p. 145-157.
48. Godley, B.F., et al., *Blue light induces mitochondrial DNA damage and free radical production in epithelial cells.* J Biol Chem, 2005. **280**(22): p. 21061-6.
49. Moon, J., et al., *Blue light effect on retinal pigment epithelial cells by display devices.* Integr Biol (Camb), 2017. **9**(5): p. 436-443.
50. Seko, Y., et al., *Blue light-induced apoptosis in cultured retinal pigment epithelium cells of the rat.* Graefes Arch Clin Exp Ophthalmol, 2001. **239**(1): p. 47-52.
51. Vila, N., et al., *Blue-light filtering alters angiogenic signaling in human retinal pigmented epithelial cells culture model.* BMC Ophthalmol, 2017. **17**(1): p. 198.
52. Fernandes, B.F., J.C. Marshall, and M.N. Burnier, Jr., *Blue light exposure and uveal melanoma.* Ophthalmology, 2006. **113**(6): p. 1062 e1; author reply 1062.
53. Marshall, J.C., et al., *The effect of blue light exposure and use of intraocular lenses on human uveal melanoma cell lines.* Melanoma Res, 2006. **16**(6): p. 537-41.
54. Manning, W.S., Jr., P.G. Greenlee, and J.N. Norton, *Ocular melanoma in a Long Evans rat.* Contemp Top Lab Anim Sci, 2004. **43**(1): p. 44-6.
55. Di Cesare, S., et al., *The effect of blue light exposure in an ocular melanoma animal model*. Vol. 28. 2009. 1-9.
56. Olah, J., et al., *Long-term hazards of neonatal blue-light phototherapy.* Br J Dermatol, 2013. **169**(2): p. 243-9.
57. Csoma, Z., et al., *Neonatal blue light phototherapy and melanocytic nevi: a twin study.* Pediatrics, 2011. **128**(4): p. e856-64.
58. el Filali, M., et al., *Regulation of VEGF-A in uveal melanoma.* Invest Ophthalmol Vis Sci, 2010. **51**(5): p. 2329-37.
59. Boyd, S.R., et al., *Vascular endothelial growth factor is elevated in ocular fluids of eyes harbouring uveal melanoma: identification of a potential therapeutic window.* Br J Ophthalmol, 2002. **86**(4): p. 448-52.
60. Missotten, G.S., et al., *Vascular endothelial growth factor a in eyes with uveal melanoma.* Arch Ophthalmol, 2006. **124**(10): p. 1428-34.

61. Yanagi, Y., et al., *Effects of yellow intraocular lenses on light-induced upregulation of vascular endothelial growth factor.* J Cataract Refract Surg, 2006. **32**(9): p. 1540-4.
62. Cogan, D.G., *Lesions of the eye from radiant energy.* J Am Med Assoc, 1950. **142**(3): p. 145-51.
63. Hood, B.D., B. Garner, and R.J. Truscott, *Human lens coloration and aging. Evidence for crystallin modification by the major ultraviolet filter, 3-hydroxy-kynurenine O-beta-D-glucoside.* J Biol Chem, 1999. **274**(46): p. 32547-50.
64. Bennett, D.C., P.J. Cooper, and I.R. Hart, *A line of non-tumorigenic mouse melanocytes, syngeneic with the B16 melanoma and requiring a tumour promoter for growth.* Int J Cancer, 1987. **39**(3): p. 414-8.
65. Weidmann, C., et al., *Differential responses of choroidal melanocytes and uveal melanoma cells to low oxygen conditions.* Mol Vis, 2017. **23**: p. 103-115.
66. Hashimoto, S., et al., *Lysophosphatidic acid activates Arf6 to promote the mesenchymal malignancy of renal cancer.* Nat Commun, 2016. **7**: p. 10656.
67. Lopez-Mosqueda, J., et al., *SPRTN is a mammalian DNA-binding metalloprotease that resolves DNA-protein crosslinks.* Elife, 2016. **5**.
68. Salmon, P., et al., *Reversible immortalization of human primary cells by lentivector-mediated transfer of specific genes.* Mol Ther, 2000. **2**(4): p. 404-14.
69. Bustamante, P., et al., *Beta-blockers exert potent anti-tumor effects in cutaneous and uveal melanoma.* Cancer Medicine. **0**(0).
70. Horibata, S., et al., *Utilization of the Soft Agar Colony Formation Assay to Identify Inhibitors of Tumorigenicity in Breast Cancer Cells.* Journal of visualized experiments : JoVE, 2015(99): p. e52727-e52727.
71. Marous, C.L., et al., *Malignant transformation of choroidal nevus according to race in 3334 consecutive patients.* Indian J Ophthalmol, 2019. **67**(12): p. 2035-2042.
72. Halaban, R. and F.D. Alfano, *Selective elimination of fibroblasts from cultures of normal human melanocytes.* In Vitro, 1984. **20**(5): p. 447-50.
73. Hu, D.N., et al., *Studies of human uveal melanocytes in vitro: isolation, purification and cultivation of human uveal melanocytes.* Investigative Ophthalmology & Visual Science, 1993. **34**(7): p. 2210-2219.
74. LEADER, M., et al., *Vimentin: an evaluation of its role as a tumour marker.* Histopathology, 1987. **11**(1): p. 63-72.
75. Chen, Y.-T., et al., *Serological analysis of Melan-A (MART-1), a melanocyte-specific protein homogeneously expressed in human melanomas.* Proceedings of the National Academy of Sciences, 1996. **93**(12): p. 5915-5919.
76. Takahashi, K., et al., *Immunohistochemical study on the distribution of α and β subunits of S-100 protein in human neoplasm and normal tissues.* Virchows Archiv B, 1984. **45**(1): p. 385-396.
77. Weedon, D., *32 - Lentigines, nevi, and melanomas*, in *Weedon's Skin Pathology (Third Edition)*, D. Weedon, Editor. 2010, Churchill Livingstone: Edinburgh. p. 709-756.e61.
78. Valtink, M. and K. Engelmann, *Serum-free cultivation of adult normal human choroidal melanocytes.* Graefe's Archive for Clinical and Experimental Ophthalmology, 2007. **245**(10): p. 1487-1494.
79. Reform, C.A.f.I. *Exponential growth, doubling time, and the rule of 70*. 1995-2019 Mar 2020].

80. Chen, Y., et al., *Characterization and Establishment of an Immortalized Rabbit Melanocyte Cell Line Using the SV40 Large T Antigen.* International journal of molecular sciences, 2019. **20**(19): p. 4874.
81. Jiang, W., et al., *An optimized method for high-titer lentivirus preparations without ultracentrifugation.* Scientific Reports, 2015. **5**(1): p. 13875.
82. Davis, H.E., J.R. Morgan, and M.L. Yarmush, *Polybrene increases retrovirus gene transfer efficiency by enhancing receptor-independent virus adsorption on target cell membranes.* Biophys Chem, 2002. **97**(2-3): p. 159-72.
83. Lee, K.M., K.H. Choi, and M.M. Ouellette, *Use of exogenous hTERT to immortalize primary human cells.* Cytotechnology, 2004. **45**(1-2): p. 33-38.
84. Amirouchene-Angelozzi, N., et al., *Establishment of novel cell lines recapitulating the genetic landscape of uveal melanoma and preclinical validation of mTOR as a therapeutic target.* Mol Oncol, 2014. **8**(8): p. 1508-20.
85. De Waard-Siebinga, I., et al., *Establishment and characterization of an uveal-melanoma cell line.* Int J Cancer, 1995. **62**(2): p. 155-61.
86. Belmar-Lopez, C., et al., *Uveal vs. cutaneous melanoma. Origins and causes of the differences.* Clin Transl Oncol, 2008. **10**(3): p. 137-42.
87. Hu, D.N., et al., *Studies of human uveal melanocytes in vitro: isolation, purification and cultivation of human uveal melanocytes.* Invest Ophthalmol Vis Sci, 1993. **34**(7): p. 2210-9.
88. Goodall, T., et al., *Effect of melanocyte stimulating hormone on human cultured choroidal melanocytes, uveal melanoma cells, and retinal epithelial cells.* Invest Ophthalmol Vis Sci, 1994. **35**(3): p. 826-37.
89. Yang, H., J. Cao, and H.E. Grossniklaus, *Uveal Melanoma Metastasis Models.* Ocular Oncology and Pathology, 2015. **1**(3): p. 151-160.
90. Mori, S., et al., *Anchorage-independent cell growth signature identifies tumors with metastatic potential.* Oncogene, 2009. **28**(31): p. 2796-2805.
91. Hurlin, P.J., et al., *Morphological Transformation, Focus Formation, and Anchorage Independence Induced in Diploid Human Fibroblasts by Expression of a Transfected H-ras Oncogene.* Cancer Research, 1987. **47**(21): p. 5752-5757.
92. Perez, D.E., et al., *Uveal melanoma driver mutations in GNAQ/11 yield numerous changes in melanocyte biology.* Pigment Cell Melanoma Res, 2018. **31**(5): p. 604-613.
93. An, J., et al., *A comparative transcriptomic analysis of uveal melanoma and normal uveal melanocyte.* PloS one, 2011. **6**(1): p. e16516-e16516.
94. Zhang, F. and G. Du, *Dysregulated lipid metabolism in cancer.* World journal of biological chemistry, 2012. **3**(8): p. 167-174.
95. Leibovitch, M. and I. Topisirovic, *Dysregulation of mRNA translation and energy metabolism in cancer.* Advances in Biological Regulation, 2018. **67**: p. 30-39.
96. Ambrosini, G., et al., *Identification of Unique MEK-Dependent Genes in GNAQ Mutant Uveal Melanoma Involved in Cell Growth, Tumor Cell Invasion, and MEK Resistance.* Clinical Cancer Research, 2012. **18**(13): p. 3552-3561.
97. Bergeron, M.-A., et al., *Repression of genes involved in melanocyte differentiation in uveal melanoma.* Molecular vision, 2012. **18**: p. 1813-1822.
98. Hussein, M.R., et al., *Microsatellite Instability and Alterations of Mismatch Repair Protein Expression in Choroidal Melanomas.* Archives of Ophthalmology, 2005. **123**(12): p. 1705-1711.

99. Rochdi, M.D. and J.L. Parent, *Galphaq-coupled receptor internalization specifically induced by Galphaq signaling. Regulation by EBP50.* J Biol Chem, 2003. **278**(20): p. 17827-37.
100. Kalinec, G., et al., *Mutated alpha subunit of the Gq protein induces malignant transformation in NIH 3T3 cells.* Molecular and cellular biology, 1992. **12**(10): p. 4687-4693.
101. Van Raamsdonk, C.D., et al., *Effects of G-protein mutations on skin color.* Nat Genet, 2004. **36**(9): p. 961-8.
102. Field, Matthew G. and J.W. Harbour, *GNAQ/11 Mutations in Uveal Melanoma: Is YAP the Key to Targeted Therapy?* Cancer Cell, 2014. **25**(6): p. 714-715.
103. Shah, C.P., et al., *Intermittent and chronic ultraviolet light exposure and uveal melanoma: a meta-analysis.* Ophthalmology, 2005. **112**(9): p. 1599-607.
104. Singh, A.D., et al., *Sunlight exposure and pathogenesis of uveal melanoma.* Surv Ophthalmol, 2004. **49**(4): p. 419-28.
105. Okuno, T., J. Ojima, and H. Saito, *Blue-Light Hazard from CO2 Arc Welding of Mild Steel.* Annals of Work Exposures and Health, 2009. **54**(3): p. 293-298.
106. Di Cesare, S., et al., *The effect of blue light exposure in an ocular melanoma animal model.* J Exp Clin Cancer Res, 2009. **28**: p. 48.
107. King, A., et al., *Mitochondria-derived reactive oxygen species mediate blue light-induced death of retinal pigment epithelial cells.* Photochem Photobiol, 2004. **79**(5): p. 470-5.
108. Vicente-Tejedor, J., et al., *Removal of the blue component of light significantly decreases retinal damage after high intensity exposure.* PloS one, 2018. **13**(3): p. e0194218-e0194218.
109. Aldrees, S., *The effects of varying intensities of blue light on the proliferation of human uveal melanoma cell lines by using multiple blue light filters*, in *Department of Pathology*. 2017, McGill University McGill University
110. Li, C.N., et al., *Cell-free DNA is released from tumor cells upon cell death: a study of tissue cultures of tumor cell lines.* J Clin Lab Anal, 2003. **17**(4): p. 103-7.
111. Valpione, S., et al., *Plasma total cell-free DNA (cfDNA) is a surrogate biomarker for tumour burden and a prognostic biomarker for survival in metastatic melanoma patients.* European journal of cancer (Oxford, England : 1990), 2018. **88**: p. 1-9.
112. Cheng, K.P., et al. *Blue Light Modulates Murine Microglial Gene Expression in the Absence of Optogenetic Protein Expression*. Scientific reports, 2016. **6**, 21172 DOI: 10.1038/srep21172.
113. Cryan, L.M., et al., *Expression of COX-2 and prognostic outcome in uveal melanoma.* Curr Eye Res, 2008. **33**(2): p. 177-84.
114. Jr., M.N.B., et al., *The Effect of a Cox–2 Inhibitor on an Ocular Melanoma Animal Model.* Investigative Ophthalmology & Visual Science, 2006. **47**(13): p. 2218-2218.
115. Marshall, J.C.A., et al., *Inhibition of uveal melanoma cell proliferation by nepafenac, a selective cyclooxygenase–2 (COX–2) inhibitor.* Investigative Ophthalmology & Visual Science, 2004. **45**(13): p. 1204-1204.
116. Shang, F. and A. Taylor, *Ubiquitin-proteasome pathway and cellular responses to oxidative stress.* Free radical biology & medicine, 2011. **51**(1): p. 5-16.
117. Shin, S.J., et al., *Unexpected gain of function for the scaffolding protein plectin due to mislocalization in pancreatic cancer.* Proceedings of the National Academy of Sciences, 2013. **110**(48): p. 19414-19419.

118. Ong, M.S., et al., *Cytoskeletal Proteins in Cancer and Intracellular Stress: A Therapeutic Perspective.* Cancers, 2020. **12**(1): p. 238.
119. Allen, R.G. and M. Tresini, *Oxidative stress and gene regulation.* Free Radical Biology and Medicine, 2000. **28**(3): p. 463-499.
120. Miyashita, Y., et al., *Expression of Opsin Molecule in Cultured Murine Melanocyte.* Journal of Investigative Dermatology Symposium Proceedings, 2001. **6**(1): p. 54-57.
121. Mignon, C., et al., *Photobiomodulation of human dermal fibroblasts in vitro: decisive role of cell culture conditions and treatment protocols on experimental outcome.* Scientific reports, 2017. **7**(1): p. 2797-2797.
122. Chang, L.-Y., et al., *Proteomic Analysis Reveals Anti-Fibrotic Effects of Blue Light Photobiomodulation on Fibroblasts.* Lasers in Surgery and Medicine, 2020. **52**(4): p. 358-372.
123. Becker, A., et al., *Blue light inhibits proliferation of melanoma cells*. SPIE BiOS. Vol. 9695. 2016: SPIE.
124. Tyssowski, K.M. and J.M. Gray, *Blue light induces neuronal-activity-regulated gene expression in the absence of optogenetic proteins.* bioRxiv, 2019: p. 572370.
125. Hu, D.N., S.A. McCormick, and R. Ritch, *Studies of human uveal melanocytes in vitro: growth regulation of cultured human uveal melanocytes.* Invest Ophthalmol Vis Sci, 1993. **34**(7): p. 2220-7.
126. Ahmed, J., et al., *Oxygen distribution in the macaque retina.* Invest Ophthalmol Vis Sci, 1993. **34**(3): p. 516-21.
127. Linge, A., et al., *Differential Expression of Fourteen Proteins between Uveal Melanoma from Patients Who Subsequently Developed Distant Metastases versus Those Who Did NotProteomic Analysis of Metastatic Uveal Melanoma.* Investigative Ophthalmology & Visual Science, 2012. **53**(8): p. 4634-4643.
128. Yuan, Y., et al., *Effects of Blue Light Emitting Diode Irradiation On the Proliferation, Apoptosis and Differentiation of Bone Marrow-Derived Mesenchymal Stem Cells.* Cell Physiol Biochem, 2017. **43**(1): p. 237-246.
129. Becker, A., *Influence of photobiomodulation with blue light on the metabolism, proliferation and gene expression of human keratinocytes*. 2017.
130. Mignon, C., et al., *Photobiomodulation of human dermal fibroblasts in vitro: decisive role of cell culture conditions and treatment protocols on experimental outcome.* Scientific Reports, 2017. **7**(1): p. 2797.
131. Zhuang, J., et al., *Enhanced proliferation inhibition of HL60 cells treated by synergistic all-trans retinoic acid/blue light/nanodiamonds.* RSC Advances, 2017. **7**(62): p. 38895-38901.